Low field magnetotransport in manganites

2008 J. Phys.: Condens. Matter 20 273201

(http://iopscience.iop.org/0953-8984/20/27/273201)

J. Phys.: Condens. Matter **20** (2008) 273201 (43pp) doi:10.1088/0953-8984/20/27/273201

TOPICAL REVIEW

Low field magnetotransport in manganites

P K Siwach[1,3], **H K Singh**[2] **and O N Srivastava**[1]

[1] Physics Department, Banaras Hindu University, Varanasi-221 005, India
[2] National Physical Laboratory, Dr K S Krishnan Marg, New Delhi-110012, India

E-mail: pksiwach@yahoo.com

Received 27 July 2007, in final form 12 February 2008
Published 13 June 2008
Online at stacks.iop.org/JPhysCM/20/273201

Abstract

The perovskite manganites with generic formula $RE_{1-x}AE_xMnO_3$ (RE = rare earth, AE = Ca, Sr, Ba and Pb) have drawn considerable attention, especially following the discovery of colossal magnetoresistance (CMR). The most fundamental property of these materials is strong correlation between structure, transport and magnetic properties. They exhibit extraordinary large magnetoresistance named CMR in the vicinity of the insulator–metal/paramagnetic–ferromagnetic transition at relatively large applied magnetic fields. However, for applied aspects, occurrence of significant CMR at low applied magnetic fields would be required. This review consists of two sections: in the first section we have extensively reviewed the salient features, e.g. structure, phase diagram, double-exchange mechanism, Jahn–Teller effect, different types of ordering and phase separation of CMR manganites. The second is devoted to an overview of experimental results on CMR and related magnetotransport characteristics at low magnetic fields for various doped manganites having natural grain boundaries such as polycrystalline, nanocrystalline bulk and films, manganite-based composites and intrinsically layered manganites, and artificial grain boundaries such as bicrystal, step-edge and laser-patterned junctions. Some other potential magnetoresistive materials, e.g. pyrochlores, chalcogenides, ruthenates, diluted magnetic semiconductors, magnetic tunnel junctions, nanocontacts etc, are also briefly dealt with. The review concludes with an overview of grain-boundary-induced low field magnetotransport behavior and prospects for possible applications.

(Some figures in this article are in colour only in the electronic version)

Contents

[3] Author to whom any correspondence should be addressed. Present address: National Physical Laboratory, Dr K S Krishnan Marg, New Delhi-110012, India.

1. Introduction

Materials science and engineering have been at the frontier of technological advancement since the bronze and iron ages. The present information age relies on the development of 'smart' and 'smaller' magnetic materials for memory, data storage, processing and probing. These magnetic materials can be divided into numerous categories, depending on their origin and applications. One prime example is the transition metal oxides (TMOs) having perovskite (ABO_3 type) structure, which form a vitally important class of materials from the point of view of fundamental physics as well as technological applications [1]. They have been attracting intense attention because of their exotic properties such as the ferroelectricity of titanates (doped $BaTiO_3$) [2, 3], high temperature superconductivity of cuprates ($La_{2-x}Ba_xCuO_4$, $HgBa_2Ca_2Cu_3O_{8-\delta}$) [4–6], colossal magnetoresistance of manganites (doped $LaMnO_3$) [7], unconventional p-wave superconductivity of ruthenates (Sr_2RuO_4) [8] and multiferroicity [9, 10].

During the last decade, TMO based magnetoelectronics is fast emerging as future viable technology. In the early days, magnetic materials, e.g. Fe_2O_3, CrO_2, were used only in motors and generators, as permanent magnets, followed eventually by applications like magnetic media (disks and tapes) for data storage, magnetic field sensors, read heads etc. The ever-exciting field of magnetism still continues to draw attention both of scientists and the industrial community [11]. R&D for magnetic recording efforts is focused on the goal of achieving higher areal density (the number of bits/unit area on a disk surface), which is possible by increasing the linear as well as track densities. Improvement in the linear density requires advancement in materials, in the recording techniques and in miniaturization of the components. Track densities can be increased by improving the magnetic media or material characteristics. The media or material developments cover a broad range of materials and processes. The recent development of deposited metal film media makes it possible to achieve still higher magnetization values, having high linear as well as track densities. Therefore, increased attention is being paid to metal thin films. Thin films with higher coercivity are required for higher density media. The most challenging issue towards achieving high recording density media is to produce magnetic thin films which have a large signal-to-noise ratio despite the smaller size of the bit or data being detected. The flexibility of thin film technology makes it possible to tailor the magnetic properties to meet specific design requirements [12, 13].

Magnetism is still a very competitive technology not only for recording but also for other novel applications. Recently, an approach to electronics is emerging that is based on the up- or down-spin of the charge carriers rather than on electrons or holes as in traditional semiconductor electronics. Devices that rely on the electron's spin to perform their functions form the foundation of spintronics or magnetoelectronics [14–17]. These spintronics devices are being developed for applications such as ultrasensitive magnetic sensors and magnetoresistive random access memory (MRAM). The key factor for the growth of magnetism based technology is the increase in the areal density. The areal density of the state of the art production was 700 Mbit in^{-2} in 1995. In the quest to lower the cost and improve the performance, the areal density has increased more than 20-million-fold in modern disk drives and currently doubles every year (figure 1). Nonetheless, the pursuit of higher areal densities still continues, as is evident in recent laboratory experiments of recording densities beyond 100 Gbit in^{-2} [18, 19], and the next big challenge now looming ahead is to achieve 1 Tbit in^{-2} recording density [20].

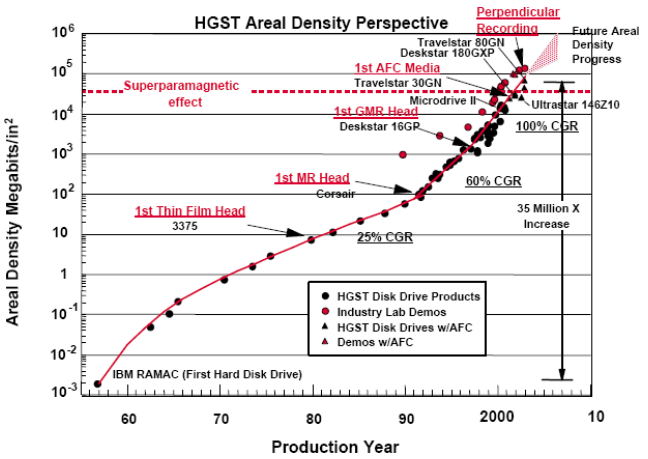

Figure 1. Progress in areal density since its invention (courtesy Ed Grochowski).

The main limitation on the size of the smallest bit depends on the design of read–write head and the intrinsic signal-to-noise ratio of the material. Herein comes the next generation devices based on giant and colossal magnetoresistive materials. Very sensitive magnetoresistive materials called giant magnetoresistive (GMR) materials and more recently the colossal magnetoresistive materials have been rediscovered in the past few years, due to the intense, new materials research. These materials exhibit a resistance change when subjected to a magnetic field and may eventually evolve into magnetoresistive (MR) heads to achieve the required areal densities. Commercialization of the GMR and CMR effects will require materials which have both high magnetization and low activation fields, of the order of few tens of gauss or even smaller. Thus, research on magnetic materials (magnetic thin films and creating new materials systems) and understanding their magnetic properties has the potential to make a significant contribution to information technology [13].

1.1. The phenomenon of magnetoresistance

Magnetoresistance (MR) refers to the relative change in the electrical resistivity of a material on the application of an external magnetic field. MR is generally defined by the equation

$$\mathrm{MR}\% = \frac{\Delta\rho}{\rho_0} \times 100 = \left[\frac{\rho_0 - \rho_H}{\rho_0}\right] \times 100,$$

where ρ_H and ρ_0 are the resistivities at a given temperature in the applied and zero magnetic fields, respectively. MR can be

positive or negative depending on the increase or decrease in resistivity, respectively.

All metals show MR, which varies from few per cent to an exceptionally high value, depending on the system and the strength and orientation of applied magnetic field [21]. Non-magnetic metals, such as Au, exhibit small MR, but the magnitude is somewhat greater (up to 15%) in ferromagnetic metals such as Fe and Co. The semimetal Bi also shows ∼18% MR in a transverse field of 0.6 T, which rises to a 40% change at 24 T [22]. Cu is more typical in that the same very powerful field (24 T) gave rise to change of only ∼2% at room temperature. This is the positive magnetoresistance that varies as B^2 (B = applied magnetic field) in half-metallic ferromagnets such as CrO_2 etc [23]. It is absent in the free electron gas [21] but appears when the Fermi surface is non-spherical (as in case of semimetal Bi) [22]. This MR originates from the impact of the Lorentz force on the moving charge carriers, similar to the Hall effect. Its value is ∼10% at 10 T. A classification of the magnetoresistance phenomenon is based on the distinction familiar in magnetism between intrinsic properties such as anisotropy constants, which depend only on the crystal structure, composition and purity, and extrinsic properties such as coercivity, which depend on the structure on various (mesoscopic or microscopic) length scales [24].

1.2. Giant magnetoresistance (GMR)

The GMR effect was originally discovered in molecular beam epitaxy grown epitaxial (100) oriented Fe/Cr/Fe sandwiches [25] and Fe/Cr multilayers [26], but the effects were quite modest at room temperature. Shortly afterward it was discovered that similar effects could be found in polycrystalline sputtered Fe/Cr multilayers [27], and subsequently very large room temperature MR was found in Co/Cu and related multilayers [28–30]. The GMR has also been observed in variety of inhomogeneous granular (clusters and alloys) systems predominantly comprised of Fe, Co, Ni and their various alloys in Cu, Ag and Au matrices [31–34]. In granular magnetic systems, where small ferromagnetic grains (e.g. Fe, Co, Ni etc) are embedded in an immiscible insulating matrix, the macroscopic properties depend on the metallic volume fraction, the grain size and the intergranular distance. When the relative orientation of grains is antiparallel, it results in a minimum in conductance. When antiparallel grains are forced to be parallel by the application of a magnetic field, conductance increases and results in large magnetoresistance [35, 36]. On the other hand, in magnetic multilayers spin-dependent scattering (SDS) at the interface is responsible for the GMR effect [37]. Parkin *et al* [38] have found that the relative orientation of the magnetic moments of two neighboring Co (magnetic) layers depends on the thickness of the intervening spacer Cu (non-magnetic) layer.

Fert and Campbell [39] have given a simple explanation to analyze the transport properties of ferromagnetic metals by mapping the electric current that flows through the magnetic multilayers. They considered a trilayer with two magnetic layers separated by a non-magnetic spacer layer. As the GMR relies on the fact that electron spin is conserved over a distance of up to several tens of nanometers, which is greater than the thickness of a typical multilayer, one can assume that electric current in the trilayer flows in two channels, one corresponding to electrons with spin-up projection ↑ and the other to electrons with spin-down projection ↓ [40]. Since the ↑ and ↓ spin channels are independent (spin is conserved), they can be regarded as two wires connected in parallel. The second essential ingredient is that electrons with spin projection parallel and antiparallel to the magnetization of the ferromagnetic layer are scattered at different rates when they enter the ferromagnet. Thus the GMR in a trilayer can be explained qualitatively using the simple resistor model as shown in figure 2. This simple physical resistor model of the GMR effect is believed to be correct but needs to be converted into a quantitative theory that can explain the difference between the current-in-plane (CIP) and current-out-of-plane (CPP) geometries, the observed dependence of the GMR on the layer thickness and also the material dependence of the effect. The simple resistor network model discussed above predicts that the resistance of a magnetic multilayer will be higher for antiparallel alignment of the magnetic layers as compared with parallel alignment [40, 41].

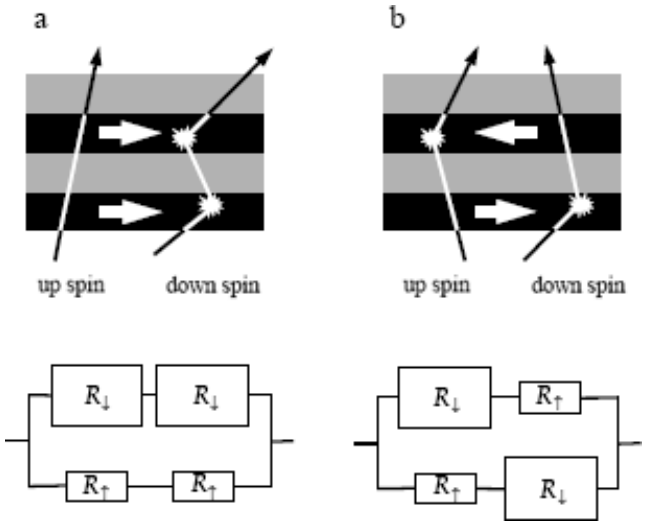

Figure 2. Schematic illustration of electron transport across a multilayer for (a) parallel and (b) antiparallel magnetizations of the successive ferromagnetic layers. The magnetization directions are indicated by the arrows. The solid lines are individual electron trajectories within the two spin channels. Bottom panels show the resistor network within the two-current series resistor model. For the parallel-aligned multilayer (a), the up-spin electrons pass through the structure almost without scattering, whereas the down-spin electrons are scattered strongly within both ferromagnetic layers. Since conduction occurs in parallel for the two spin channels, the total resistivity of the multilayer is low. For the antiparallel-aligned multilayer (b), both the up-spin and down-spin electrons are scattered strongly within one of the ferromagnetic layers, and the total resistivity of the multilayer is high [46]. Reprinted with permission from [46]. Copyright Elsevier 2001.

Several theoretical models have been developed, but most of them are based on a pioneer model of the electrical conduction in ferromagnets (FMs) proposed by Mott [42]. Mott hypothesized that the electric current in FM metal is carried independently in two conduction channels that

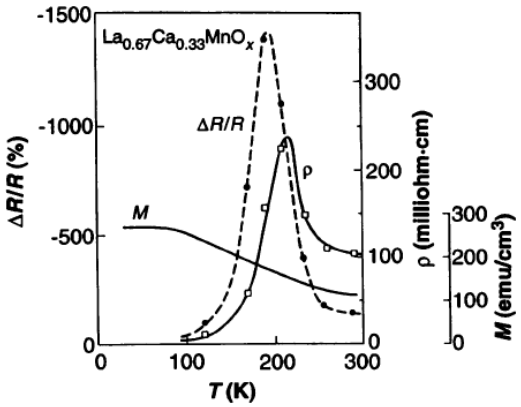

Figure 3. Temperature dependence of $\Delta R/R$, the resistivity ρ and the magnetization M for thin films of $La_{1-x}Ca_xMnO_3$ at $x = 0.33$ from [49]. Reprinted with permission from AAAS.

correspond predominantly to the spin-up and spin-down s–p electrons. These electrons are in broad energy bands with low effective masses. This assumption is believed to be good at temperatures significantly below the magnetic ordering temperature of the magnetic material so that there is little spin mixing between two conduction channels. Mott established that the conductivity can be significantly different in the two channels, which is related to the corresponding spin-up and spin-down density of empty states at the Fermi level. These states will be largely of d character, and as a result of the exchange split d bands the ratio of spin-up to spin-down density of empty states at the Fermi level can be significantly different in the ferromagnetically ordered states of Fe, Co, Ni and their alloys. Consequently this leads to the possibility of substantially different mean free paths $\lambda^{\pm}$ and spin-down (minority) electrons as compared with spin-up (majority) electrons [43–45]. An extensive review covering all aspects of the giant magnetoresistance effect is given by Tsymbal and Pettifor [46].

2. Emergence of a new type of magnetoresistance: colossal magnetoresistance (CMR)

Another magnetoresistive material which has drawn considerable attention in the last decade is the unique intrinsically layered perovskite (ABO_3 type) manganites of the form $RE_{1-x}AE_xMnO_3$, where RE is a trivalent rare earth cation, e.g. La, Pr, Nd etc, and AE is a divalent alkaline earth cation, e.g. Ca, Ba, Sr etc. Chahara *et al* [47], von Helmholtz *et al* [48] and Jin *et al* [49] observed a high magnetoresistance in these doped rare earth manganites (bulk as well as thin films) in a magnetic field of several tesla (∼6 T) (figure 3). As the physical origin of the magnetoresistance in manganites was completely different from the giant magnetoresistance effect (GMR), the term colossal was coined (Jin *et al*) [49] to describe the effect. Since doped perovskite manganites are the theme of the present review, the basics of colossal magnetoresistance materials are described and discussed in detail.

2.1. Brief history of manganites

About half a century ago Jonker and Santen [50–52] described the preparation of polycrystalline samples of (La, Ca)MnO_3, (La, Sr)MnO_3 and (La, Ba)MnO_3 manganites and reported ferromagnetism and anomalies in the conductivity at the Curie temperature with variation in lattice parameter as a function of hole doping. A few years later Volger (1954) observed a notable decrease of resistivity for $La_{0.8}Sr_{0.2}MnO_3$ in the FM state, in applied magnetic fields [53]. Soon after, a significant research effort started on the studies of low temperature measurements in manganites such as specific heat, magnetization, dc and ac resistivity, magnetoresistance, magnetostriction, I–V curves, dielectric constant, Seebeck effect and Hall effect [53, 54].

After these pioneering experiments, Wollan and Koehler [55] carried out extensive neutron diffraction study to characterize and draw the first ever magnetic structures (phase diagram) of $La_{1-x}Ca_xMnO_3$ in the entire composition range. (Wollan and Koehler (1955) were among the first to use the technique of neutron scattering to study magnetism in materials.) They found that in addition to FM phase many other interesting antiferromagnetic phases were also present in manganites (figure 4(a)). Among them the most exotic spin arrangement is the CE-type state, which following their classification is a mixture of the C phase with the E phase (figure 4(b)). This CE state was also the first evidence of charge ordering and mixed phase (phase separation) tendencies in the manganites. Further progress came somewhat later when the group at Manitoba grew a high quality millimeter long single crystal of another interesting manganite, (La, Pb)MnO_3, which has a Curie temperature well above room temperature [56]. Jirak *et al* [57] and Pollert *et al* [58] studied the structure and magnetic properties of another very popular manganite (Pr, Ca)MnO_3 by x-ray and neutron diffraction techniques. They have also observed charge-ordered phases which are totally different from the ferromagnetic phases of other manganites [57].

A burst of research activity on manganites started during 1990 because of the observation of large magnetoresistance. Work by Kusters *et al* [59] on bulk $Nd_{0.5}Pb_{0.5}MnO_3$ reveals the large MR effect. Another work by von Helmholtz *et al* [48] on thin films of $La_{2/3}Ba_{1/3}MnO_3$ also revealed a large MR effect at room temperature. Thereafter, a similar conclusion was reached by Chahara *et al* [47] using thin films of $La_{3/4}Ca_{1/4}MnO_3$ and by Ju *et al* [60] for films of $La_{1-x}Sr_xMnO_3$. They all observed MR values larger than those observed in artificially engineered multilayers (GMR) [38]. A defining moment for the field of manganites was the publication by Jin *et al* [49] of results with truly colossal magnetoresistance (CMR). Jin *et al* reported MR close to ∼1500% at 200 K and over ∼100 000% at 77 K for thin films of $La_{0.67}Ca_{0.33}MnO_3$. This enormous factor corresponds to a thousand-fold change in resistivity with and without the field. One year later Xiong *et al* [61] reported an MR ratio of over ∼100 000% (MR $= (\rho_0 - \rho_H) \times 100/\rho_H$) using thin films of $Nd_{0.7}Sr_{0.3}MnO_3$ near 60 K and in the presence of a magnetic field of 8 T. These studies led to the obvious conclusion that manganites were a potential alternative for 'giant' MR systems.

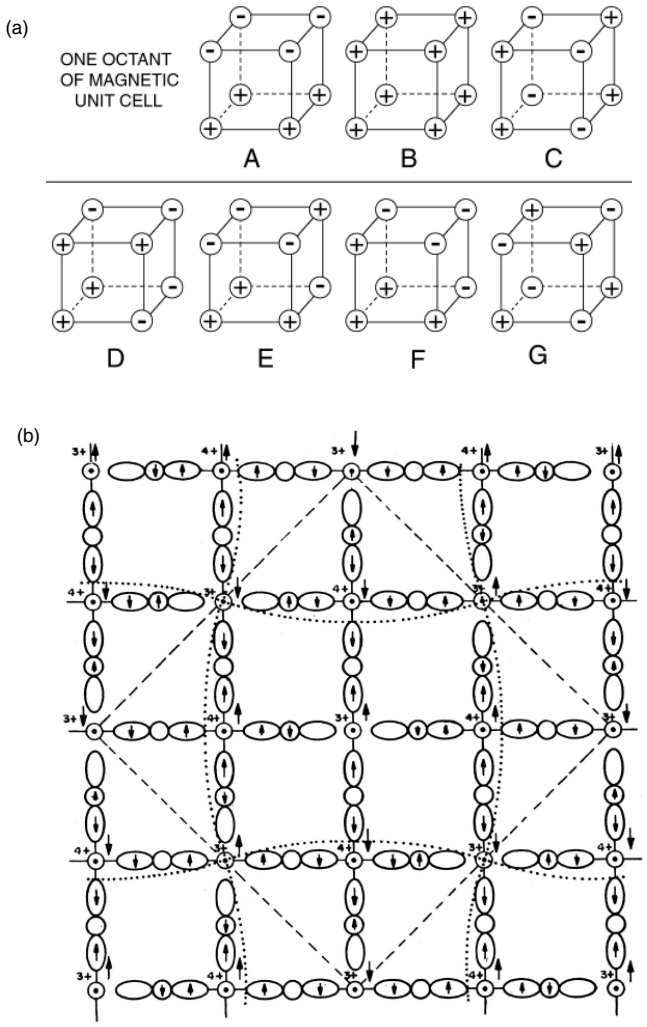

Figure 4. (a) Possible magnetic structures of Mn oxides by Wollan *et al* [55]. The circles are the Mn ions, and the signs the orientation of the z-axis spin projection. For example, A type has planes that are ferromagnetic, with antiferromagnetic coupling between them. The B-type structure is the standard ferromagnetic arrangement, while G type corresponds to an antiferromagnet in all three directions. The C type has antiferromagnetism in two directions, and ferromagnetism along the third. Reprinted figure with permission from [55]. Copyright 1955 by the American Physical Society. (b) Schematic representation of the CE state proposed by Goodenough [63]. This figure shows the spin, charge and orbital order states in Mn oxides. Reprinted figure with permission from [63]. Copyright 1955 by the American Physical Society.

2.2. Salient features of manganites

2.2.1. Crystal structure and its relevance. The characteristic properties of doped perovskite manganites like the CMR effect and the strong correlation between the structure and electronic–magnetic phases can all be attributed to the ratio of the Mn^{3+} and Mn^{4+} ions [50]. The parent compound crystallizes in $AMnO_3$ type perovskite structure having general formula $RE_{1-x}AE_xMnO_3$, where RE stands for a trivalent rare earth cation such as La, Pr, Nd, Sm, Eu, Gd, Tb, Y etc and AE stands for a divalent alkaline earth cation such as Ca, Br, Sr etc. In this perovskite-like structure (RE, AE) occupies the vertices of the cubic unit cell, Mn occupies the body center and O occupies the six faces of the cube, which forms the MnO_6 octahedra (figure 5) [62–64]. The (RE, AE) site (so-called perovskite A site) can in most cases form a homogeneous solid solution. Both the end members $LaMnO_3$ (A type) and $CaMnO_3$ (G type) are antiferromagnetic insulators having single-valent Mn ions, i.e. Mn^{3+} ($3d^4$, $t_{2g}^3e_g^1$) and Mn^{4+} ($3d^3$, $t_{2g}^3e_g^0$) respectively [55]. Partial doping of the trivalent RE ion by divalent alkaline earth cation AE leads to the formation of a mixed valence state of the Mn, i.e. Mn^{3+} and Mn^{4+}, to maintain the charge neutrality of the system [50]. The mixed valence of the Mn ions may also be controlled by varying the oxygen content [65, 66]. This doping with some divalent cation causes the structure to become distorted due to the differences in the size of the various atoms and leads to the Jahn–Teller effect, which is discussed in section 3.1 [67].

Perovskite-based structures occasionally show lattice distortion as modifications from the cubic structure due to doping. One of the possible origins of the lattice distortion is the deformation of the MnO_6 octahedron arising from the Jahn–Teller effect that is inherent to high-spin ($S = 2$) Mn^{3+} with double degeneracy of e_g orbitals. Another lattice deformation comes from the connection pattern of the MnO_6 octahedra in the perovskite structure (tilting of the octahedra), forming rhombohedral or orthorhombic lattices. In these distorted perovskites, the MnO_6 octahedra show alternate buckling [68, 69]. Such a lattice distortion of the perovskite $AMnO_3$ (where $A = RE_{1-x}AE_x$) is governed by the Goldschmidt tolerance factor t [70, 71], which measures the deviation from perfect cubic symmetry ($t = 1$) and is defined as

$$\left[t = \frac{d_{A-O}}{\sqrt{2}d_{Mn-O}} = \frac{\langle r_A \rangle + r_O}{\sqrt{2}\left(\langle r_{Mn} \rangle + r_O\right)} \right],$$

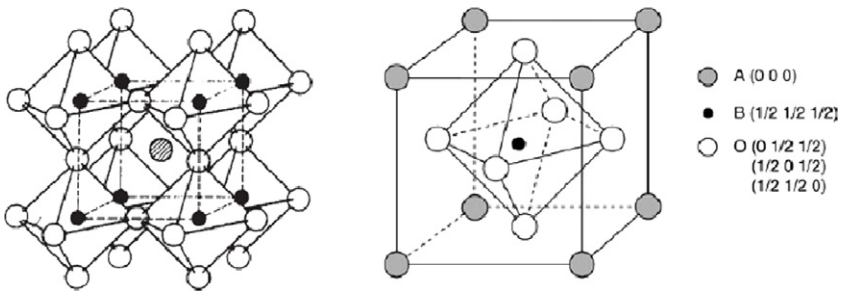

Figure 5. The ideal cubic $LaMnO_3$ perovskite structure (two views), where A = (RE, AE) (RE = trivalent rare earth cation e.g. La, Pr, Nd etc and AE = divalent alkaline cation e.g. Ca, Ba, Sr etc), B = Mn and O = oxygen.

where d_{A-O} is the distance between the A site, where the lanthanide or alkaline earth ions are located, and the nearest oxygen ion, i.e. $(\langle r_A \rangle + r_O)$, and d_{Mn-O} is the Mn–O shortest distance, which are calculated from the sum of the ionic radii for 12-coordinated A-site cations and 6-coordinated Mn cations [72]. However, the tolerance factor is dependent on both temperature and pressure. The A–O bond has a larger thermal expansion coefficient and is normally more compressible than the Mn–O bond of an $AMnO_3$ perovskite, which makes $dt/dT > 0$ and $dt/dP < 0$ [71].

Since for an undistorted cube the Mn–O–Mn bond is straight ($d_{A-O} = \sqrt{2} d_{Mn-O}$), $t = 1$. However, sometimes the A ions are too small to fill the space in the cubic centers, and due to this the oxygens tend to move toward this center, reducing d_{A-O} (d_{Mn-O} also changes at the same time). For this reason, the tolerance factor becomes smaller than one, $t < 1$, as the A-site radius is reduced, and the Mn–O–Mn angle becomes smaller than 180°. Thus as the tolerance factor decreases the tendencies of charge localization increase due to the reduction in the carrier mobility and hence hopping amplitude also decreases between Mn^{3+} and Mn^{4+} [73]. This has been observed experimentally and proved theoretically in doped manganites [74–76]. For the ideal cubic structure $t = 1$, but the stable perovskite structure occurs over a range of $0.89 < t < 1.02$. For lower values of t, the cubic structure is distorted to optimize the A–O bond lengths. For values of t between 0.75 and 0.9, the MnO_6 octahedra tilt cooperatively to give an enlarged orthorhombic unit cell [73]. This distortion (reduction of Mn–O–Mn angle from 180°) affects the conduction band, which appears as hybridization of the p level of the oxygen and the e_g levels of the Mn. The orbital overlap decreases with decrease in tolerance factor and the relation between the bandwidth ω and θ has been estimated as $\omega \propto \cos^2 \theta$ [77].

Hwang *et al* [78] have carried out a detailed study of the structure–property correlation as a function of temperature and tolerance factor t, for the $RE_{0.7}AE_{0.3}MnO_3$ compound for a variety of RE (trivalent rare earth ion) and AE (divalent) ions. The typical relationship is shown in figure 6 and it shows the clear presence of three dominant regions: a paramagnetic insulator at high temperature, a low temperature ferromagnetic metal at large tolerance factor and a low temperature charge-ordered ferromagnetic insulator (FMI) at small tolerance factor. Zhou *et al* [79] have also investigated the influence of the tolerance factor t and differences in the ionic radii of the A-site cations in Curie temperature, resistivity, coercive field and magnetoresistance. They observed that large difference between the ionic radii of the A-site cations is detrimental for magnetotransport properties. In another study Sun *et al* [80] examined a series of compounds at constant 33% doping level $La_{2/3-x}R_xCa_{1/3}MnO_3$ (R = Pr, Nd, S, Eu, Gd, Tb, Y, Er, Tm) with x chosen to be fixed at $t = 0.911$. Under the constraints of constant doping level x and t, the picture developed by Hwang *et al* [79] would predict no variation of the insulator–metal transition temperature (T_{IM}) with rare earth. Sun *et al* did observe a dependence of T_{IM} on the choice of rare earth ion, which demonstrates that a single, average tolerance factor t is inadequate for describing the behavior of perovskite manganites where A-site components have widely different radii. They attributed the discrepancy to an inhomogeneous distribution of cations on the A site [80].

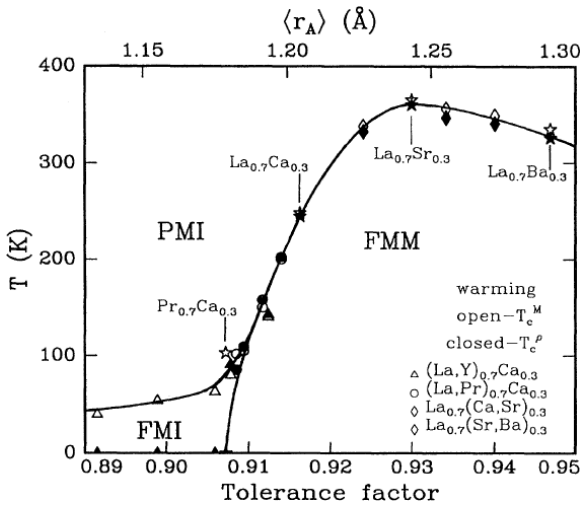

Figure 6. Phase diagram of temperature versus tolerance factor for the system $RE_{0.7}AE_{0.3}MnO_3$, where RE is a trivalent rare earth ion and AE is a divalent alkaline earth ion. Open symbols denote T_c^M measured at 100 Oe. Closed circles denote T_c^ρ. Reprinted figure with permission from [78]. Copyright 1995 by the American Physical Society.

2.2.2. Phase diagram. Phase diagrams of doped perovskite manganites are exceptionally rich with different resistive/magnetic as well as structural phases [81–83]. The phase diagrams that have been established so far for different compounds, e.g. $La_{1-x}Ca_xMnO_3$ (LCMO), $La_{1-x}Ba_xMnO_3$ (LBMO), $La_{1-x}Sr_xMnO_3$ (LSMO) etc, are constructed from detailed measurements of macroscopic physical quantities such as resistivity (ρ), susceptibility (χ) and magnetization (M) on single-crystal and bulk ceramic samples [84, 85]. Even though the phase diagram of each composition is different due to the variation in sizes of different atoms involved, they have some common features [86]. The Ca doped $LaMnO_3$ i.e. $La_{1-x}Ca_xMnO_3$ (LCMO) is the prototype of the intermediate bandwidth mixed-valent perovskite manganite because the ionic size of Ca (∼1.16 Å) is almost identical to the ionic size of La (∼1.18 Å) and thus a true solid solution forms in the entire range of Ca concentration [82]. Furthermore, the structure, unlike other perovskite manganites, remains orthorhombic below ∼700 K in the entire doping concentration. So, $La_{1-x}Ca_xMnO_3$ (LCMO) is a good candidate material for basic understanding and hence its phase diagram has been described in detail.

The first ever magnetic phase diagram for $La_{1-x}Ca_xMnO_3$ as a function of temperature was reported by Schiffer *et al* [84], but the complete phase diagram for $La_{1-x}Ca_xMnO_3$ was given by Cheong and Hwang [85] on the basis of magnetization and resistivity data, as shown in figure 7. Similar phase diagrams have been obtained using thin films [88, 89]. In figure 7 we have shown the phase diagram of intermediate bandwidth manganite i.e. $La_{1-x}Ca_xMnO_3$. At high temperature (>275 K), for all doping levels, the system

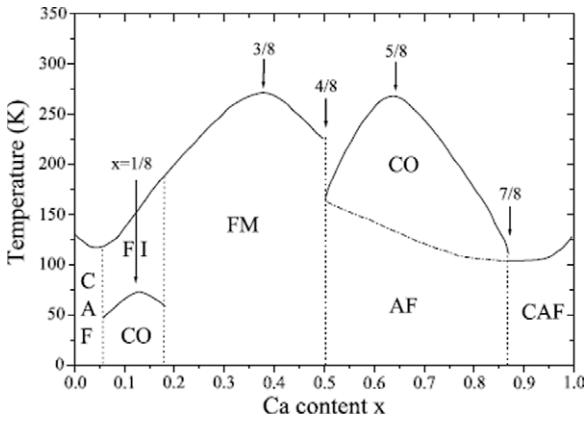

Figure 7. Phase diagram of $La_{1-x}Ca_xMnO_3$, constructed from measurements of macroscopic quantities such as the resistivity and magnetic susceptibility. PI, paramagnetic insulator; FM, ferromagnetic metal; FI, ferromagnetic insulator; AF, antiferromagnetism; CAF, canted antiferromagnet; CO, charge/orbital order. The ferromagnetic–insulating and canted antiferromagnetic states could be spatially inhomogeneous states with ferromagnetic and antiferromagnetic coexistence. Reprinted figure with permission from [85].

is a paramagnetic insulator (PI). At low temperature, LCMO undergoes the following transitions: the end compositions $LaMnO_3$ ($x = 0$) and $CaMnO_3$ ($x = 1$) are insulators at all temperatures and canted antiferromagnetic insulators at low temperature. For $x = 0.175$, a complicated regime with FI (ferromagnetic insulator), CO (charge-ordered) and CAF (canted antiferromagnetic) phases has been realized. On further Ca substitution from 0.175 to 0.50, the regime of CMR effect has been found. In this region, the material undergoes an insulator–metal transition, T_{IM}, which is usually very close to the paramagnetic–ferromagnetic transition, T_c. Close to $x = 0.5$, where the Mn^{4+} to Mn^{3+} ratio is about 1:1, a charge-ordered antiferromagnetic insulating phase starts to evolve at low temperature. This phase has been observed up to 87% of Ca, beyond which a canted antiferromagnetic regime (mixture of ferromagnetic and antiferromagnetic regions) exists. Thus the phase diagram of $La_{1-x}Ca_xMnO_3$ consists of various phases such as canted antiferromagnetic, charge ordered, ferromagnetic metallic, paramagnetic insulating and others, which makes the physics of manganites interesting and challenging [84, 85].

As can be seen from the phase diagram in figure 7, there are well defined special features at the commensurate Ca concentration of $x = N/8$ ($N = 1, 3, 4, 5$ and 7) [85]. At $x = 3/8$ (0.375), T_c becomes maximum whereas T_{CO} peaks at $x = 5/8$ (0.625). The compound at the phase boundary with $x = 4/8$ (0.5) undergoes first a ferromagnetic transition and then a simultaneous antiferromagnetic and charge ordering transition at low temperature. The system at $x = 1/8$ concentration also undergoes two transitions, first a ferromagnetic transition and then an antiferromagnetic transition accompanied by a charge ordering transition. There is another well defined phase boundary at $x = 7/8$ (0.875), and a magnetic transition with a significant ferromagnetic moment is observed for $x > 7/8$. The phase diagram also shows that there exists pronounced electron–hole symmetry in the ground state properties of $(La, Ca)MnO_3$. First of all, the ground state is a ferromagnetic metal for the hole concentration of $1/8 < x < 4/8$, but the electron concentration $1/8 < x < 4/8$ shows charge ordering at low temperatures. Furthermore, at the carrier concentration of $0 < x < 1/8$, ferromagnetism is much more pronounced for the hole carrier as compared to the electron carrier. In general, holes in LCMO tend to induce metallicity along with ferromagnetism at low temperatures, while electron carriers are susceptible to charge ordering. These anomalies at the commensurate concentrations clearly indicate the importance of electron–lattice coupling (which induces charge localization) in the mixed-valent manganites [90, 91].

Another important manganite, $La_{1-x}Sr_xMnO_3$ (LSMO), is widely studied as a representative of large bandwidth Mn oxides and has a high Curie temperature of 370 K at intermediate hole doping [92]. In the LSMO compound a structural transition from orthorhombic ($x > 20\%$) to rhombohedral ($x < 20\%$) is present [81]. However, the structural phase diagram is even more rich [82, 83]. In general, the orthorhombic phase is stable at lower temperatures, while the rhombohedral phase requires higher temperature. Thus, depending on the doping, one can obtain ferromagnetic or antiferromagnetic metallic phases, as well as antiferromagnetic insulating phases. Ferromagnetic insulators are less common, since the occurrence of ferromagnetism is associated with the movement of free carriers in the lattice, but can be obtained for some partial orbital ordering cases [93, 94]. A large amount of theoretical as well as experimental work has been devoted to disclosing the orbital effects on the magnetic phases of CMR manganites [95]. There are differences in the phase diagram for different manganites, e.g. $La_{1-x}Ca_xMnO_3$ [84, 85], $La_{1-x}Sr_xMnO_3$ [92, 96], $Pr_{1-x}Ca_xMnO_3$ [87], $Nd_{1-x}Sr_xMnO_3$ [97] etc; however, in general they have some common features.

3. The known mechanisms: their salient features and inadequacies

3.1. Crystal field splitting and Jahn–Teller effect

The physical properties of the doped perovskite manganite ($LaMnO_3$) involve a complex interplay between the spin, charge, orbital and lattice degrees of freedom, which strongly depend on the site of occupancy of the d orbitals. The basic building blocks of the manganites are the MnO_6 octahedra. In the cubic environment of the MnO_6 octahedron, hybridization and electrostatic interaction with oxygen 2p electrons will create a crystal field for the outer 3d electrons in Mn^{3+}. As the d orbitals are fivefold degenerate (figure 8), this crystal field lifts the fivefold degeneracy of d electrons present in free Mn^{3+} ions by splitting the energy levels and forming lower lying triply degenerate t_{2g} states and higher doublet e_g states [98]. The low lying t_{2g} triplet consists of the d_{xy}, d_{yz} and d_{zx} orbitals. These orbitals have lobes oriented between the O^{2-} ions. The higher energy e_g doublet consists of the $d_{x^2-y^2}$ and $d_{3z^2-r^2}$ orbitals. Their lobes point in the directions of the O^{2-} ions, which raises their energy because of the stronger Coulombic repulsion of

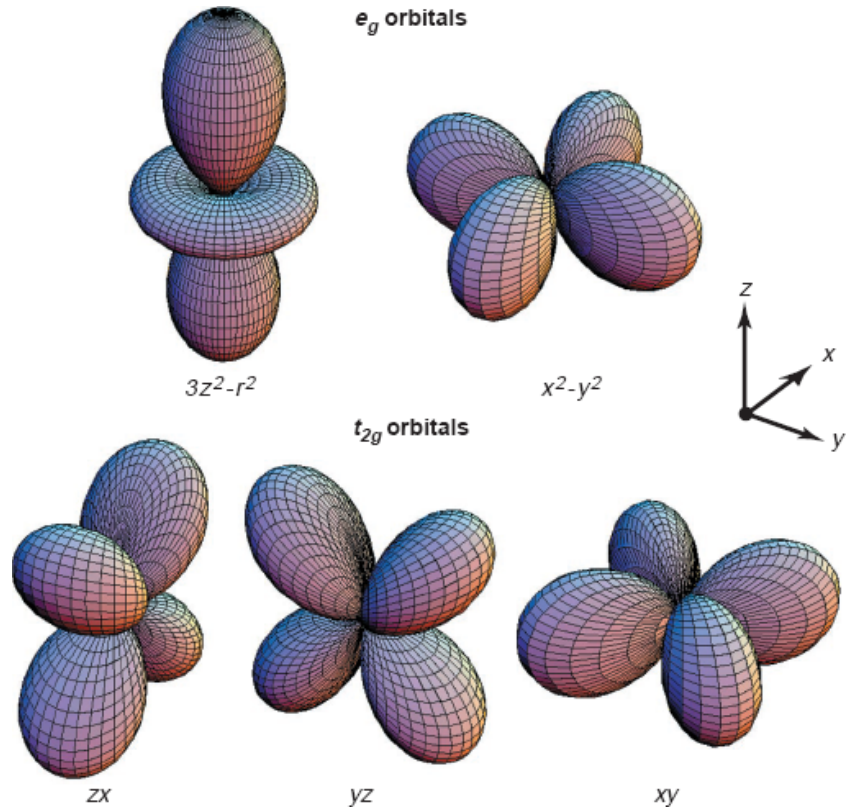

Figure 8. Five d orbitals. In the cubic crystal field, this fivefold degeneracy is lifted to two e_g orbitals ($(x_2 - y_2)$ and $(3z_2 - r_2)$) and three t_{2g} orbitals ((xy), (yz) and (zx)) from [168]. Reprinted figure with permission from AAAS.

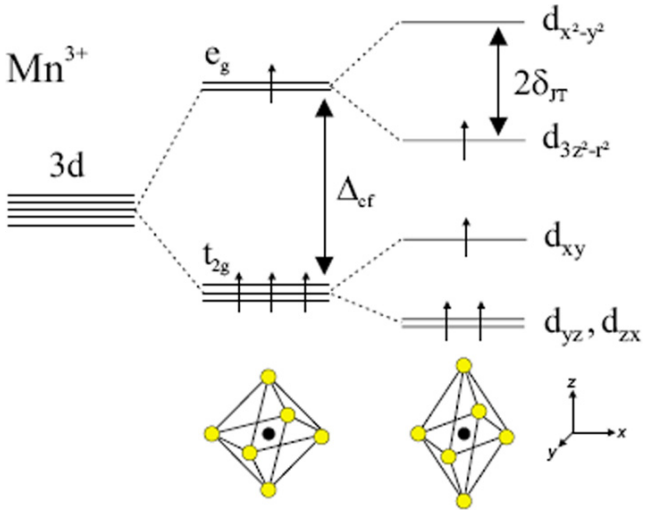

Figure 9. Lifting of the degeneracy of 3d orbitals in Mn^{3+} ions by the Jahn–Teller distortion. The crystal field splitting (CFS), Δ_{cf}, is around 1.5 eV, while the energy difference $2\delta_{JT}$ between the e_g states is about 1 eV [7].

the MnO_6 octahedra in doped $LaMnO_3$. The energy difference due to crystal field splitting (CFS) between t_{2g} and e_g levels for $LaMnO_3$ is approximately 1.5 eV (figure 9) [99]. Due to strong intra-atomic Hund's coupling, all electrons of Mn^{3+} and Mn^{4+} are aligned parallel in the ground state, leading to a total spin of $S = 2$ and $S = 3/2$, respectively. All three outer electrons of Mn^{4+} occupy the t_{2g} sites, while the extra electron of Mn^{3+} is situated in one of the e_g levels. The t_{2g} orbitals overlap relatively little with the p orbitals of nearby oxygen atoms, so that the t_{2g} electrons can be considered as forming a localized core spin ($s = 3/2$). The e_g orbitals on the other hand overlap with the p orbitals of neighboring oxygen atoms. Although strongly coupled ferromagnetically to the t_{2g} spin, the e_g electron ($s = 1/2$) is more mobile and can hop between different Mn ions. Thus the partial degeneracy of the 3d orbitals has been removed by CFS. The remaining degeneracy is usually broken by the lattice motion. The oxygen ions surrounding the Mn^{3+} ions can slightly readjust their locations, creating an asymmetry between the different directions that effectively removes the degeneracy. This lifting of degeneracy due to the orbital–lattice interaction is named as the Jahn–Teller distortion/effect. This effect tends to occur spontaneously because the energy penalization of the lattice distortion grows as the square of this distortion, while the energy splitting of the otherwise degenerate orbitals is linear. For this reason, it is energetically favorable to spontaneously distort the lattice, thus removing the degeneracy. As far as manganites are concerned there are 21 degrees of freedom (modes of vibration) for the movement of oxygen and Mn ions [100]. Out of these only two types of distortion (modes of vibrations) are relevant for the splitting of the e_g doublet, i.e. JT distortion: Q_2 and Q_3 [101], which are shown in figure 10. Q_3 is a tetragonal distortion, which results in elongation or contraction of MnO_6 octahedra. However, in the case of manganites the effective distortion is the basal plane distortion (called the Q_2 mode) in which one diagonally opposite O pair is displaced outwards and the other pair

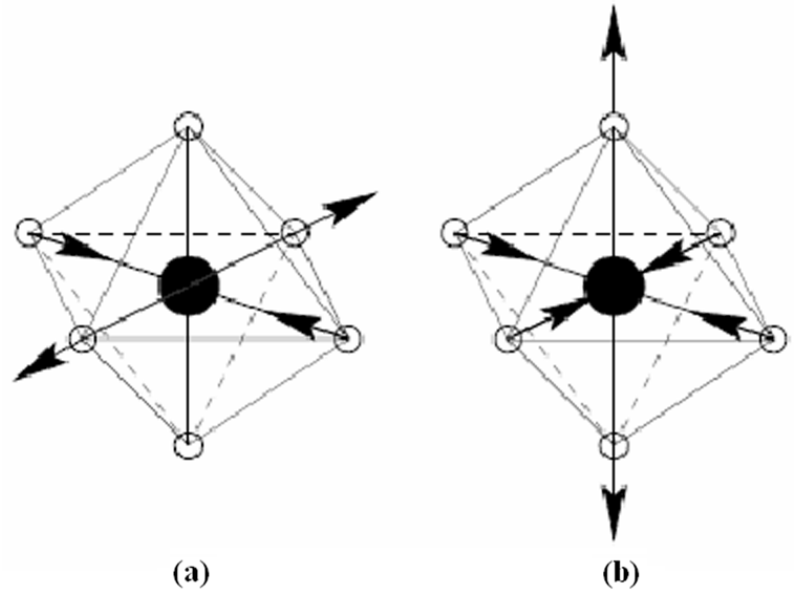

Figure 10. The relevant modes of vibration are (a) Q_2 and (b) Q_3 for the splitting of the e_g doublet (Jahn–Teller distortion) [7].

displaced inward. As Mn^{4+} does not have an electron in the e_g states, it will not act as a JT ion.

Lattice distortion of the octahedral can be static or dynamic. When the carriers have a certain mobility, the distribution of Mn^{3+} and Mn^{4+} ions is random and changes with time. Therefore, electron–phonon coupling arises and, in fact, Millis *et al* [102] and Roder *et al* [103] have claimed that it is necessary to take account of the lattice vibrations to explain the change in curvature of the resistivity close to T_C. Moreover, due to the large Hund's coupling, magnetic polarons can be formed [104]. The localization of the carrier in lattice and/or magnetic polarons can explain the activated behavior of the resistivity for $T > T_C$ [89]. When the bandwidth is narrow, the localization induced by lattice deformations is very relevant and leads to charge/orbital ordering and stripe formation [93, 94, 105].

3.2. Double exchange and related effects

Soon after Jonker and Santen [50, 51] discovered the strong correlation between ferromagnetism and metallic conductivity in doped manganites, Zener [62] proposed a qualitative explanation that remains at the core of our understanding (of simultaneous ferromagnetic–paramagnetic and metal–insulator transition) in manganites even today.

Zener interpreted ferromagnetism as arising from an indirect coupling between 'incomplete d shells' of Mn^{+3} and Mn^{4+} via 'conducting electrons' of oxygen, as shown in figure 11. Zener pointed out that on doping with a divalent ion at a rare earth site, i.e. $RE_{1-x}AE_xMnO_3$, the Mn ions become mixed valent, with Mn fraction x in the tetravalent Mn^{4+} ($3d^3$, $t_{2g}^3e_g^0$, $S = 3/2$) and $1 - x$ in the trivalent Mn^{3+} ($3d^4$, $t_g^3e_g^1$, $S = 2$) state, which forms a cluster comprising oxygen and two Mn ions i.e. Mn^{3+} and Mn^{4+}. The basic idea of double exchange is that the initial state φ_1 (Mn^{3+}–O–Mn^{4+})

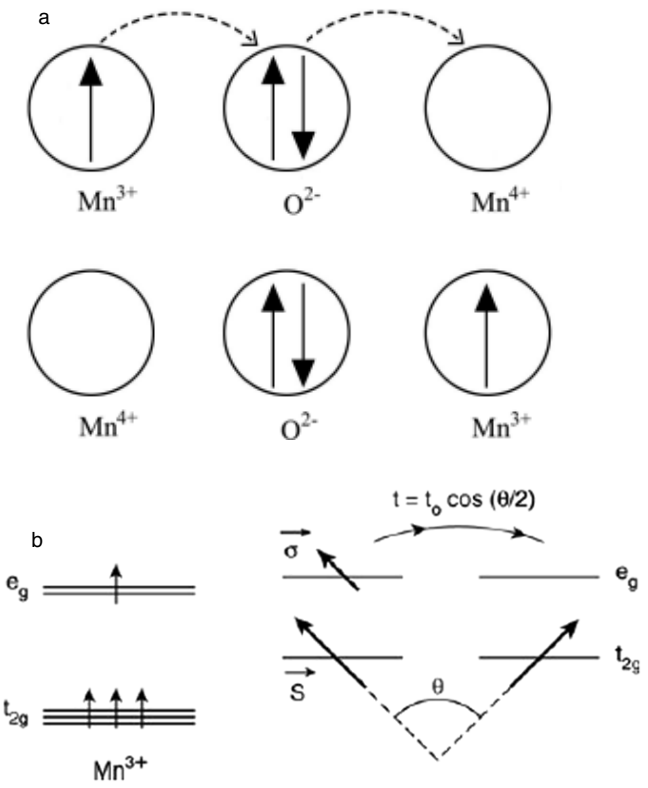

Figure 11. (a) Schematic representation of the double exchange mechanism proposed by Zener; (b) sketch of de Gennes spin-canted states.

and final state φ_2 (Mn^{4+}–O–Mn^{3+}) are degenerate, leading to a delocalization of the hole on the Mn^{4+} site or electron on the Mn^{3+} site. Thus the transfer of an electron occurs simultaneously from Mn^{3+} to O^{2-} and from O^{2-} to Mn^{4+}; this process is a real charge transfer process and involves an overlap integral between Mn 3d and O 2p orbitals. Because

of strong Hund's rule coupling, the transfer-matrix element has finite value only when the core spins of the Mn ions are aligned ferromagnetically. The Hund's rule coupling of degenerate states lifts the degeneracy and the system resonates between φ_1 and φ_2 if the core spins are parallel, leading to simultaneous occurrence of metallicity and ferromagnetism. Zener's model was based on the assumption that the manganites are uniform and homogeneous without any form of coexisting clusters of competitive phases.

Anderson and Hasegawa [106] modified Zener's model by treating the core spin (t_{2g}) of each Mn ion classically and the mobile electron (e_g) quantum mechanically. They showed that electron transfer between neighboring Mn ions depends on the angle between their magnetic moments as $t_{\text{eff}} = t\cos(\theta/2)$. The transfer probability varies from 1 for $\theta = 0$ to zero for $\theta = 180°$ and the exchange energy is lower when the itinerant electron's (e_g) spin is parallel to the total spin of the Mn cores. Further, de Gennes [107] in a mean field type description revisited the problem, treating the effect of double exchange in the presence of antiferromagnetic background. He formulated the DE problem for a lattice and derived a band model for the motion of holes. de Gennes considered a layered material with N magnetic ions per unit volume, each spin S coupled ferromagnetically to its Z' neighbour on the same layer with exchange energy J' and antiferromagnetically to Z neighbours on adjacent layers with energy J. de Gennes predicted that at low doping level an antiferromagnetic superexchange interaction competes with the ferromagnetic DE interaction, which leads to a spin-canted state. However, recent studies have shown that a strong alternative to canted states is provided by the tendency to phase separation. de Gennes further considered localization and self-trapping of charge carriers, which gives rise to local distortion of the spin lattice, i.e. the concept of the magnetic polaron [108]. Another pioneer theoretical study in manganites was carried out by Goodenough [109] regarding the charge, orbital and spin arrangements in the non-ferromagnetic regime of the phase diagram of LCMO [52]. The approach of Goodenough was based on the notions of 'semicovalent bond' and elastic energy considerations. A semicovalent bond or semicovalency arises when the overlap of spin-polarized sp orbitals of Mn ions with occupied orbitals of the oxygen allows only covalent bonds involving electrons of one spin direction [109].

Kubo and Ohata [110] considered a fully quantum mechanical approach employing mean field theory for metallic double exchange ferromagnets. They calculated a magnetic phase diagram, resistivity and the magnetoresistance. Their results show a ferro-to-paramagnetic transition at T_c, accompanied by a change in the temperature dependence of resistivity, and diverging magnetoresistance at T_c. They have calculated low temperature resistivity due to second order electron–magnon process and found that resistivity is proportional to $T^{9/2}$. However, neither the predicted low temperature resistivity dependence nor the constant resistivity above T_c agree with the experiments. Further, Furukawa [111, 112] proposed an unconventional one-magnon scattering process in manganites using the dynamical mean field theory and found that the low temperature resistivity follows a T^3 power law.

3.3. Electron–phonon coupling and subsequent theories

The double-exchange [62] and subsequent theories by Anderson–Hasegawa [106], de Gennes [107] and Goodenough [108] only explain the transport properties of manganites qualitatively. They overestimate the Curie temperature of most manganites, cannot describe the huge magnitude of the CMR effect, underestimate the resistivity values in the paramagnetic phase by several orders and cannot account for the existence of various antiferromagnetic phases, charge/orbital ordering, phase separation scenario and strong lattice effects/anomalies seen experimentally due to their inherent limitations. Millis *et al* [102] invoke the idea that double exchange alone does not explain the resistivity of $La_{1-x}Sr_xMnO_3$. Their argument hinges mainly on an estimate of the Curie temperature in a pure double-exchange model, which turns out to be an order of magnitude larger. Moreover, Millis *et al* calculated the resistivity within the double-exchange model including spin fluctuations and found that resistivity decreases below T_c and a positive magnetoresistance above T_c, both features in contradiction to the experimental results. Millis *et al* argued that the electron–phonon coupling due to the dynamic Jahn–Teller distortion plays an important role, and that a strong interplay between electron–phonon coupling, including charge localization, and Hund's coupling, generating a FM metallic phase, is responsible for the observed properties of manganites [113, 119, 120]. The strong e–ph coupling in manganites is mainly caused by the Jahn–Teller effect of Mn^{3+}. The JT effect causes local distortion of the crystal structure in which some of the Mn–O bonds become shorter and other longer. This breaks the local cubic symmetry and splits the degeneracy of the e_g levels on this site. By occupying the orbital with the lowest energy, the e_g electron can become effectively self-trapped to form together with the surrounding deformed lattice a quasiparticle called a lattice polaron or Jahn–Teller polaron. This transport of lattice and spin distortions is also called a magnetic polaron. Calculations by Millis *et al* [104, 113–115] predict the localization of charge carriers by temporal and spatial JT distortions around and above T_c. This would lead to the observed activated resistivity behavior in the paramagnetic phase. Below T_c, the self-trapping of carriers ends, leading to a relaxation of the lattice and an enhancement of the conductivity. In this theory both JT coupling and DE are needed to explain the properties in the various magnetic phases. This leads to the prediction of lower more correct T_c values, and can explain the high resistivity and large CMR effect in manganites. The work of Millis *et al* marked a new stage in the study of the CMR manganites by making use of the concept of static and dynamic JT instabilities [116–118]. Several recent experimental observations, such as resistivity [119], thermoelectric power [120, 121], Hall effect [122], low temperature optical conductivity [123, 124], mobility [125], neutron scattering [126], volume thermal expansion [127], a large nuclear magnetic resonance [128], isotope effect [129], electron energy loss spectroscopy [130], photoemission spectroscopy [131], x-ray absorption fine structure

spectroscopy [132] and Raman scattering [133], clearly indicate that self-trapping of a charge carrier as a small polaron in doped perovskite manganites above T_c due to Jahn–Teller-induced electron phonon coupling should be taken into account to explain the distinctive properties of perovskite manganites.

Roder *et al* [103, 134] incorporated Jahn–Teller (electron–phonon) coupling into the double-exchange model and suggested that the e_g charge carrier becomes self-trapped as localized lattice distortions with a spin polarization around the position of the charge carrier, having a coherence length of the order of five Mn sites. These quasi-self-trapped small polarons can therefore be called magnetoelastic polarons, since they are associated with spin clusters and essentially form metallic islands in a paramagnetic lattice. Ample experimental evidence regarding the existence of magnetic polarons has been reported. It has been demonstrated by neutron diffraction that for both perovskite [76] and layered manganites [135] a volume reduction and relaxation of the lattice is observed as the temperature decreases below T_c. This is due to change in the Mn–O bonds and indicates the existence of localized e_g electrons above T_c, which become delocalized in the ferromagnetic phase [136].

The close agreement between the theoretical predictions and the experimental evidence strongly indicates that the lattice effects in CMR materials are caused by the existence of small magnetic Jahn–Teller polarons above T_c and 'melting' of these entities below T_c. In this theoretical picture, the properties of manganites like the value of T_c, the magnitude of the CMR effect and whether the ground state becomes metallic or stays insulating depend on the relative strength of DE mechanism and the electron–phonon coupling, which is determined mainly by the nominal hole concentration x. There are various other theories/models, e.g. the vibronic model of Goodenough [137], the bi-polaronic model of Alexandrov [108, 138] and the magnetoimpurity theory of Nagaev [139], that explain some aspect or other of doped perovskite manganites. Recently, Ramakrishnan and co-workers [140] have proposed a theory for doped manganites where they argued that due to strong JT interactions the doubly degenerate e_g electrons dynamically reorganize themselves into two types of coexisting electron fluid. The majority of the electrons (labeled l) become localized polarons, trapped by large local JT distortions exponentially, with reduced intersite hopping, and a minority of them (labeled b) can remain mobile and non-polaronic, with no associated lattice distortions, and undiminished hopping amplitudes. A virtual adiabatic transition to empty neighboring sites induces a ferromagnetic exchange referred to as virtual double exchange in doped manganites. The resulting Falicov–Kimball type, lb model Hamiltonian in a simple dynamical mean field treatment in the framework of an 'orbital liquid' description gave a good account of the distinctive properties of these doped manganites.

Very recently, Mannella *et al* [141] describe the electronic properties (Fermi surface) of manganites, revealing that the interaction of electrons and lattice vibrations (phonons) is crucial and should be taken into account to explain their distinctive properties. They carried out ARPES of the low temperature ferromagnetic–metallic ground state of $La_{1.2}Sr_{1.8}Mn_2O_7$ (LSMO). Their results indicate that the spectral weight of LSMO is too small. In addition, they have also found that the measured energy spectrum is not isotropic, but depends strongly on the direction of electron propagation. The electron propagates readily in a direction that is diagonal to the square lattice of the Mn atom but poorly along the axes of the lattice. The reduced spectral weight and the velocity seem to imply that, even in the metallic state, in which conduction electrons supposedly move freely throughout the lattice, electrons and phonons are interdependent. The nested shape of the Fermi surface (having large parts that are nearly parallel) itself provides strong evidence of electron–phonon coupling. Nesting provides a channel through which an electron can be scattered between different parts of the Fermi surface. The scattering centers are phonons in the present LSMO case and they could also be magnetic fluctuations. Thus scattering reduces the electronic spectral weight around the Fermi energy and induces a gap in the energy spectrum, which is very similar to the 'pseudogap' observed in high temperature cuprate superconductors. Thus, Mannella *et al* confirmed that in manganites the electron–phonon coupling is an essential microscopic ingredient.

3.4. Ordering phenomenon

A fascinating phenomenon of charge ordering (CO) is found to occur in various transition metal oxides (TMOs) wherein electrons become localized due to ordering of cations of different charges (oxidation states) on specific lattice sites. Such ordering generally localizes the electrons in the material, rendering it insulating or semiconducting. This phenomenon of charge ordering (CO) is well known in Fe_3O_4 (magnetite), which undergoes a disorder–order transition accompanied by a resistivity anomaly, popularly known as the Verwey transition, at 120 K [142, 143]. Charge ordering (CO) has been found to occur in a few other TMOs [144, 145] as well, but the evidence of CO in doped rare earth manganites is overwhelming due to the discovery of colossal magnetoresistance and other interesting properties [7]. The first evidence of CO in doped manganites was observed by Wollan and Koehler [55] through neutron diffraction and latter examined by Jirak *et al* [146]. The phase diagram of $La_{1-x}Ca_xMnO_3$ (figure 7) depicts well defined features at the commensurate carrier concentration (Ca) of $x = N/8$ ($N = 1$, 3, 4, 5 and 7) [84, 85]. CMR has been observed for Ca concentration x of $\sim$1/8–4/8. For the high doping range with $x \geqslant 4/8$, the doped charge carriers localize and order with stripe modulation at low temperatures along with antiferromagnetic ordering [109, 147–149].

The general tendency of charge carrier localization and ordering in doped Mott insulators [85, 150] is particularly strong in doped manganites, due to the relatively enhanced (electron/hole) carrier–lattice coupling. In addition, there exists an orbital degree of freedom of the e_g electrons in Mn^{3+} ions. This orbital ordering can lower the electronic energy through the Jahn–Teller mechanism. Therefore, there exists orbital ordering (OO) in addition to charge ordering in mixed-valent manganites. The first direct evidence of charge ordering in $La_{0.5}Ca_{0.5}MnO_3$ ($T_c \approx 220$ K) was provided by electron

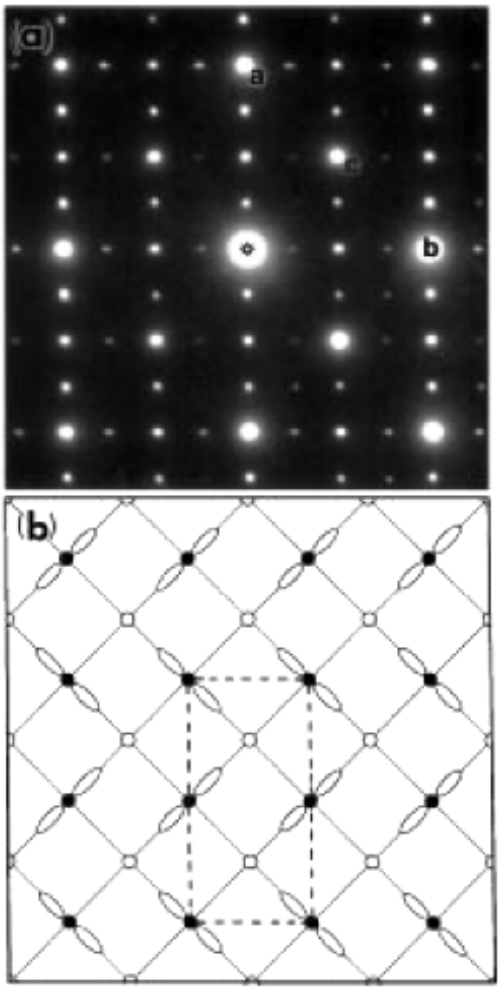

Figure 12. (a) [001] zone-axis electron diffraction pattern obtained at 95 K. The fundamental Bragg peaks labeled a, b and c can be indexed as (200), (020) and (110), respectively. The presence of superlattice spots with modulation wavevector (1/2, 0, 0) or (0, 1/2, 0) is evident. Kinematically forbidden (100) and (010) spots also appear as a result of multiple scattering. (b) Schematic charge ordering picture of Mn^{4+} and Mn^{3+} ions. Open and closed circles represent Mn^{4+} and Mn^{3+} ions, respectively. The orientational order of d_z^2 orbitals of Mn^{3+} ions, which results in the cell doubling along the a axis, is also indicated. Reprinted figure with permission from [149]. Copyright 1996 by the American Physical Society.

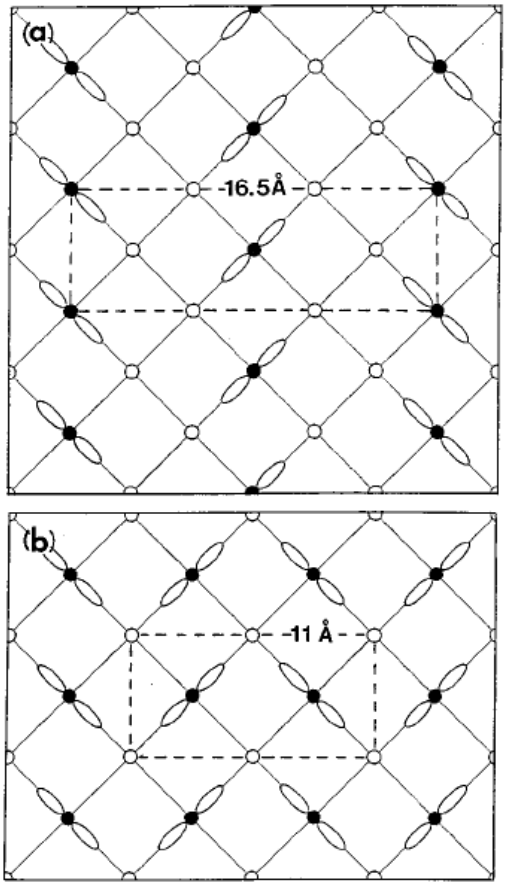

Figure 13. (a) Schematic real space charge ordering picture of Mn^{4+} (open circles) and Mn^{3+} (closed circles) ions for the 16.5 Å diagonal stripes appearing in the $x = 0.67$ sample. The orientational order of d_z^2 orbitals of Mn^{3+} ions is also indicated. For comparison, a similar schematic diagram for the sample of $x = 0.5$ is shown in (b), which demonstrates 11 Å periodic stripes. Dashed lines in (a) and (b) indicate the unit cell of the superlattice. Reprinted figure with permission from [149]. Copyright 1997 by the American Institute of Physics.

diffraction studies reported by Chen and Cheong as shown in figure 12 [149]. Close to the onset of antiferromagnetism, quasi-commensurate satellite reflections were observed, with a modulation wavevector $2\pi/a$ $(1/2 - \epsilon, 0, 0)$. They interpreted these reflections as a result from the coherent ordering of $Mn^{3+}O_6$ and $Mn^{4+}O_6$ octahedra, as expected for a charge-ordered phase. Radaelli *et al* [151] reported a detailed synchrotron x-ray and neutron diffraction investigation of 50% Ca doped $LaMnO_3$. They observed weak satellite reflections in the x-ray diffraction pattern, which was consistent with that of Chen and Cheong [149]. In $La_{1/3}Ca_{2/3}MnO_3$, there are twice as many Mn^{4+} ($3d^3$) ions as Mn^{3+} ($3d^4$) ions, and the ordering of diagonal rows of Mn^{4+} and Mn^{3+} ions plus the orientational ordering of the d_z^2 orbitals in Mn^{3+} gives rise to the striped pattern as shown in figure 13. In figure 13(a), diagonal charge stripes are evident, and their periodicity is ∼16.5 Å. These ∼16.5 Å charge stripes from the pattern in the real space image (figure 14) [152] are obtained from electron microscopy for $x = 2/3$. Shown in figure 13(b) is the similar charge/orbital ordering scheme for $x = 0.5$, where there are just as many Mn^{4+} ions as Mn^{3+} ions. In this case, the diagonal charge stripes adopt a wavevector $\delta = 0.5$ with a spacing of ∼11 Å.

Mori *et al* [152] have reported a different pattern of charge localization in the charge-ordered phase of $La_{1-x}Ca_xMnO_3$ ($x \geqslant 0.5$), employing transmission electron microscopy at 95 K (figure 14). They observed extremely stable pairs of $Mn^{3+}O_6$ stripes, with associated large lattice contraction (due to the Jahn–Teller effect), separated periodically by stripes of non-distorted $Mn^{4+}O_6$ octahedra. These periodicities, which adopt integer values between two and five times the lattice parameter of the orthorhombic unit cell, corresponds to the commensurate carrier concentrations of $x = 1/2$, $2/3$, $3/4$ and $4/5$; for other values of x, the pattern of charge ordering is a mixture of the two adjacent commensurate configurations. These paired Jahn–Teller stripes appear

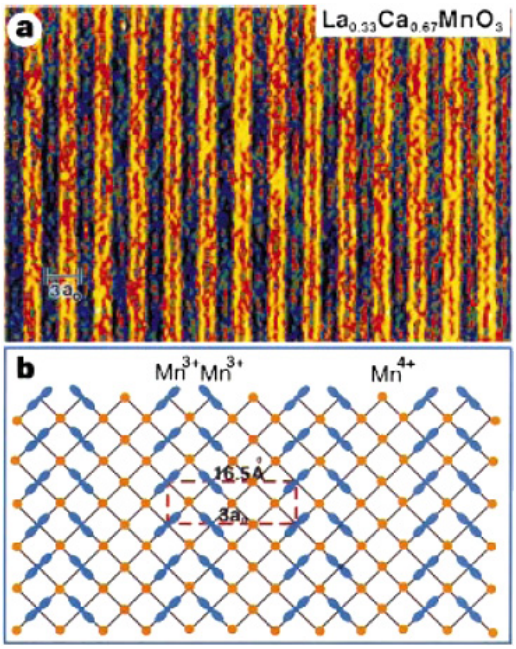

Figure 14. Pairing of charge-ordered stripes in $La_{0.33}Ca_{0.67}MnO_3$. (a) High resolution lattice image obtained at 95 K showing $3a_0$ pairing of the JTS. (b) Schematic model in the *a*–*b* plane showing the pairing and orbital ordering of the Mn^{3+} JTS in blue, and the Mn^{4+} in orange [152]. Reprinted with permission from Macmillan (*Nature*), copyright 1998.

therefore to be the fundamental building blocks of the charge-ordered state in the manganites. The charges ordering in manganites have been accompanied by an increase in sound velocity, change in lattice parameters and anomalies in heat capacity, magnetization, resistivity and the activation energy for conduction. These orbital/charge orders can readily be melted to the ferromagnetic metallic state by application of various impulses such as magnetic field [153], pressure [154], exposure to x-ray photons [155], high voltage (250–700 V) [156], electric field [157] and visible–IR light laser pulses [158].

Charge ordering (CO) similar to that found in $La_{0.5}Ca_{0.5}MnO_3$ has been reported for $Nd_{0.5}Sr_{0.5}MnO_3$ [159] and $Pr_{0.5}Ca_{0.5}MnO_3$ [145]. Both these compounds exhibit the CE-antiferromagnetic structure. However, not all $RE_{0.5}AE_{0.5}MnO_3$ compounds exhibit charge ordering behavior. For example, $Pr_{0.5}Sr_{0.5}MnO_3$ [160] has a A-type antiferromagnetic insulating ground state. It has also been demonstrated that equal numbers of Mn^{3+} and Mn^{4+} are not a prerequisite to charge-ordered behavior. $Pr_{0.7}Ca_{0.3}MnO_3$ has also been reported to exhibit the CE-type antiferromagnetic structure, suggesting a similar charge ordering as in $La_{0.5}Ca_{0.5}MnO_3$ [106]. Rao *et al* [105] have carried out detailed investigations on the effect of average radius of the A-site cations $\langle r_A \rangle$ on CO properties and concluded that T_{CO} (charge ordering temperature) increases with decrease in $\langle r_A \rangle$. The phenomenon of charge/orbital ordering in manganites is very interesting and relevant to explain various peculiar properties such as colossal magnetoresistance and phase separation [105, 161–163]. Recently, Loudon *et al* [164] have observed the CO–FM phase in $La_{0.5}Ca_{0.5}MnO_3$ employing Lorentz electron microscopy at 90 K. They observed an inhomogeneous mixture of ferromagnetic ($3.4 \pm 0.2\mu_B$ per μ_N) and antiferromagnetic (zero-moment) regions, which extend for several micrometers, and can span several crystallographic grains. Loudon *et al* have suggested that CO occurs not only in regions with no net magnetization, but can also occur in ferromagnetic regions; this is consistent with the similar coexistence in $La_{0.25}Pr_{0.375}Ca_{0.375}MnO_3$, as observed by Mori *et al* [165]. Recently Sagdeo *et al* [166] have given evidence of room temperature charge ordering in $La_{1-x}Ca_xMnO_3$ ($0.55 < x < 0.67$) through electron diffraction. In another study, Cepas *et al* [167] have given a few model calculations on CO in manganites by extending the *lb* model of Ramakrishnan *et al* [140]. They discuss the phase diagram of the two-orbital model of half-doped manganites by calculating self-consistently the Jahn–Teller (JT) distortion patterns, charge, orbital and magnetic order at zero temperature. They analyze the instabilities of these phases caused by electron or hole doping away from half-doping, or by the application of a magnetic field. For the CE insulating phase of half-doped manganites, in the intermediate JT coupling regime, they have shown competition between canting of spins (which promotes mobile carriers) and polaronic self-trapping of carriers by JT defects. By studying the properties of electronic excitations coupled with JT distortion, they suggest the incipient instabilities of the CE phase indicative of the doping- and magnetic-field-induced phase transitions, as well as the presence of localized and mobile carriers. Tendeloo *et al* (2004) have extensively reviewed the structure and microstructural aspects of colossal magnetoresistive materials with special reference to charge ordering [69].

3.5. Phase separation (PS) scenario

The physics of solids with strongly correlated electrons such as transition metal oxides (TMOs) [1, 168] and related compounds such as doped manganites [169–173], cuprates [174] and cobaltates [175] appears to be dominated by states that are microscopically and intrinsically inhomogeneous in the most interesting range of temperatures and charge carrier (hole and electron) densities. The most relevant examples are the cuprates at the hole densities in the underdoped region and the manganites in the regime of colossal magnetoresistance (CMR). In cuprates the competition occurs between antiferromagnetic insulating and superconducting or metallic phases [174]. On the other hand, in manganites the inhomogeneities arise from phase competition between ferromagnetic metallic and charge-ordered insulating phases. These microscopic and intrinsic inhomogeneities lead to phase separation (PS) in manganites [169–173]. Indeed, the existence of phase separation (PS) was envisioned by Nagaev [176] in an antiferromagnetic semiconductor, where the doping of electrons is expected to create a ferromagnetic phase embedded in an antiferromagnetic matrix. Nagaev [177] remarked that if the two phases have opposite charge the coulomb forces would break the macroscopic clusters into microscopic ones, typically of nanometer scale size. Percolative transport has been considered to result from the coexistence of ferromagnetic metal-

lic and insulating phases. The tendency of PS is entirely reversible, and is generally the result of a competition between charge localization and delocalization, the two situations being associated with contrasting electronic and magnetic properties. An interesting feature of PS is that it covers a wide range of length scales anywhere between 1 and 200 nm and is static or dynamic [169–173].

These intrinsically inhomogeneous states are more pronounced and universally accepted for manganites. These phase-separated states give rise to novel electronic and magnetic properties with colossal magnetoresistance (CMR) in doped perovskite manganites. CMR and related properties essentially arise from the double-exchange mechanism of electron hopping between the Mn^{3+} ($t_{2g}^3e_g^1$, JT ion) and Mn^{4+} ($t_{2g}^3e_g^0$, non-JT-ion) ions, which favors the ferromagnetic metallic phase below T_c and the paramagnetic insulating state above T_c. In the insulating state, the Jahn–Teller distortion associated with the Mn^{3+} ions localizes the electrons and favors charge ordering (CO) of Mn^{3+} and Mn^{4+} ions. This CO competes with double exchange and promotes the antiferromagnetic insulating (AFI) behavior [105]. Even in many of the manganites (exhibiting CMR) which are in FMM state at low temperatures, CO clusters occur. Thus in doped rare earth manganites CO (AFM) and FM clusters or domains coexist, the sizes of which are affected by the carrier concentration or composition, average size of the A-site cations, temperature and other external factors such as magnetic and electric fields [178–181]. Phases with different charge densities and transport properties coexist as carrier-rich FM clusters or domains along with carrier-poor antiferromagnetic (AFM) phase. Such an electronic phase separation gives rise to microscopic or mesoscopic inhomogeneous distribution of electrons, and results in rich phase diagrams that involve various types of magnetic structures [107]. Thus there is a clear evidence of electronic phase separation in many manganite systems. Rao *et al* [169] and Dagotto *et al* [182–184] have extensively reviewed all aspects of phase separation in manganites.

The phase separation (PS) scenario in manganites is somewhat complex because the transition from the metallic to the insulating state is not sharp and the domains of the two phases are often sufficiently large to give rise to well defined signatures in neutron scattering or diffraction experiments. In electronic phase separation for manganites, the concentration of the charge carriers giving rise to ferromagnetism and/or metallicity in a part of the crystal causes mutual charging of the two phases. This gives rise to strong coulomb interaction, which may mix the conducting ferromagnetic and insulating antiferromagnetic phases in order to lower the coulomb energy (stabilization of microscopically charged inhomogeneous states) and gives rise to cluster of one phase embedded in another. The size of clusters depends on the competition between DE and Coulomb force. Electronic phase separation of different charge densities is generally expected to give rise to nanometer scale clusters. This is because large phase separated domains would break up into small pieces because of Coulomb interaction. Depending on the strength of interaction the shapes of these pieces could be droplets or stripes. One can visualize PS arising from disorder due to size mismatch of the A-site cations in doped manganites. Such phase separation is seen in the $(La_{1-y}Pr_y)_{1-x}Ca_xMnO_3$ (LPCMO) systems in terms of the insulator–metal transition induced by disorder [185]. The size of the cluster depends on the magnitude of the disorder. The smaller the disorder, the larger would be the size of the cluster. These microscopically homogeneous clusters are usually ∼1–2 nm in diameter dispersed in an insulating or charge-localized matrix. Such a phase separation scenario bridges the gap between the double-exchange model and the lattice models. In the last couple of years, phase separation have been reported in several rare earth manganites and the phenomenon has been investigated by a variety of techniques [183]. Keeping in view the wide implication of this phenomenon in solid state and material science, it is important as well as necessary to give an idea about the concept of phase separation in manganites.

The first evidence of phase separation in manganites was given in the pioneer neutron diffraction study of $La_{1-x}Ca_xMnO_3$ by Wollan and Koehler [55] in 1955. They reported the coexistence of ferromagnetic and A-type antiferromagnetic reflections in non-stoichiometric $LaMnO_3$ (14, 18 and 20% Mn^{4+}) and in $La_{0.89}Ca_{0.11}MnO_3$. The most important results that have convincingly shown the presence of coexisting clusters of metallic and insulating phases in the CMR regime of manganites were obtained by Uehera *et al* in their study of $La_{5/8-Y}Pr_YCa_{3/8}MnO_3$ using transport, magnetic and electron microscopy techniques [186]. They observed an enormous low temperature resistivity in spite of the fact that $\partial\rho/\partial T > 0$ suggests metallic behavior. In itself this shows that a homogeneous picture of manganites will likely fail, since only a percolative state can produce such large but metallic resistivity. The magnetoresistance is large and increases rapidly as T_c is reduced. The value of MR can be very large even at low temperature where the resistivity is flat, far from the actual ferromagnetic transition, suggesting again the mixed phase tendencies in the system. Uehara *et al* [186] interpreted their results in terms of two-phase coexistence of a stable FM state at small y (Pr content) and a stable CO state in the large y LPCMO compound. They proposed a percolative transition in the intermediate regime of composition. To further strengthen their results they carried out transmission electron microscopy and found 500 nm coexisting domains of CO insulator and FM metallic phases for $Pr = 0.375$ at 20 K. At 120 K, these clusters become nanometer in size (figure 15). However, the experimental results for LPCMO are in excellent agreement with the ideas presented by Moreo *et al* [185], where first order transitions are transformed into regions of two-phase coexistence by the intrinsic disorder of the manganites, which is called a disorder-induced phase transition.

Further remarkable evidence of mixed phase tendencies in $La_{0.7}Ca_{0.3}MnO_3$ single crystals and thin films has been given by Fath *et al* employing scanning tunneling spectroscopy (STS) [187]. Below T_c, phase separation was observed where inhomogeneous clusters of metallic and insulating phases coexist. The cluster size was found to be as large as a fraction of a micrometer and depends strongly on magnetic field. They believe that T_c and the associated MR behavior

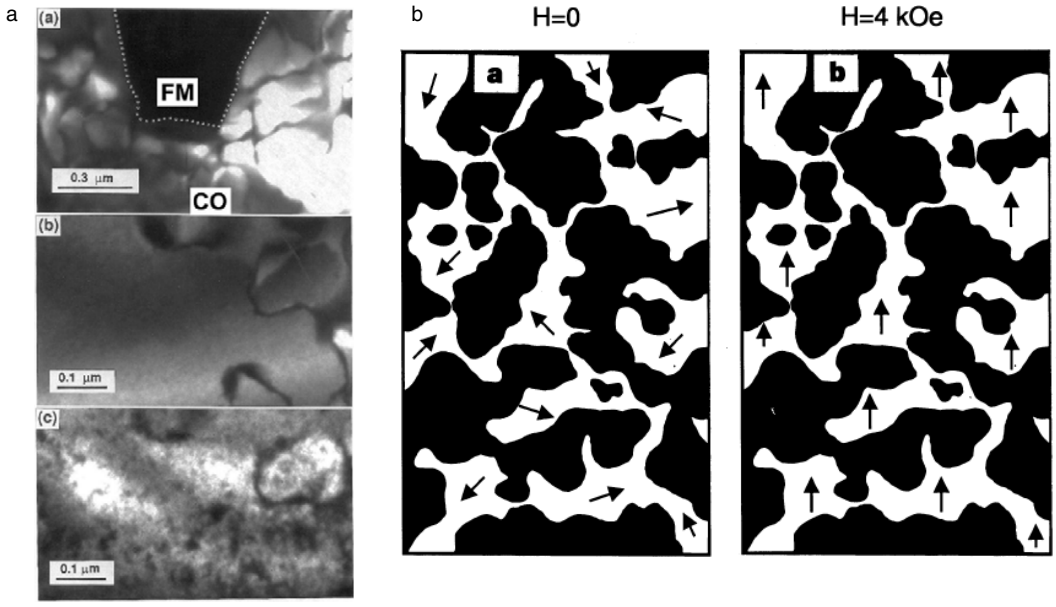

Figure 15. (a) Dark field images for $La_{5/8-y}Pr_yCa_{3/8}MnO_3$ obtained by using a superlattice peak caused by CO. Panel a shows the coexistence of charge-ordered (insulating) and charge-disordered (FM metallic) domains at 20 K for $y = 0.375$. The charge-disordered domain (dark area) is highlighted with dotted lines for clarity. The curved dark lines present in CO regions are antiphase boundaries, frequently observed in dark field images for the commensurate CO states of $La_{0.5}Ca_{0.5}MnO_3$ [163]. Panels (b) and (c), obtained from the same area for $y = 0.4$ at 17 K and 120 K, respectively, show the development of nanoscale charge-disordered domains at $T > T_C$. The curved lines in (a), (b) and (c) signify the presence of antiphase boundaries of the CO domains. (b) Schematic illustration of the sub-micrometer-scale coexistence of the $x = 1/2$-type CO insulating (dark area) and FM metallic (white area) domains. The typical size of domains is ∼0.5 mm. In zero field (a), the magnetizations of FM domains are random, but all magnetizations of FM domains can be aligned by applying field of about 4 kOe (b). With the variation of y (that is, the abundance of CO domains), the residual ρ_0 follows $\rho_0 \propto (y_c - y)^p$ with $P \approx -6.9$ and $P \approx -2.6$ for (a) and (b), respectively. Reprinted by permission of Macmillan Publishers Ltd: *Nature* [186], Copyright (1999).

is caused by percolative transition. Fath *et al* (STS gives a real space picture at microscopic level) remarked that the presence of 'clouds', which can be metallic or insulating, having size of tens to hundreds of nanometers, is not at all compatible with the picture of homogeneously distributed small polarons, which is a competing theory to the mixed phase scenario. Other workers have also studied the mixed phase tendencies by STS [188, 189], STM [190, 191] and low temperature MFM [192]. The results provide an atomic scale basis for description of the manganites as a mixture of electronically and structurally distinct phases, in excellent agreement with modern theoretical studies [182] and a wide range of experiments [183].

Several other experimental techniques, e.g. EXAFS [193], PDF (x-ray as well as neutron) [194], neutron scattering [195], Raman scattering [196], Mossbauer spectroscopy [197], muon spin relaxation [198], infrared reflectivity [199], photoabsorption spectroscopy [200], isotope effect [201], specific heat [202], thermal expansion measurements [203], optical studies [204], internal friction [205] and others, give strong evidence of phase separation in a variety of manganite systems. Further evidence of phase separation in manganites comes from inhomogeneous conductivity in the vicinity of the insulator–metal transition for the noise characteristics of film and single-crystal samples. The noise measurements provide direct proof of conduction in perovskite manganites dominated by mixed phase tendencies leading to a percolative process below T_c [206–209]. Merithew *et al* [210] and Raquet *et al* [209] have carried out detailed analysis of voltage spectral density $(1/f)$ for $La_{2/3}Ca_{2/3}MnO_3$ and concluded that the effect arises from fluctuations between local states with different conductivities. These fluctuations are likely located along the percolative backbone expected in manganites. The domains have a size of 10^4–10^6 unit cells. These effects are not caused by chemical inhomogeneity but seem to be intrinsic to the material. Similar results were reported for $Pr_{2/3}Ca_{1/3}MnO_3$ by Anane *et al* [211] and for $(La_{1-y}Pr_y)_{1-x}Ca_xMnO_3$ in the mixed phase regime by Podzorov *et al* [206, 212]. Recently Sarma *et al* observed the formation of distinct electronic domains by direct spatially resolved spectroscopy [213]. Very recently, Viret *et al* [214] and Saurel *et al* [215] have shown a 'red cabbage' sheet-like distribution of FM clusters in an AFI matrix having a few nanometers width by employing the polarized small angle neutron scattering technique. In another recent study, Ma *et al* [216] have imaged for the first time both occupied and unoccupied states simultaneously in $(La_{5/8}Pr_{0.3})Ca_{3/8}MnO_3$ epitaxial thin film by *in situ* scanning tunneling microscopy. The direct visualization of the doped holes and intriguing electron inhomogeneity in real space for TMO provide insights into polaron correlation in manganite films.

There has been considerable theoretical work, motivated by experimental results on perovskite manganites, on the analysis of models for these materials. Several many body techniques for modeling strongly correlated electron systems were developed and improved during recent efforts to understand high temperature superconductors, thus it is natural to apply some of these models to manganite systems;

of particular relevance here are the computational technique that allows unbiased analysis of correlated models on finite clusters [217]. Intimately related to the concept of phase separation is the idea of percolation of insulating and metallic regions. The effective medium approach suggests that metallic and insulating regions coexist as interpenetrating clusters, also suggesting a percolative mechanism for the insulator–metal transition. One such percolative model was proposed by Bastiaansen and Knops [218] based on a random resistor network. A Monte Carlo simulation (MCS) of resistor networks with the 2D Ising model formed the basis of the calculation, with unit resistors connecting aligned nearest-neighbor and next-nearest-neighbor sites and infinite resistance linking unlinked sites. The MCS is in good agreement with experimental data concerning both the temperature variation of the resistivity and the influence of the magnetic field. Quite similar results for the resistivity of manganites by the random resistor network model have been reported recently by Mayr *et al* [219]. Weibe *et al* [220] proposed a two-phase scenario of competing ferromagnetic metallic and insulating polaronic phases; the balance between these two states/phases can be tuned by the variation of various parameters. The magnetization exhibits a first order transition, which is consistent with the neutron scattering data of Lynn *et al* [221] and the magnetization data of Mira *et al* [222] and Ziese [223]. A more relativistic model was proposed by Lyuksyutov and Pokrovsky [224], which is based on Varma's theory [225] of magnetic polaron formation, modified to include Jahn–Teller effects. Magnetic polarons, which coexist with small lattice polarons, are assumed to be large, basically comprising magnetically correlated regions. As the temperature is lowered, the magnetic polaron density increases until the magnetic polaron overlaps, which defines the percolation point. They argue that long range Coulomb effects render implausible suggestions that macroscopic charge separation underlies the CMR effect [169, 226, 227]. Recently, Dzero *et al* [228] modeled the metallic phase as a two-band Fermi liquid and applied the percolative model to study the phase separation at low doping ($x = 0.16$). In addition, a variety of mean field and variational calculations also led to phase separation. This shows that the evidence of phase separation in manganites is not restricted to computational methods only. The dynamical mean field theory of Millis *et al* [104] and the simple mean field model of Jaime *et al* [229] and several other MFTs only give a qualitative description of phase separation rather than the essential contributions of magnetic/conducting fluctuations. In fact, using approximate analytic techniques, Ahn *et al* [230] have shown that the strong coupling between the electronic and elastic degrees of freedom is essential in explaining self-organized inhomogeneities over both nanometer and micrometer scales (phase coexistence). In another work, Sagdeo *et al* [231] have carried out extensive comparative structural studies on the powder (nearly strain free) and the compressed pellets (strained) of $La_{1-x}Ca_xMnO_3$. They have shown that the structural phase coexistence occurs only in the pellets (strained) and not in the powder, which is in agreement with theoretical calculation of strain-induced phase coexistence by Ahn *et al* [230]. Recently Shenoy *et al* [232] adopted a different approach to explain the nanoscale inhomogeneities in manganites. They modified the proposed *lb* model by adding two critical ingredients, namely the long range Coulomb interaction and dopant ion disorder [140, 169]. On the basis of numerical simulation they concluded that the nanoscale electronic inhomogeneities in doped manganites are not due to 'phase-competition'-induced 'phase separation' between 'insulating' and 'metallic' phases frustrated by disorder as suggested by earlier studies [182–184, 230]. Rather, they arise due to the long ranged Coulomb interactions frustrating the phase separation induced by strong local correlations.

In short, we can say that the instability towards phase separation and the formation of inhomogeneous states or competing phases (e.g. CO/AF and FM) is an intrinsic property of doped perovskite manganites. The existence of these preformed clusters (inhomogeneous state or competing phase of CO/AF and FM) and their easy alignment with modest magnetic fields leads to colossal magnetoresistance. Thus phase separation appears to be at the heart of various magnetotransport phenomena in manganites. So, one has to be careful in attributing CMR and the associated insulator–metal transition to percolation of FMM domains.

4. Magnetoresistance at low magnetic fields ($\leqslant$10 kOe)

Depending on the origin, the magnetoresistance (MR) [7] effect is of two types. First, observed in the vicinity of T_C in good quality single crystals and epitaxial films of doped manganite perovskites it is intrinsic in nature and usually referred to as the colossal magnetoresistance (CMR) effect. Since CMR is observed at high magnetic fields it has a limited application potential [47–49, 233–235]. The second is the extrinsic MR effect, observed deep in the ferromagnetic regime and at moderately low magnetic field ($<$0.1 T), in which the grain boundary plays the central role. This grain-boundary- (both natural as well as artificial) induced MR is more promising for device applications and hence is of great interest. Since significant MR is observed at low magnetic field the extrinsic MR effect is generally referred to as low field magnetoresistance (LFMR). The initial works on polycrystalline bulk and thin films have shown substantial MR at temperatures much lower than T_C, having relatively flat or monotonic temperature dependence. In contrast, in the low temperature regime, single crystals and epitaxial films of the same composition exhibit vanishingly small MR at low magnetic fields [84, 236]. A number of subsequent studies, both on bulk and thin film samples, have confirmed the important role of grain boundaries as a source of LFMR and VLFMR (very low field magnetoresistance at magnetic field of $\sim$few mT) [238–292]. The LFMR is usually interpreted in terms of spin-polarized tunneling (SPT) through electronic barriers across the grain boundaries. Hence the nature and size of grain boundaries (GBs) plays a major role in the LFMR mechanism. For example, the low magnetic field magnetotransport properties in these materials have been found to be sensitive to the nature and

size of the GBS. This brings out the importance of grain-size-dependent study of the magnetotransport properties of manganites. In this regard, a variety of grain boundary configurations (natural as well as artificial) have been explored. The effect of natural GBs on magnetotransport properties has been probed in a wide spectrum of samples, such as nano/polycrystalline bulk [236–257], thick/thin film samples [258–333], manganite-based composites [334–356] and intrinsically layered manganites [357–385]. To achieve the desired control over the magnetotransport, artificial GBs have been tailored in different junctions such as bi-crystals [395–406], step-edge [407–411], laser patterned [410, 411] etc. All these have been explored to figure out the role of the nature and size of GBs in the low field magnetotransport of manganites. As low field magnetotransport properties of polycrystalline manganite are the theme of the present review, it is opportune and important to give a overview of various GB systems and the effect they have on LFMR in doped manganites [236–294]. In the following subsections some important contributions to low field MR are summarized.

4.1. Natural grain boundary systems

4.1.1. Polycrystalline and nanocrystalline bulk. In view of the fact that transformation from multiple domains to a single domain leads to disappearance of intrinsic MR and also that micro/nanoscale inhomogeneities (and phase separation) play an important role in manganites, several groups have centered their research on nanosize manganites. Nanocrystalline manganites exhibit distinct magnetotransport properties due to both the inherent nanoscale phase inhomogeneities and additional surface effects.

Mahesh *et al* [237] were the first to explore the size effect in polycrystalline $La_{0.7}Ca_{0.3}MnO_3$ (LCMO) prepared by a citrate-gel route and having different particle sizes (0.025–3.5 μm). The Mn^{4+} concentration, which is a crucial factor in controlling the transport and magnetic properties, was kept similar in the different samples. They observed an increase in resistivity (ρ) with decreasing particle size (figure 16). Furthermore, the ratio of ρ at 4.2 K and at the T_{IM}, corresponding closely to the T_C, decreased with increasing particle size. The T_C has also been observed to broaden with decreasing particle size, with the 0.025 μm sample not exhibiting a well defined transition temperature. They noted that, despite these changes, the MR near the T_C did not show any significant changes with the size of the particle. However, the MR at 4.2 K is found to have both low and high field components, with the former increasing with decrease in particle size (figure 16). Based on this and the observation that single-crystal and epitaxial films exhibit very small MR at 4.2 K, they concluded that a substantial part of the MR at low temperatures ($T \ll T_C$) arises from the GBs.

In another study Hwang *et al* [236] further elaborated the role of GBs in manganites by direct comparison of the MR and field-dependent magnetization for a $La_{0.67}Sr_{0.33}MnO_3$ (LSMO) single crystal and two ceramic samples of the same composition sintered at 1300 and 1700 °C. Both single-crystal and polycrystalline samples show a sharp ferromagnetic

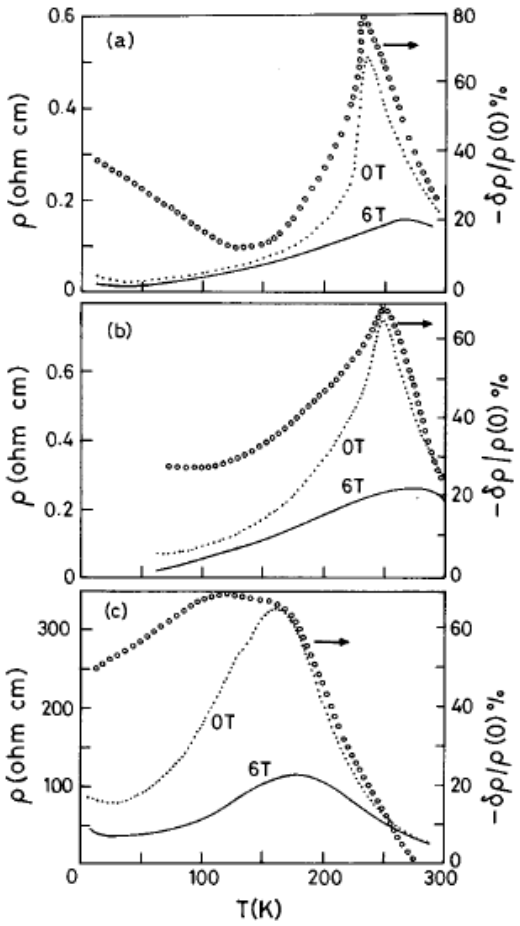

Figure 16. Temperature variation of resistivity at $H = 0$ and 6 T and magnetoresistance of $La_{0.7}Ca_{0.3}MnO_3$ samples with particle size (a) 3.5, (b) 1.5 and (c) 0.025 μm [237]. Reprinted with permission from [238]. Copyright 1999 by the American Institute of Physics.

transition at $T_C \sim 365$ K. However, at low temperatures, ρ of the polycrystalline samples is significantly higher than that of the single crystal, as shown in figure 17. At 5 K, a ρ of 35 $\mu\Omega$ cm is observed for the single-crystal LSMO; the ρ *of* the 1700 °C sintered polycrystalline sample is about an order of magnitude higher owing to scattering introduced by the grain boundaries. Furthermore, the ρ of the 1300 °C sintered sample is almost an order of magnitude larger than the 1700 °C sintered sample because of increased scattering that is due to smaller grain size. As shown in figure 17, the low temperature resistivity depends strongly on the microstructure, whereas the magnetization at 0.5 T is virtually identical for the three samples. The effect of the GBs on the LFMR is even more surprising. Figure 18 shows the field-dependent magnetoresistance and magnetization of the samples investigated. For a single crystal there is negligible MR at low temperatures, and with increasing temperature there is increasing negative MR. Correspondingly, the magnetization shows a rapid rise because of magnetic domain rotation at low applied fields, followed by a slow approach toward saturation at higher fields. The variation in the magnetization at various temperatures for the single crystal closely tracks the MR, strongly suggesting that the suppression of magnetic fluctuations is the origin of the negative MR in the single-

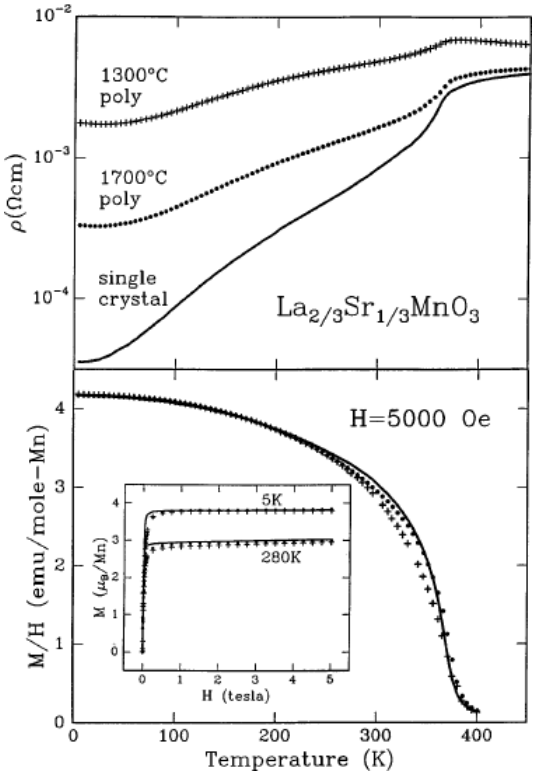

Figure 17. Top panel: $\rho(T)$ of $La_{2/3}Sr_{1/3}MnO_3$ for a single-crystal sample and two polycrystalline samples with final sintering temperatures of 1300 and 1700 °C. Bottom panel: the temperature dependence of the magnetization for these three samples at 0.5 T. Inset: the field-dependent magnetization of these samples at 5 and 280 K. Reprinted figure with permission from [236]. Copyright 1996 by the American Physical Society.

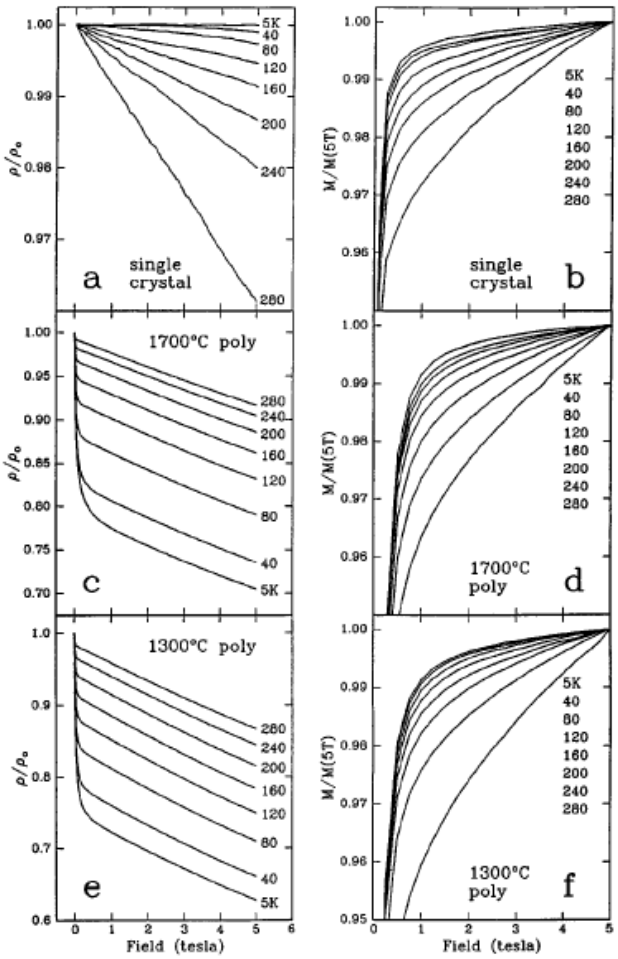

Figure 18. (a), (c), (e) The magnetic field dependence of the normalized resistance at various temperatures from 5 to 280 K. (b), (d), (f) The magnetic field dependence of the magnetization (normalized to the 5 T value) at various temperatures from 5 to 280 K. Reprinted figure with permission from [236]. Copyright 1996 by the American Physical Society.

crystal sample. In contrast, both polycrystalline samples exhibit a sharp drop in the resistance at low fields followed by a slower background negative MR at higher fields. The sharp drop is greatest at the lowest temperatures and decreases with increasing temperature. In contrast to the resistivity variations, the magnetization data are quite similar for three samples. The magnitude of LFMR increases with decreasing temperature, while the intrinsic MR that has a maximum near the T_C decreases with lowering temperature. This suggests that the MR in the polycrystalline samples is dominated by intergrain effects, with the magnetic field associated with the sharp drop in resistance identical to that associated with magnetic domain rotation. Another important observation, apparent from figure 18, is that above 0.5 T and for the entire temperature range 5–280 K the MR in the polycrystalline samples has the field dependence of type $\sim H^2$ in addition to the obvious dominant linear term in H. They concluded that LFMR in polycrystalline samples is due to spin-polarized tunneling between misaligned grains. It was further shown by Wang *et al* [238] that, for a phenomenological analysis, one has to distinguish between weak and strong link GBs. Only weakly linked GBs give considerable LFMR. The microstructural characteristics of the two types of links (weak and strong), that is, the formation of weak or strong links, can be controlled by the fabrication methods.

The Hwang proposal of SPT as the main source of LFMR was provided strong support by the results of Bibes *et al* [239]. Bibes *et al* analyzed the magnetic properties and nuclear magnetic resonance response of LCMO ceramics with different grain sizes, and observed that the surface of the grain contained poorly conducting regions, some ferromagnetic and some weakly magnetic. This region envelopes a thickness of 1–2 nm and can thus constitute the barrier involved in the spin-polarized tunneling mechanism invoked by Hwang *et al* to explain LFMR in powders of half-metallic oxides. The SPT predicts that LFMR magnitude decreases with increasing temperature. However, an anomaly has been observed in the temperature dependence of LFMR in nanosize samples. Hueso *et al* [240] have found that in polycrystalline LCMO having particle size lower than ∼150 nm the intrinsic CMR disappears, but large intergrain LFMR still remains. They invoked the presence of domain walls in the bigger particles that arises due to transition from single domain (small grain size) to multiple domain (large grain size), resulting in a decrease in intrinsic CMR. These walls are dynamic and act

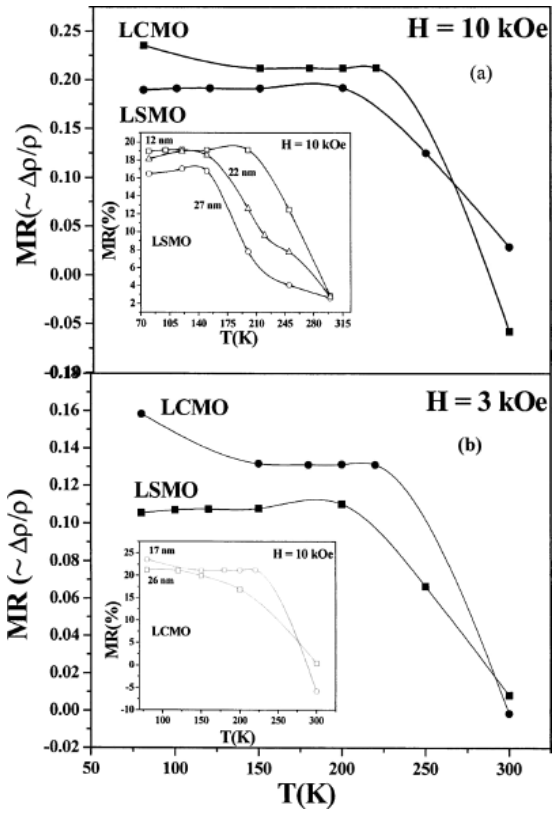

Figure 19. MR versus T in the temperature range of 80–300 K for LSMO and LCMO samples at (a) 10 and (b) 3 kOe, respectively. Insets of (a) and (b) show the MR–T curves at 10 kOe for varying particle sizes of LSMO and LCMO, respectively. For both LSMO and LCMO nanomanganites the MR (at 3 and 10 kOe) remains constant up to 200 K. Reprinted figure with permission from [243]. Copyright 2005 by the American Institute of Physics.

as scattering centers altered by the presence of a magnetic field, which results in appearance of the intrinsic CMR mechanism. This has also been theoretically confirmed by Zhang *et al* [241]. Kim *et al* [242] prepared hollow colloidal nanospheres of LCMO on a porous carbon template having a magnetic transition near 250 K. Recently, Dey and Nath [243] probed the effects of nanometric grain size on temperature-dependent LFMR of single-phase nanocrystalline granular $La_{0.7}Sr_{0.3}MnO_3$ and $La_{0.7}Ca_{0.3}MnO_3$ having average grain size in the nanometric regime (12 and 17 nm). They observed that the magnitude of LFMR, arising from spin-polarized tunneling of conduction electrons, remains constant up to a sufficiently high temperature (200 K) (figure 19), and then drops sharply with temperature. In the case of polycrystalline materials grain boundaries provide defect sites where the anisotropy energy of the surface spin is the lowest. So at the disordered surface of polycrystalline grains strong pinning of surface spins is expected. In the case of nanometric-size grains defects are expected to occur to a higher extent at the enhanced grain surface due to a high degree of (i) contamination, (ii) breaking of Mn–O–Mn bonds, (iii) deviation of stoichiometric composition, (iv) termination of crystal structure and (v) dislocation. With the application of magnetic field, strong freezing of surface spins occur at the defect sites of the disordered grain surface as a consequence

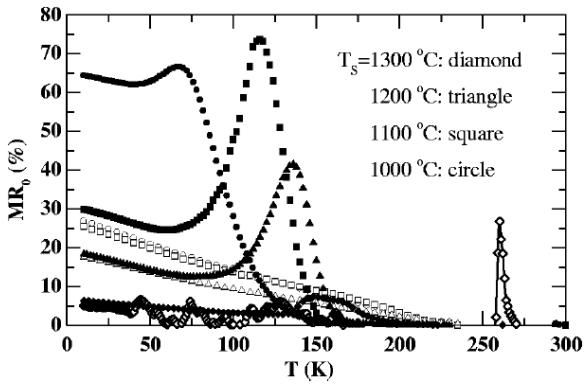

Figure 20. Variation of magnetoresistance at 0.3 T field in $La_{2/3}Ca_{1/3}Mn_{1-x}Cu_xO_3$ with $x = 0$ (open symbols) and 4% (solid symbols) synthesized at 1000, 1100, 1200 and 1300 °C. The sample at 1300 °C shows a characteristic CMR peak near T_{IM}, while the samples $\leqslant$1200 °C have no peak MR but the LFMR increases with decreasing temperature [245]. Reprinted with permission from [246]. Copyright 2003 by the American Physical Society.

of interactions between grain boundary pinning strength and magnetic field. Thermal energy (k_BT), up to a considerably high temperature, remains unable to flip them from their strained condition, resulting in such a temperature insensitive behavior of MR. They proposed a phenomenological model based on SPT similar to Raychaudhuri *et al* [244] to explain the magnetotransport behavior of LCMO having grain size of ∼14–27 nm. They found that the temperature dependence of MR is decided predominantly by the nature of the temperature response of surface magnetization of these nanosize magnetic particles as proposed by Lee *et al* [245].

Anomalously large LFMR was reported by Yuan *et al* [246] in sol–gel prepared polycrystalline samples of nominal $La_{2/3}Ca_{1/3}Mn_{1-x}Cu_xO_3$. LFMR showed a strong dependence on sintering temperature (T_S). Lowering T_S causes a large decrease of the T_{IM} and a substantial increase in resistivity at $T < T_{IM}$. In samples sintered at $T_S < 1200$ °C a colossal LFMR ∼ 74% was found at a low magnetic field 3 kOe near T_{IM} as shown in figure 20. Interestingly, the sample at $T_S \sim 1000$ °C exhibits an almost constant magnetoresistance with a value ∼ 65% for the 3 kOe field over the whole low temperature range. Rivas *et al* [247] have also shown the importance of the surface contribution in small grain size $La_{0.67}Ca_{0.33}MnO_3$. The surface contribution seems to be responsible for a great variety of extrinsic effects. LFMR arises in smaller grain size samples and, at the same time, intrinsic CMR around the phase transition is destroyed. They emphasized the importance of the domain wall contribution and a spin-polarized tunneling below phase transition temperature. They suggested that in small enough particles the observed electrical resistivity increase at very low temperatures could be ascribed to an electrostatic barrier present between grains. Nam *et al* [248] have systematically studied the magnetotransport in $La_{1-x}Ba_xMnO_3$. LFMR ∼ 12–16% at $H = 500$ Oe and $T = 77$ K was found in the overdoped regime in the range $0.5 \leqslant x \leqslant 0.75$.

Siwach *et al* [252] have extensively studied the effect of sintering temperature on the low field magnetotransport

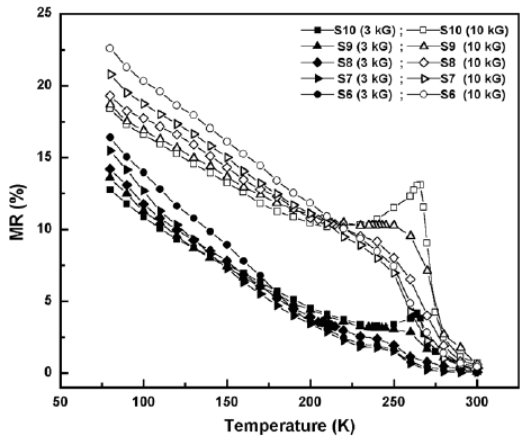

Figure 21. Magnetoresistance (MR) as a function of temperature for applied magnetic field of 3 and 10 kG for the samples sintered at different temperatures. The peak MR values are ∼13.07 and 10.34 % at 10 kG field for S10 and S9, whereas for S8 and S7 there is a hump in the MR variation around T_C. At 80 K, the MR values are measured to be ∼12.87, 13.66, 13.85, 15.46 and 16.51 for S10, S9, S8, S7 and S6, respectively, at the field of 3 kG [252].

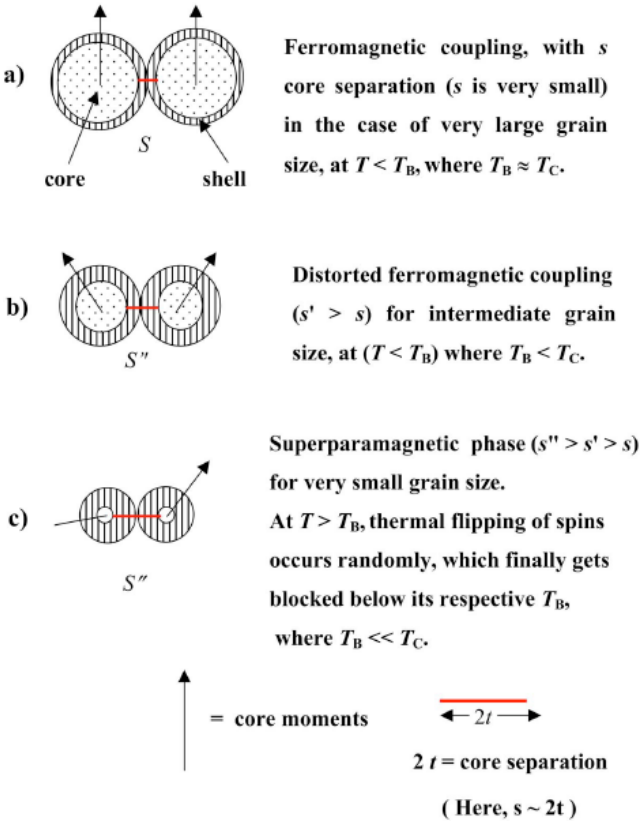

Figure 22. Phenomenological demonstrative representation of the possible ordering of core moments in the core–shell structure of nanometric manganite grains with the grain size as a variable parameter in different temperature ranges. Reprinted figure with permission from [243]. Copyright 2006 by the American Physical Society.

of sol–gel-synthesized LCMO manganite and observed that decreasing grain size leads to the enhancement in LFMR at lower temperatures while the MR in the higher temperature regime is suppressed. The T_C, being an intrinsic characteristic, does not show significant change as a function of the sintering temperature, whereas T_{IM} is an extrinsic property, that strongly depends on the synthesis conditions and microstructure (e.g. grain boundary density). The disappearance of the high temperature MR can be explained by weakening of the DE mechanism around the respective PM–FM transition temperatures due to decrease in particle size, which results from low sintering temperature, which is consistent with previous studies on spin-polarized-tunneling-enhanced LFMR in polycrystalline samples [251]. At 80 K, the MR values are increased from ∼12.9 (600 °C) to ∼16.5 (1000 °C) at the field of 3 kOe as shown in figure 21. Thus, decreasing grain size leads to the enhancement of LFMR at lower temperatures while the MR in the higher temperature regime is suppressed. Peng *et al* [253] synthesized an ordered surface pattern consists of grain chains located on regular orthogonal cracks on the $La_{0.5}Ca_{0.5}MnO_3$ films due to the thermal mismatch between the film and the substrate. These cracks act as natural in-plane weak link grain boundaries, which leads to enhanced low field MR up to ∼214% in 400 Oe at 90 K, which can be ascribed to the intergrain spin-polarized tunneling.

It is well known that as the grain size becomes smaller and smaller the surface to volume ratio increases. This results in an enhanced contribution from the surface region to the various physical properties of the materials. Consequently, in nanosize materials the surface effects are responsible for anomalous behavior because a large fraction of atoms reside at the GBs. These grains and the GBs have different temperature dependences of relaxation processes, which affect the transport properties to a great extent [254]. In the case of nanostructured manganites, magnetotransport studies reveal that the spatial confinement of free and bound charges and the volume fraction of highly disordered GBs play an important role in these materials [255]. In order to understand the magnetotransport behavior of polycrystalline manganites, the concept of a core–shell-type structure has been proposed by Zhang *et al* [256]. In the core–shell structure the inner part of the grain, i.e. the core, would have the same properties as the bulk manganite, whereas the outer layer, i.e. the shell (thickness t), would contain most of the oxygen defects and crystallographic imperfections, which would lead to a magnetically disordered dead layer. As the surface to volume ratio becomes larger, that is, the grain size is reduced, the shell thickness (t) increases. Basically, the net intercore barrier thickness ($s = 2t + d$), namely the total shell thickness ($2t$) of two neighboring grains together with the intergranular distance (d), increases with the reduction of grain size. As shown in figure 22, with the decrease in grain size, core separation ($s \sim 2t$) increases significantly with the thickness of the shell (t), even if we consider the grains to be in intimate contact ($d = 0$) for all grain size samples. Another important fact is that in the absence of magnetic field the contributory portion of each individual grain to the magnetization is the core and not the shell, as in the absence of applied magnetic field the net magnetization of the shell is considered to be zero. Since the surface would contain most of the oxygen defects and faults in the crystallographic structure that will lead to a

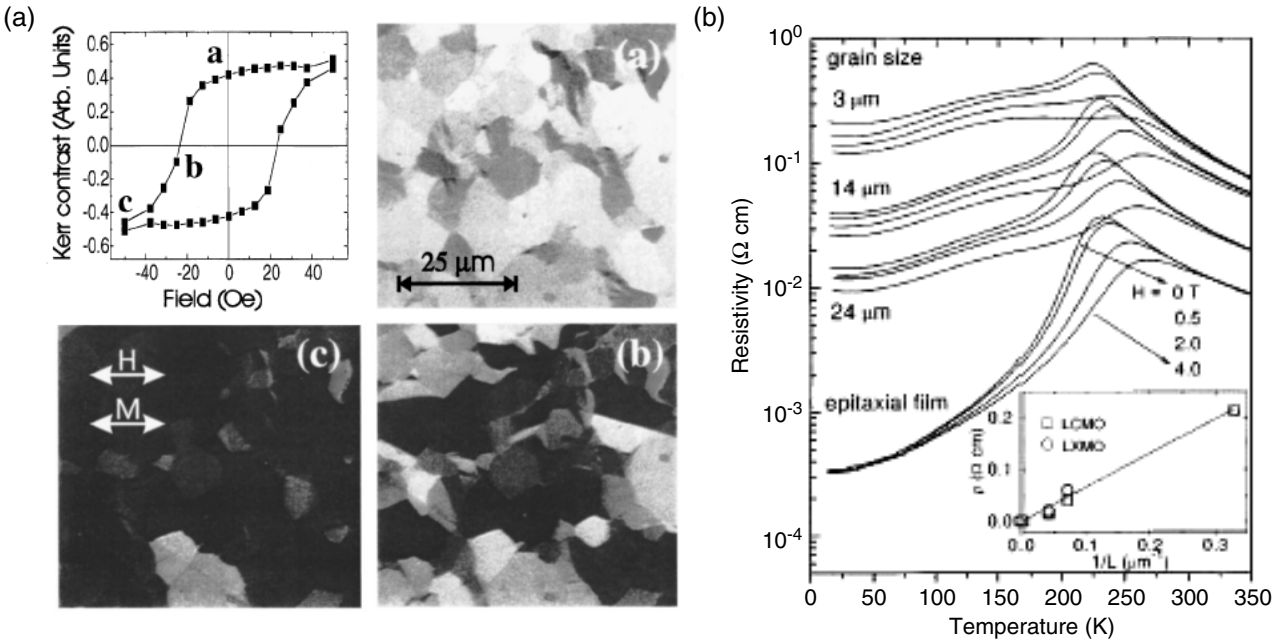

Figure 23. (a) Kerr hysteresis loop of a polycrystalline LSMO film sample averaged over a number of grains. The three Kerr images correspond to the points (a), (b) and (c) marked in the hysteresis loop. The external field has been applied horizontally, as indicated in the image, and swept between plus and minus 200 Oe. The Kerr signal is sensitive to changes in the horizontal component of the magnetization. (b) Resistivity (in log scale) as a function of temperature for polycrystalline (average grain size of 3, 14 and 24 mm) and epitaxial LCMO films. For each sample, data measured at magnetic fields of 0, 0.5, 2 and 4 T are presented. The inset shows a plot of the zero-field resistivity at 10 K as a function of the inverse grain size ($1/L$) for LCMO and LXMO films. Reprinted with permission of [272]. Copyright 1996 by the American Physical Society.

magnetically disordered state, which may lead to formation of spin canting or antiferromagnetic state at the manganite grain surface [257, 258], large magnetoresistance has been observed in the core–shell type structure.

4.1.2. Polycrystalline and epitaxial films. The discovery of high temperature superconductivity (HTSC) in doped cuprates and more recent observation of colossal magnetoresistance (CMR) in doped manganites has seen the emergence of epitaxial transition metal oxide (TMO) films as one of the most attractive and overwhelming subjects for the materials scientist not only because of the fundamental physics but also due to their application potential [259]. Since most technological applications such as ferroelectric field effect [260], bolometric [261], optical [262] and spintronic devices [14–17] require manganite thin films having good magnetotransport properties on suitable substrates, the ability to prepare such high quality single-crystal epitaxial films and understand their properties is of prime importance. The synthesis (growth optimization) for manganite thin films has become possible by benefiting from studies of high temperature superconducting thin films in the late 1980s. Another reason for this quick transfer of growth technology is that these oxides crystallize in the same perovskite structure like HTSCs, and in several respects they are quite similar [263]. Different growth techniques, such as sputtering [264], molecular beam epitaxy (MBE) [265], electron beam/thermal co-evaporation [266], chemical vapor deposition (CVD) [267], pulsed laser deposition (PLD) [233–235], nebulized spray pyrolysis [268–270] and the sol–gel technique [271] have been extensively used for deposition of manganite epitaxial and polycrystalline thin films. An excellent review on various aspects of deposition and properties of manganite thin film has been given by Haghiri-Gosnet *et al* [234] and Prellier *et al* [235].

Gupta *et al* [272] systematically explored the properties of epitaxial and polycrystalline films of LCMO, $La_{0.67}Sr_{0.33}MnO_3$ (LSMO) and $La_{0.75}MnO_3$ manganites having mean grain sizes ∼3, 14 and 25 μm. They found that the polycrystalline films show substantial MR over a wide temperature range, similar to polycrystalline ceramics (figure 23(b)). They used a wide angle Kerr microscope to image the domains in the polycrystalline manganite films of LSMO. Because these domains have different coercivities, they are weakly coupled and orient successively in an increasing field. Figure 23(a) shows a Kerr M–H loop of a 14 μm grain size polycrystalline LSMO film and three corresponding Kerr images of the film recorded at room temperature. Image (*a*) displays the nearly uniform magnetic state of the sample at remanence. Near the coercive point, half the grains switch orientation, as seen in image (*b*). In image (*c*) most of the grains have switched as the loop nears saturation. Individual grains can be observed to switch at different fields, and the loop data are an average over the many grains contained in the images. Some of the grains are also observed to switch by wall motion. For example, in the top right corner of (*b*), a wall can be seen to cross a grain boundary. Wall motion can be impeded by surface defects such as scratches on the film. This work clearly brings out the dif-

ference between magnetization in polycrystalline and epitaxial LSMO films at microscopic level, which gives a qualitative idea that the LFMR in polycrystalline samples is due to spin-polarized tunneling of polarized electrons at the grain boundaries.

The LFMR has been found to depend on the degree of texturing in polycrystalline thin film. Walter *et al* have studied $La_{0.7}Sr_{0.3}MnO_3$ thin films on YSZ(100) substrates [273]. Experimental data on such films indicate that a key role is played by high grain boundary resistance that results from misorientation of adjacent grains, for both the low field and the high field magnetoresistance of polycrystalline ferromagnetic lanthanum manganites. Based on their results, they have suggested that high angle grain boundaries may cause structural disorder in a region at the grain boundary. This could lead to magnetic disorder because the balance of competing double exchange and superexchange interactions in lanthanum manganites is very sensitive to local structure. Then, magnetic disorder strongly enhances the resistivity of the grain boundary due to the double-exchange transport mechanism that dominates in these compounds. The highly resistive GB provides both a kind of thin insulating barrier for electron tunneling and magnetic decoupling of grains. Cheng *et al* [274] have observed appreciable LFMR $\sim$ 27% at 75 K in the low temperature regime in nanocrystalline $La_{0.7}Sr_{0.3}MnO_3$ films with thickness $t = 10$ nm grown on $LaAlO_3$ (100) substrates by RF magnetron sputtering. The temperature dependent MR of the 10 nm thick film has the inverse of temperature dependence as shown in figure 24, which is consistent with the model of spin-polarized tunneling.

Liu *et al* [275] investigated the low field transport properties of both polycrystalline and epitaxial films of doped lanthanum manganite prepared by the sol–gel method. The polycrystalline films show the same magnetic transition temperature as the epitaxial films with the same composition, but the transport properties are quite different from those of epitaxial films and show strong grain size dependence. The polycrystalline films show much lower resistivity peak temperature than that of the corresponding epitaxial films, and the resistivity peak temperature increases when the grain size becomes larger due to the higher annealing temperature. When the grains become very small, the intergrain conduction dominates over the intragrain conduction. On the other hand, the polycrystalline samples become magnetically harder with reducing grain size, implying a higher degree of spin disorder at the grain boundaries. Spray pyrolysis [268–270], which is a rather cheap but very handy technique for making good quality thin/thick films [233–235], has also made a significant contribution to the study of manganites. Singh *et al* [269] observed $\sim$18% MR at a low field of 3 kOe in spray-deposited LCMO polycrystalline films having average grain size of $\sim$125 nm. These films show broad insulator–metal transition temperature (T_{IM}) at $\sim$195 K and increasing MR with decreasing temperature, which has been ascribed to the presence of insulating regions around grain boundaries and domain rotation as suggested by Pignard *et al* [276]. The increasing LFMR is due to the presence of a large number of grain boundaries, which dilutes the interdomain interactions in each weak link region as proposed by Wang *et al* [239].

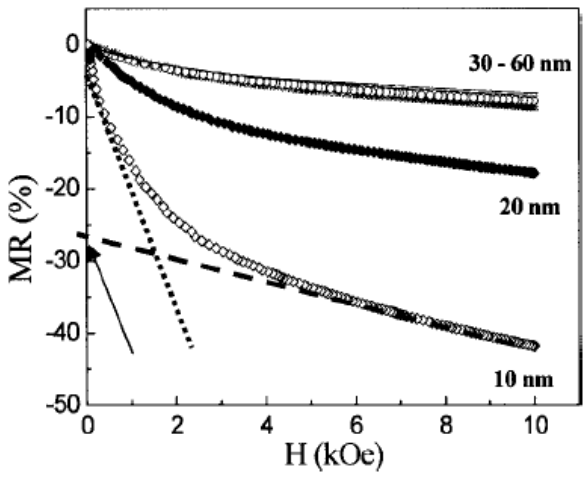

Figure 24. Dependence of the magnetoresistance of the $La_{0.7}Sr_{0.3}MnO_3$ films with thicknesses in the range of $\sim$10–60 nm on applied magnetic field. The dotted and solid lines denote the first and the second linear terms, respectively. The arrow indicates the intercept obtained by backwardly extrapolating the high field data to zero field. The MR–H dependence shows two gradients: One corresponds to the intergranular tunneling effect (at low fields), and the other corresponds to the intragranular magnetic fluctuation, which is reflected above 5 kOe. Reprinted with permission of [274]. Copyright 2005 American Institute of Physics.

Magnetotransport characteristics of manganites are governed by DE interaction between Mn ion spins via the Mn^{3+}–O–Mn^{4+} path [62, 106, 107]. Therefore, even a small perturbation in the Mn^{3+}–O–Mn^{4+} path affects MR properties significantly. In addition, the strong electron–phonon-coupling-induced Jahn–Teller (JT) distortion is crucial for magnetotransport properties [102, 104, 113]. There are two types of distortions of the ideal perovskite structure in bulk samples. The first is the rotational distortion of the MnO_6 octahedra due to the mismatch between the average A-site and Mn-site ionic radii, which is similar to the strain effect induced by substitution [277, 278]. The other is JT distortion of MnO_6 octahedra. However, for manganite thin films, in addition to doping level and average size of dopant, the substrate-induced lattice strain (caused by the lattice mismatch between the film and substrates) also plays a key role [279]. This kind of biaxial strain is different from the strain induced by hydrostatic [280] or chemical pressure [277, 278], since an in-plane strain generally accompanies an out-of-plane strain with a different sign, which can cause electronic behavior not found in bulk materials of the same chemical composition [279]. Substrate-induced lattice strain has been reported to change a wide variety of properties, with examples including the crystal symmetry [281–283], transport [284, 285] and magnetic anisotropies [286], the magnitude of ferromagnetic (T_C) [287] and charge ordering melting field [65], the spin and orbital order structure [288] and the tendency towards phase separation [279]. In most cases, these changes are interpreted in terms of substrate-induced strain, which relaxes with increase in thickness [289–291]. The lattice mismatch δ along the interface is defined by $\delta = (a_{p\ \text{substrate}} - a_{p\ \text{bulk}})/a_{p\ \text{substrate}}$. When the film is grown on a substrate whose lattice parame-

ter is smaller or larger than that of the bulk material, the epitaxial strain is expected to be compressive (the cell is elongated along the growth direction and compressed in the film's plane) or tensile (the cell is elongated in the film's plane and compressed along the out-of-plane growth direction), respectively. Compressive strain usually reduces the resistivity and shifts T_C towards higher temperature. These effects have been confirmed in $La_{0.7}Ca_{0.3}MnO_3$ films [281] and $La_{0.7}Sr_{0.3}MnO_3$ films [292–294] grown on various substrates.

For manganite films, the study of strain-dependent film properties is important from the physics standpoint as well as from the point of view of applications, because most devices are based on supported thin-film configurations. A biaxial strain is induced by lattice mismatch and in some cases by a large thermal expansion coefficient mismatch with the substrate. Jin *et al* found that insulator–metal transition is suppressed in very thin films because of strain [295]. A theoretical analysis has suggested that ferromagnetic T_C is extremely sensitive to biaxial strain, that can have an impact on both the Mn–O bond distance and the Mn–O–Mn bond angle [287]. Konishi *et al* [296] have shown that thin films of LSMO under tensile strain are metallic while under compressive strain they are insulating. They attributed the difference to strain-induced orbital polarization on the magnetic state of the films. Strain effects on magnetoresistance, magnetic anisotropies and magnetic domain structure have also been studied [297, 298]. Duo *et al* [294] have studied the magnetotransport properties of the LSMO epitaxial thin film with varied oxygen background pressure and thickness in relation to lattice strain. They observed that T_C, T_{IM} and T_{MR} are more sensitive to oxygen pressure than film thickness and concluded that the oxygen partial pressure is associated with the oxygen defect that leads to magnetic and structural inhomogeneities and hence affect the magnetotransport. Nelson *et al* [299] observed that substrate-induced lattice strain for $Pr_{0.6}Ca_{0.4}MnO_3$ thin films have a dramatic effect on the crystal symmetry, low temperature charge and orbital ordering, transport and magnetization behavior. They found low temperature ordering to be more robust under compressive strain as compared to tensile strain and suggested the importance of Mn–O–Mn bond angle in the formation of low temperature charge and orbital ordering. Wu *et al* [300] have investigated $La_{0.67-x}Pr_xCa_{0.33}MnO_3$ ($x = 0.13, 0.20, 0.27$) thin films under both internal chemical pressure from Pr doping and external strain from lattice mismatch with substrates. They found that lattice strain not only produces a wide span of insulator–metal transition temperatures, as shown in figure 25, but also induces tendencies towards multiphase coexistence in films. Large tensile strain eliminates the metallic behavior altogether and produces a ferromagnetic–insulating phase-separated mixture. Dale *et al* [301] have tuned the strain state of epitaxial $La_{1/2}Sr_{1/2}MnO_3$ thin films on $BaTiO_3$(BTO). As BTO undergoes numerous phase transitions as a function of temperature, so the BTO surface lattice can be dynamically changed in an attempt to significantly alter the strain state of the epitaxial film. They correlated the temperature dependence of the structure with that of the fractional changes

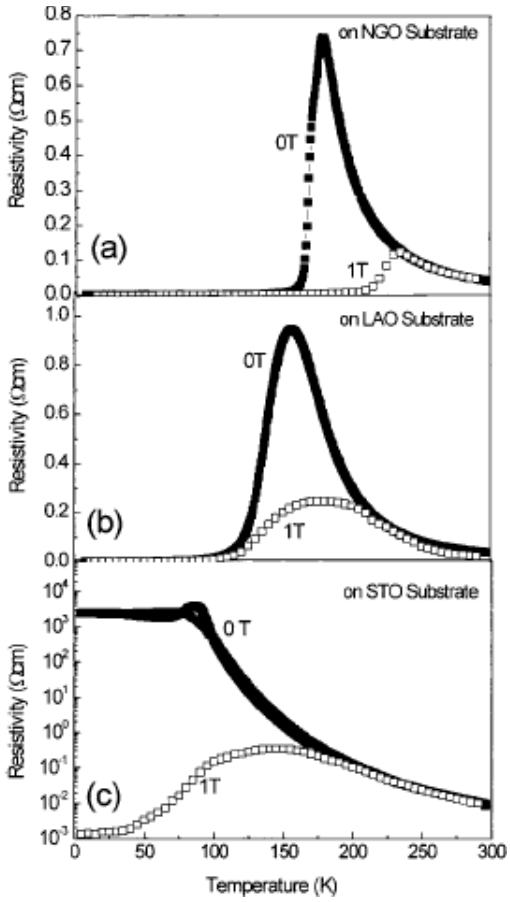

Figure 25. The magnetotransport of $La_{0.4}Pr_{0.27}Ca_{0.33}MnO_3$ (∼600 Å) films on (a) NGO, (b) LAO and (c) STO substrates at 0 and 1 T having characteristic MR and shift in T_{IM}. The film on STO shows melting of the charge-ordered state evident by a huge resistivity drop [300]. Reproduced with permission from [300]. Copyright 2003 by the American Institute of Physics.

in magnetization and magnetoresistance. Valencia *et al* [302] have grown 50 nm thick fully strained epitaxial films of $La_{2/3}Ca_{1/3}MnO_3$ on $SrTiO_3$ (001) substrates. After detailed analysis of the structural and magnetotransport properties of high temperature annealed film, they have found a progressive increase of out-of-plane cell parameter, as the annealing temperature rises but no change in the in-plane cell parameters are observed. Simultaneously, the magnetic transition temperature T_C and saturation magnetization, M_s, substantially increases. They argued that high temperature annealing promotes an enhancement of the itinerant charge carriers likely to be due to an oxygen uptake accompanying the lattice relaxation. Kanki *et al* [303] have deposited $La_{0.8}Ba_{0.2}MnO_3$ (LBMO) thin films on $SrTiO_3$ substrate by PLD having atomically flat surface (width of atomically flat surface was 150 nm with step height of 0.4 nm, corresponding to one unit cell of LBMO). They found room temperature ferromagnetism down to 5 nm thick films. The 5 nm thick film shows T_C at 290 K. They also observed several tens of nanoscale ferromagnetic (local magnetization) domains at room temperature (figure 26) by using non-contact magnetic force microscopy (NC-MFM). The observation of nanoscale magnetic domain behavior makes it possible to create workable

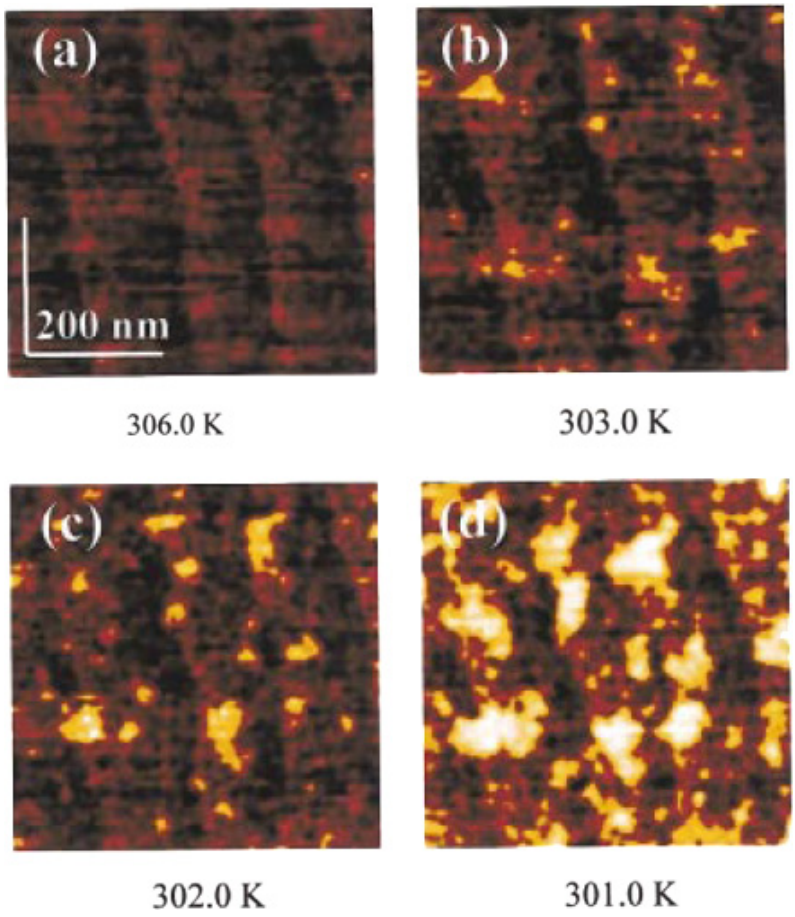

Figure 26. Temperature dependence of local magnetic domain by NC-MFM imaging of LBMO film around $T_C \sim 3003$ K. The rms roughnesses are (a) 0.156 nm at 306 K, (b) 0.191 nm at 303 K, (c) 0.223 nm at 302 K and (d) 0.267 nm at 301 K, respectively. Above T_C (a) no magnetic domain exists. At ∼303 K, a ∼20 nm wide magnetic domain appears, which goes on increasing with decreasing temperature [303]. Reproduced with permission from [303]. Copyright 2003 by the American Institute of Physics.

spintronic devices using a perovskite system, and that NC-MFM techniques will also be applicable to decide the magnetic state of nanostructural devices. Andres *et al* [304] have studied structural and magnetic properties of $La_{0.7}Ca_{0.3}MnO_3$ epitaxial films with varying thickness from 2.4 to 80 nm on $SrTiO_3$ substrate. By extensive x-ray diffraction study employing synchrotron radiation they demonstrated that for fully strained films (<12 nm) the origin of T_C reduction is due to limitation of the spin fluctuation by the film thickness. Only recently, it has been realized that, because of phase separation, different lattice parameters associated with various phases can result in large scale inhomogeneous strain in the interfacial regions of supported thin films [190], but the relation between strain, magnetic properties and electronic phase separation in manganite films remains unclear.

The interplay between substrate and film allows the modification of properties and can even enhance the magnetoresistive effect [48, 49]. There are two mechanisms by which substrates modify film properties. The first one is associated with the lattice distortion of epitaxially grown films. The substrate induces both bulk and biaxial strains in the film, which alters the physical properties of films [305–307]. The other one is associated with the dynamics of film growth and the manner of strain relaxation [308], which induce phase separation and inhomogeneities in films [309, 310]. These suggest that interesting phenomena may be observed in highly strained thin films of manganite. The influence that lattice strain appears to exert over so many properties of manganite film suggests that it could be used advantageously to tailor magnetotransport properties. These strain effects have been evaluated by the dependence of properties on the thickness and lattice matching between the films and substrates. Although consistent behaviors have been reported concerning the thickness dependence of T_C of the manganite films [290, 311, 312], disagreement exists concerning the origin of the observed phenomena. Some investigators have argued that the difference in oxygen content is the most important factor responsible for the T_C variation in manganites and that strain has less effect [293, 312], while others have claimed that a change in structure, which is strongly coupled with the electronic system, must account for the origin of the behaviors observed [290, 313].

Large LFMR has also been observed in epitaxial thin films [314–317]. It has been shown by de Andrés *et al* [317] that controlled chemical defects introduced in order to change the electron–lattice coupling in LCMO result in formation of polaron clusters just below T_C. These defects act as pinning centers for magnetic domain walls and increase their density,

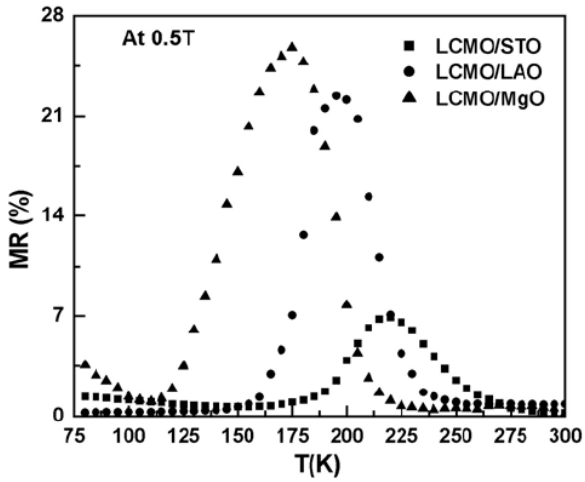

Figure 27. The temperature dependence of MR for LCMO films deposited on STO, LAO and MgO in an applied magnetic field of 0.5 T [314].

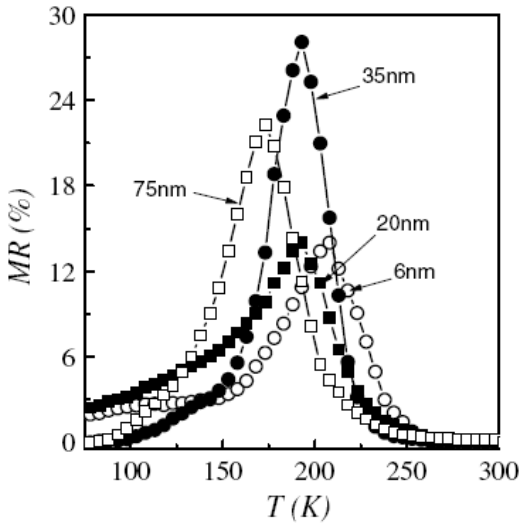

Figure 28. Temperature dependence of low field MR, measured at 3 kOe, of all $La_{0.88}Sr_{0.12}MnO_3$ films having different thicknesses (∼6–75 nm) [315].

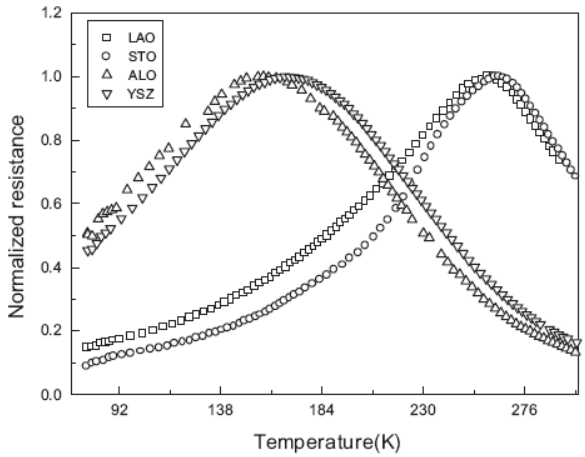

Figure 29. The temperature dependence of low field MR measured at constant dc magnetic field of 1.5 kG. Low strain relaxed films (STO and LAO) have peak MR close to the transition temperature which remains constant at ∼2–3% at low temperature, whereas the MR for high strain relax films goes on increasing as we lower the temperature (∼9%, ALO; ∼7%, YSZ) [319].

leading to enhancement of a very low field component of the magnetoresistance that is not observed at low temperature. The origin of the larger MR around T_C than the one predicted from a double exchange mechanism in LCMO is due to the delocalization of the polaron clusters below T_{MI} by moderate external magnetic fields (mostly below 5 kOe). The MR at 5 kOe increases with chemical defects, which is equivalent to an increase in electron–phonon coupling, and occurs only around T_C when the balance between extended and localized carriers is critical. Similar results have been reported by Siwach *et al* [314] and Prasad *et al* [315] for PLD-grown LCMO and DC magnetron-sputtered $La_{0.88}Sr_{0.12}MnO_3$ thin films. Siwach *et al* [314] have shown that lattice defects resulting from lattice relaxation also cause large LFMR just below T_{IM}. Increase in lattice relaxation has been found to enhance LFMR; e.g., the LCMO film on MgO (100) that has highest degree of lattice relaxation exhibits the highest LFMR ∼ 21% at 5 kOe as shown in figure 27. Prasad *et al* [315] show that in a 35 nm thin film of lightly doped manganite such as $La_{0.88}Sr_{0.12}MnO_3$ deposited on LAO(100) a large LFMR ∼ 27% at 3 kOe is observed (figure 28). This LFMR is thickness dependent, being smaller at lower film thickness. This thickness-dependent enhancement has been explained in terms of the delocalization of weakly localized carriers around T_{IM} by small magnetic fields.

Li *et al* [318] have investigated $La_{2/3}Ca_{1/3}MnO_3$ thin films have been grown on YSZ-buffered silicon-on-insulator substrates by the pulsed laser deposition technique. While full cube-on-cube epitaxy was achieved for the YSZ layer, the top manganite layer was found to be multioriented in plane, with a coexistence of cube-on-cube and cube-on-diagonal epitaxial structures. The local spin orientation was found to vary across the large angle grain boundaries as a result of combined influence from the magnetocrystalline, shape and stain-induced magnetic anisotropy, in zero field and at low temperatures. As a result, a quite large LFMR based on spin-dependent tunneling was observed. The film shows a resistance change of 20% in a magnetic field, 1 kOe at 50 K. Recently Siwach *et al* [319] found that polycrystalline thick films behave differently to lattice strain and affect LFMR by producing disorders (grain boundary density, stacking faults etc) depending on the amount of strain relaxation. A larger film–substrate lattice mismatch (as in the case of films deposited on ALO and YSZ) results in higher disorder density, that reduces T_C and gives rise to larger zero-field resistance and higher LFMR. The T_C values of the films deposited on ALO and YSZ are 254 K and 243 K respectively and corresponding LFMR (H_{dc} = 1.5 kG, 77 K) values are ∼9% and ∼7% respectively (figure 29). Similar lattice-distortion-induced disorder has also been observed for epitaxial films of LCMO by Yeh *et al* [316] and Andres *et al* [317].

Besides synthesis techniques the GBs and oxygen deficiencies are the major cause of noise in polycrystalline

CMR films, which leads to higher resistivity with low T_{IM} and T_c values [320–322]. Shreekala *et al* [323] reported that the LCMO–Ag epitaxial films exhibit enhanced T_{IM} and T_C with improved homogeneity of the films. Prokhorov *et al* [324] reported that in an epitaxial film of $La_{0.8}Ca_{0.2}MnO_3$ kept at room temperature for six months structural phase transformation occurs, which changes the characteristics of the film. Recently, Srivastava and co-workers [269, 325] studied the Ag admixing effect on polycrystalline LCMO films in relation to magnetotransport, conduction noise and stability. They observed that T_{IM} shifts to lower temperature but T_c remains the same in all the subsequent measurements for LCMO films, whereas for Ag–LCMO films both T_{IM} and T_c remain constant, which indicates improved stability of Ag–LCMO films. For LCMO film only T_{IM} shifts to a lower value while T_c remain the same with thermal cycling, which indicates that the thermal cycling is bringing change only at the grain boundaries and not inside the grains. In the polycrystalline films T_{IM} depends on the properties of both the grains and the grain boundaries, whereas T_c is the bulk property, depending mainly on the grains. They concluded that the role of Ag admixing is manifold. During the synthesis, the Ag segregation at the grain boundaries not only increases conductivity of the grain boundaries but also reduces the effect of thermal strain, i.e. disorder at the grain boundaries and hence Ag–LCMO films are stable for longer durations [323, 325]. Finally, the nascent oxygen from the decomposition of $AgNO_3/Ag_2O$ combines with LCMO [332], improves the inhomogeneity of the films by decreasing the microstructural deficiency and also enhances the conductivity of carriers through a change in Mn^{3+}/Mn^{4+} ratio [269, 330]. The reduction in conduction noise for polycrystalline LCMO film is similar to that observed by Rajeswari *et al* [333] in epitaxial LCMO film. Thus the role of Ag in CMR films is mainly that of catalyzing the grain boundary diffusion of manganite species by providing the nascent oxygen and improving the grain boundary ordering, which offers better possibility for applications.

4.1.3. Manganite-based composites. Manganite-based composites form an interesting system to study magnetotransport at low magnetic field. The extrinsic LFMR effect observed in polycrystalline materials is mainly due to spin-polarized tunneling (SPT) [236, 237] as the conduction electrons traverse the grain boundaries (GBs). Extrinsic CMR, a function of the intergrain transport between ferromagnetic (FM) particles, plays a crucial role in enhancing low field magnetoresistance (LFMR) or increasing room temperature magnetoresistance. Since extrinsic CMR is a grain-boundary-controlled phenomenon, magnetically dirty GBs in the virgin sample help in achieving a high LFMR or increase the field sensitivity and it is generally ascribed to the spin polarized intergrain tunneling of conduction electrons. Since the tunneling process takes place across the interfaces or grains separated by an energy barrier (related to the magnetic disorder), dilution of these GBs by secondary phases in manganites such as insulators, metal, polymer or another manganite etc [326–328, 334–353], which impede the magnetic homogeneity near the grain boundary, adjusts the barrier layer influencing the tunneling process, which takes place across the GBs and also influences the degree of magnetic disorder present therein. Also, since these extraneous effects act as pinning centers in remagnetization by domain wall displacement [334], a small field will align the neighboring ferromagnetic (FM) grains and hence an enhanced MR response can be achieved at low fields and at low temperatures. This is why a spin misorientation of the magnetically virgin state of the system is crucial to achieve enhanced MR at low fields, which is more useful for device application.

Recent efforts are being directed to synthesize composite materials consisting of two (or more) different manganites or manganites and polymer/insulator materials which may show large LFMR near room temperatures [326–328, 334–353]. Several groups have attempted to enhance the low temperature LFMR or the room temperature MR by making a composite of manganites with a secondary phase like an insulating oxide, a hard FM material, a polymer etc [326–328, 334–353]. Balcells *et al* [335] and Petrov *et al* [336] were the first who reported the magnetoresistance of $LSMO/CeO_2$ and $LSMO/SrTiO_3$ composites and they found enhanced LFMR near the percolative threshold. The LFMR was also found to be enhanced in composites comprising manganites like $La_{0.67}Ca_{0.33}MnO_3$(LCMO) and $La_{0.67}Sr_{0.33}MnO_3$(LSMO) with secondary phases such as an insulators (YSZ, V_2O_5, SiO_2, Al_2O_3 etc) [337–342], a hard ferromagnetic material [343], a soft magnetic material [344], a polymer material (PPP, polyparaphenylene; PMMA, poly(methyl methacrylate)) [345–347], a glass (borosilicate) [348], a metal/metal oxide (Ag, Ag_2O etc) [325–327] or with other CMR oxides (PSMO, SSMO etc) [349–351]. But in every case the basic objective is to increase the height of the tunnel barrier between the neighboring FM grains.

In a recent study Kumar *et al* [347] admixed insulating poly(methyl methacrylate) (PMMA) polymer in the nanocrystalline $La_{0.7}Ba_{0.2}Sr_{0.1}MnO_3$ (LBSMO) and observed the absence of any intrinsic physico-chemical reaction between LBSMO and PMMA [345, 346]. The LBSMO exhibits the broad T_{IM} and T_C respectively at ∼150 and 303 K with a discrepancy that can be attributed to the strong disorder due to small grain size, which may include oxygen deficiency, high density of blocked Mn spins at the GBs, increased misalignment of the neighboring FM domains etc. This grain boundary segregation of insulating PMMA affects the DE by decoupling the FM grains [343–345]. In fact, it has been shown by Yan *et al* [345] that addition of polymer (PPP) leads to the dilution of the magnetization as well as yielding additional magnetic disorder. PMMA admixing leads to a kind of inhomogeneity comprising FM metallic clusters that are separated by insulating PMMA [345], and as its concentration increases the spatial separation of these grains/clusters further increases. On application of field, these FM clusters grow in size, resulting in improved connectivity, and consequently the resistance decreases and the composites exhibit significant LFMR of ∼14% for 10% PMMA admixed LBSMO nanocomposites at 1.2 kOe, as shown in figure 30.

The GBs in polycrystalline manganites mimic the role of the thin insulating layer sandwiched between two

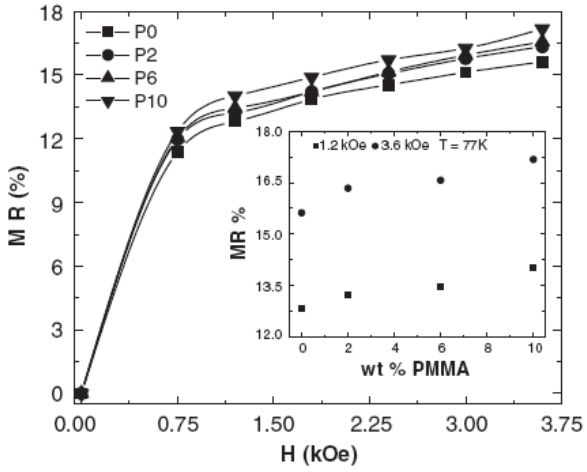

Figure 30. Magnetic field dependence of magnetoresistance of LBSMO–PMMA composite samples measured at 77 K. The MR for the LBSMO sample is 12% and it increases to 14% for 10 wt% PMMA admixed LBSMO composite. The inset shows the variation of MR with PMMA concentration [347].

FM manganite grains, which are magnetically as well as structurally disordered, having disordered Mn spins. In fact, as Mn spin disorder density increases due to PMMA admixture, the carrier scattering increases, leading to further enhancement in the resistivity, and the magnetic interaction energy also increases, and hence a higher magnetic field is needed to suppress them. When a magnetic field is applied, the spin disorder is suppressed, resulting in slightly higher MR, especially above a magnetic field $H \sim 1.5$ kOe. Thus the overall positive change in MR at lower temperatures is due to the slightly enhanced spin disorder in the intragranular regions, which leads to enhanced spin-polarized tunneling. Recently, in nanocrystalline LCMO–PMMA composites an enhancement of LFMR of ∼30–35% has been observed [347]. In another interesting study Yao *et al* [354] prepared nanocrystalline composites of LCMO–CeO_2 by means of a dispersing particle polymer-network gel method, which leads to both high field (∼70% at 50 K and 5 T) and low field magnetoresistance of ∼16% at 5 K and 0.05 T at the percolation threshold of ∼35% CeO_2 content (figure 31). They invoked that smaller grain sizes and good connectivity among neighboring grains because of the dispersing particle polymer-network gel causes enhanced LFMR in the LCMO–CeO_2 nanocomposites. The importance of manganite composites has been emphasized in a recent report on epitaxial $(La_{0.7}Ca_{0.3}MnO_3)_{1-x}$:$(MgO)_x$ [355] and $(La_{0.7}Sr_{0.3}MnO_3)_{0.5}$:$(ZnO)_{0.5}$ [356] nanocomposite films. Oriented $(La_{0.7}Sr_{0.3}MnO_3)_{0.5}$:$(ZnO)_{0.5}$ nanocomposite thin films grown by Kang *et al* [356] having fine intermixed grains have shown an enhanced LFMR of ∼12% at 1 T, whereas negligible LFMR has been observed in the postannealed films with large phase separated grains, as shown in figure 32. Bhadhur *et al* [352] and Chaudhuri *et al* [353] have extensively reviewed the low field magnetotransport properties of manganite composites.

4.1.4. Intrinsically layered manganites. Most of the studies so far have been carried out on doped $LaMnO_3$ type

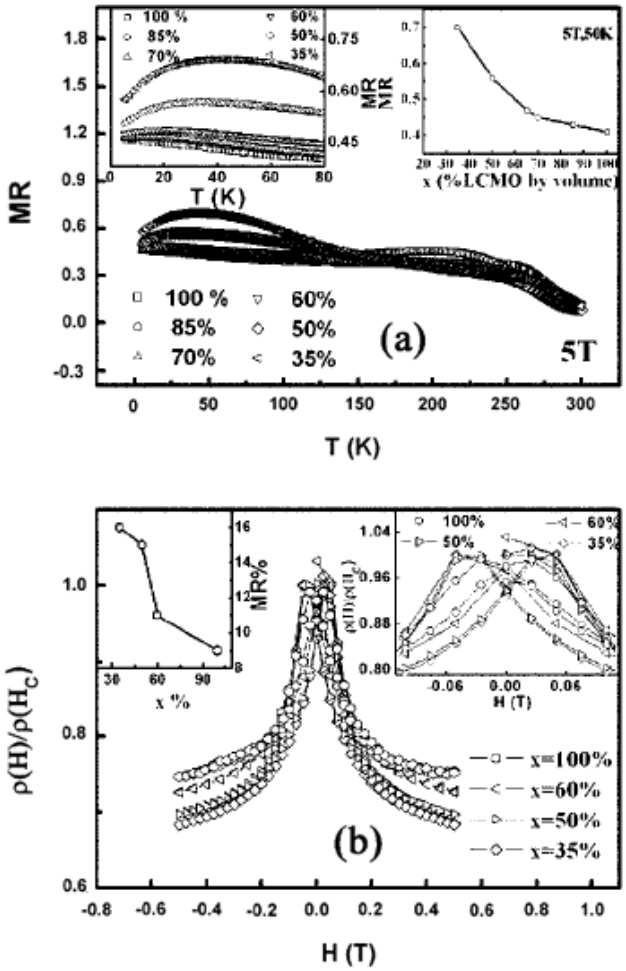

Figure 31. (a) High field MR of all composites versus temperature for different metallic (LCMO) volume fraction x. Left inset: the partial enlarged figure. Right inset: the variation of MR value with increasing x in a 5 T field at 50 K. (b) Low field dependence of resistance $\rho(H)/\rho(H_C)$ of several composites recorded at 5 K. Right inset, the partial enlarged figure; left inset, the variation of LFMR value with increasing x in a 0.05 T field at 5 K [354]. Reproduced with permission from [354]. Copyright 2007 by the American Institute of Physics.

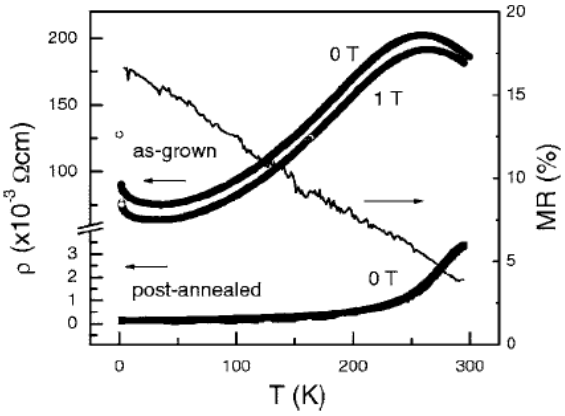

Figure 32. Resistivity, $\rho(T)$, of the as-grown films (solid circles at $H = 0$ T, open circles at $H = 1$ T) and the postannealed films (solid square) at $H = 0$ T as a function of temperature. The MR (solid line) of the as-grown films is also exhibited [356]. Reproduced with permission from [356]. Copyright 2006 by the American Institute of Physics.

perovskites such as $La_{1-x}Sr_xMnO_3$, with three-dimensional Mn–O networks (isotropic MnO_6 octahedra). They become ferromagnetic metal at hole doping of $x > 0.2$ and exhibit CMR effects [7, 232–235] along with various exotic phenomena [69, 163, 173–176, 182–184]. However, very recently Moritomo *et al* [357] discovered CMR properties in the layered $La_{1.2}Sr_{1.8}Mn_2O_7$ system ($n = 2$) akin to their 3D counterparts ($n = \infty$); thereafter followed a flurry of activity on these double-layered manganites [358, 359]. A very large CMR effect has been observed for the $n = 2$ compound above the Curie temperature. At 129 K, the MR of 200% at 0.3 T has been observed, which is significantly higher than the equivalent 3D Sr-based compound. The CMR at a few tesla is observed in a very broad temperature range from 100 K to close to room temperature. In another study, Kimura *et al* [358] reported a large MR effect in $La_{2-2x}Sr_{1+2x}Mn_2O_7$, which reveals that the magnetotransport behavior of Sr = 0.3 composition is very different from that of Sr = 0.4. In fact, at Sr = 0.3 the resistivities in plane and out of plane behave qualitatively differently. These bilayered manganites undergo a charge ordering transition at ∼210 K, having CE state ($(3x^2 - r^2)/(3y^2 - r^2)$ type). The $x = 0.5$ compound also exhibits a substantial MR effect, although the charge-ordered state could not be melted completely at a magnetic field as high as 7 T [360]. In addition to the CMR effect these bilayered manganites also show phase transitions from an FM metal to either an AFM insulator or to a PM insulator. In some compounds, the strong competition between the ferromagnetic (FM) and the antiferromagnetic (AFM) phases, below T_c, drives the system to a host of other new magnetic orders, such as a cluster glass, spin-glass-like state or to a charge- or orbital-ordered state. They also show an extremely rich variety of magnetic structures as a function of doping, which allow for the study of dimensionality effects on the charge transport and magnetic properties in these bilayered manganites [360–370]. The reduced dimensionality of these structures is anticipated to enhance the magnetic and electronic fluctuations in the critical temperature region just above T_C and in this region where external fields can harness these fluctuations to generate ordered phases and the CMR effect [360–370].

The doped double-layered perovskite manganites are a stack of FM metal sheets composed of MnO_2 bilayers, which are separated by the insulating $(RE, AE)_2O_2$ layers and thus form a natural array of ferromagnetic–insulator–ferromagnetic (FM–I–FM) junctions [357, 363]. It has been observed that the incorporation of the MnO_2–$(RE, AE)_2O_2$–MnO_2 junctions in the structure naturally leads to higher magnetoresistance, especially low field magnetoresistance (LFMR), in these layered manganites than the infinite layer simple perovskite counterparts [357, 362, 363, 371, 372]. The individual bilayers consisting of the FM–I–FM (MnO_2–$(RE, AE)_2O_2$–MnO_2) layers are themselves weakly coupled along the *c*-axis, resulting in a quasi-two-dimensional FM order in these materials and anisotropic exchange interaction. Around room temperature the double-layer compounds with $x = 0.3$ and 0.4 are paramagnets and around $T \sim 270$ K a short range FM order due to in-plane spin coherence evolves and the long range FM order corresponding to both in-plane and out-of-plane spin coherence evolves at a much lower temperature [357, 363, 373, 374].

The double-layer manganites consist of two building blocks, namely, the perovskite block incorporating MnO_6 octahedra and the rock salt separation layer containing $(RE, AE)_2O_2$. Thus the RE(AE) ions are located in the perovskite block as well as in the rock salt layer, and the distribution of the various RE(AE) cations between these two building blocks is dependent on the dopant ion size. Consequently, the magnetotransport properties are expected to show a rather complicated correlation with the average RE(AE) site radius. It is well known that the average or effective cationic radius of the rare earth site plays a crucial role in determining the magnetotransport properties of the infinite layer manganites [375, 376], and some studies in this direction have also been carried out on the double-layer manganites [371, 372, 377, 378]. Shen *et al* [371] have studied the effect of Ca^{2+} (∼1.18 Å) substitution in $La_{1.2}Sr_{1.8}Mn_2O_7$, in which the average La-site radius is ∼1.272 Å, and have observed a gradual decrease in the paramagnetic to ferromagnetic transition temperature T_C from 135 K for Ca = 0.0–82 K for Ca = 0.6. This observed decrement in T_C has been attributed to the contraction of the lattice unit cell due to substitution of smaller Ca^{2+} cations in place of larger Sr^{2+} (∼1.31 Å) cations. Somewhat similar results have been observed by Chi *et al* [377] for $La_{1.4}Sr_{1.6}Mn_2O_7$ ($\langle R \rangle = 1.266$ Å). They report that the T_C and the insulator–metal temperature (T_{IM}) both decrease when Sr^{2+} is partially substituted by either a bigger cation like Ba^{2+} (∼1.47 Å) or a smaller cation, Ca^{2+} (∼1.18 Å). Chi *et al* [377] suggests that a preferential distribution of various cations between the rock salt and the perovskite blocks is responsible for the observed trends in the T_C and T_{IM}. However, this study leaves a fair amount of ambiguity regarding the correlation between the average La-site cationic radius and the various transport parameters. Recently Zhu *et al* [374, 379] have studied the compound $La_{1.4}Sr_{1.6-x}Ba_xMn_2O_7$ and found that with increasing Ba content the long range or 3D FM order diminishes and finally disappears beyond $x = 0.3$, and on further increasing the Ba content the 2D or in-plane FM phase fraction increases and induces a IM transition at the percolative threshold [374, 379]. In another study Singh *et al* [380] studied the effect of co-doping Ca and Ba at the La site in $La_{1.4}Ca_{1.6-x}Ba_xMn_2O_7$ ($x = 0.0, 0.2, 0.4, 0.6$) bulk polycrystals. They observed that large Ba^{2+} cations occupy the perovskite block while the smaller La^{3+} and Ca^{2+} cations go preferentially to the rock-salt layer, which leads to anisotropic change in the unit cell. This leads to reduction in the distortion of the MnO_6 octahedra in the perovskite block, which consequently leads to a reduction in the electron–lattice coupling via weakening of the cooperative Jahn–Teller distortion. They show that both T_C and T_{IM} increase with Ba content and Ba ∼0.6 has a maximum T_C and T_{IM} of ∼185 K and ∼136 K respectively. The drastic difference in the T_C and T_{IM} is a known feature and is due to the intrinsic anisotropy in the magnetic exchange interaction [357, 362, 371, 372]. All the samples show the low field magnetoresistance (LFMR) (figure 33(a)), which increases with the Ba content, and

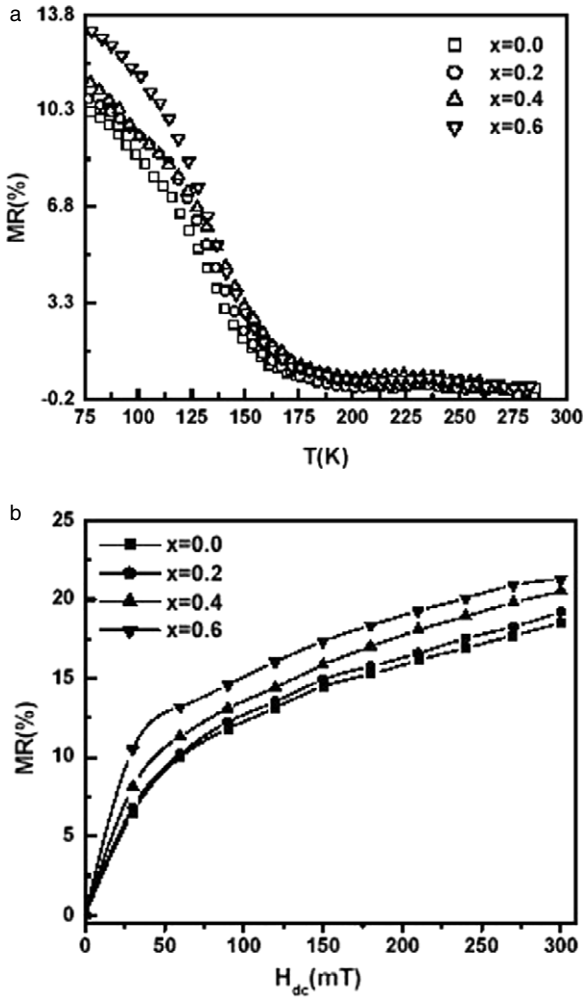

Figure 33. (a) Variation of low field magnetoresistance (LFMR) with Ba content with temperature at 150 mT. The MR at 77 K increases from ∼10.2% for Ba = 0.0 to ∼13.5% for Ba = 0.6. (b) Variation of low field magnetoresistance (LFMR) with Ba content at different magnetic fields at 77 K. The LFMR values are measured to be ∼18.5, 19.1, 20.7 and 23.8 respectively for Ba content of 0.0, 0.2, 0.4 and 0.6 [380].

maximum LFMR of ∼13.5% has been observed at 77 K. The field evolution of LFMR shows (figure 33(b)) that the Ba-doped samples have much larger MR than the virgin sample. They do not observe any saturation-like features in the LFMR–H curves, which are usually seen in the infinite layered manganites, and such a behavior may be attributed to the intrinsic contribution to the LFMR by the stacking of the $La(Ca, Ba)_2O_2$–MnO_2–$La(Ca, Ba)_2O_2$ layers in the unit cell of the layered manganites.

The epitaxial films of $La_{2-2x}Sr_{1+2x}Mn_2O_7$ have also been observed to exhibit anisotropy in transport properties and high field magnetoresistance in excess of 99% [381, 382]. The Ca-doped double-layer compound, namely $La_{2-2x}Ca_{1+2x}Mn_2O_7$ has been reported to exhibit higher T_C values; e.g., $La_{1.6}Ca_{1.4}Mn_2O_7$ ($x = 0.2$) has a $T_c \approx 170$ K, which rises to 215 K for a doping level $x = 0.25$ [360, 362, 363], and they have significant LFMR below T_C [360–362]. In another study of double-layered manganite films Siwach *et al* [383] observed reasonable low field magnetoresistance of ∼5% at 0.6 kOe and ∼13% at 3 kOe in polycrystalline spray-deposited $La_{1.4}Ca_{1.6}Mn_2O_7$ films. Weak short range in-plane FM spin coherence sets in at 125 K [361], which transforms to a complete long range FM ordering below $T_C \sim 95$ K. On further lowering the temperature a spin-glass-like state is observed at $T_{CA} \sim 50$ K, suggesting the magnetic frustration between competing FM double-exchange (itinerant e_g electrons) and the antiferromagnetic (AFM) superexchange (localized t_{2g} electrons) interaction [382]. Metal–insulator transition occurs at a lower temperature $T_{IM} \sim 55$ K. Resistivity shows an upturn in the spin-canted regime, suggesting increased scattering of the conduction electrons due to the canting of Mn spins [382, 384, 385]. The low field magnetoresistance (∼5% at 0.6 kOe and ∼13% at 3 kOe) has been attributed to complete spin-polarized tunneling of charge carriers through the insulating $(La, Ca)O_2$ layers between the adjacent MnO_2 bilayers, supported by strong non-linearity in I–V characteristics below T_C. Similarly, Asano *et al* [373] and Zhou *et al* [360] also obtained significant MR of ∼40% at 18 kOe applied field and ∼25% at 10 kOe, respectively.

4.2. Artificial grain boundaries system

Several other studies [386–394] using polycrystalline films have probed the role of grain boundaries in samples consisting of multiple grains with different orientations over the measurement distance of the probe contacts, which gives only qualitative information, because the total MR contribution is a complex convolution of the MR due to the 'intrinsic' CMR contribution inside the grain and the 'extrinsic' contribution coming from the GBs. Bicrystal [395–406] and step-edge/laser-patterned [407–411] junctions consisting of a single grain boundary, with a well defined misorientation between the grains, are ideal for the growth of films in order to isolate the contribution of a single grain boundary. In order to enhance the grain boundary contribution to the total ρ, the number of grain boundary intersections is increased by patterning a meander track on the substrate. Reduction of the grain region that is probed will lead to further enhancement of the grain boundary signal.

4.2.1. Bicrystal grain boundary junctions. Mathur *et al* [395] have followed such an approach to pattern thin film devices on a bicrystal substrate in order to isolate the contribution of a single grain boundary. They deposited epitaxial LCMO (∼2000 Å) films by PLD on $SrTiO_3$ (001) bicrystal substrates with a misalignment between two crystallographic directions by 24°. In order to study the artificial grain boundary directly, the manganite films are patterned into a meander-like track (Wheatstone-bridge structures) crossing the grain boundary many times, using optical lithography and ion milling, as shown in figure 34(a). The symmetry of the bridge structures ensures that all resistance contributions balance to zero, except those arising from the grain boundary. The devices have been characterized in a liquid nitrogen cryostat in a magnetic field up to 300 mT by passing a constant current through each bridge and measuring the voltage across the output

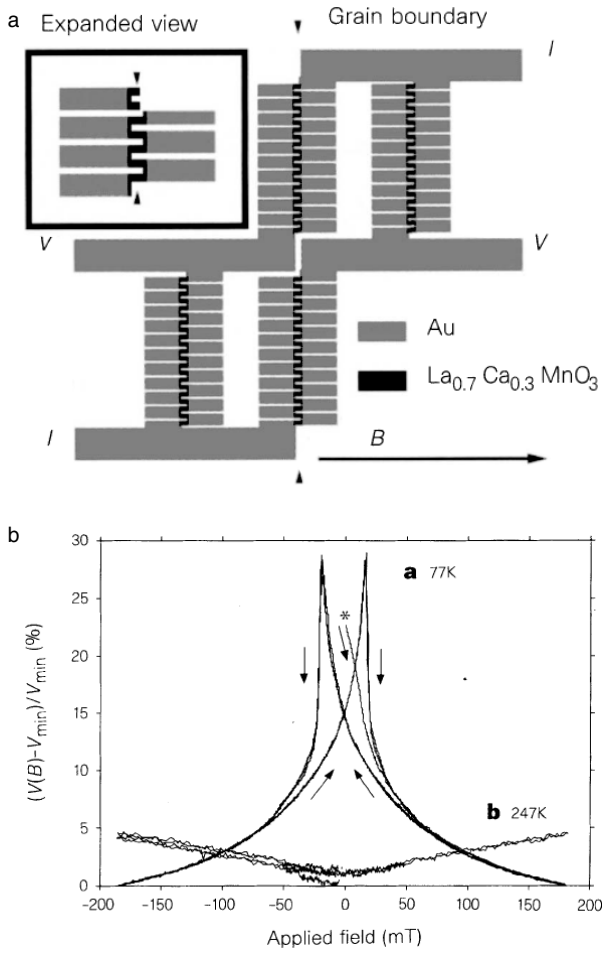

Figure 34. (a) The meander track Wheatstone-bridge geometry used for the grain boundary measurements. Each arm consists of 19 CMR elements, 2 μm wide (shown black), those on two of the arms crossing the grain boundary (dashed line), the other two-sample control material. The gold (marked in gray) was added to the structure to reduce the resistance of the wiring between the arms and the links between the elements. The bridge structure for measurement along the grain boundary was similar except that the meander was replaced by a single straight track in each case. (b) Wheatstone-bridge measurements with $I = 1.5$ μA with B in-plane and perpendicular to the grain boundary, at (a) 77 K and (b) 247 K. Voltages $V(B)$ and V_{min} are the field-dependent output voltage and the minimum output voltage measured. The asterisk indicates data taken following zero-field cooling to 77 K. Data taken following cooling to 77 K in 300 mT are also presented, but can barely be distinguished. Reprinted by permission of Macmillan Publishers Ltd: *Nature* [395], copyright (1997).

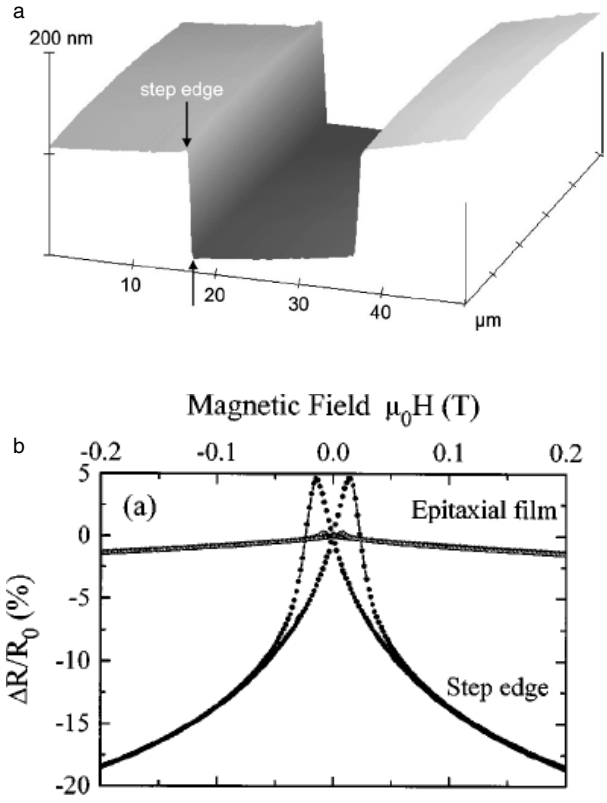

Figure 35. (a) Atomic force microscopy image of two step edges on a $LaAlO_3$ substrate. Grain boundaries might nucleate near the edges, such that there are two grain boundaries per step-edge. (b) Magnetoresistance ratio at 100 K of an epitaxial film and step-edge arrays along [100] and [110], respectively [407]. Reprinted with permission from [407]. Copyright 2002 by the American Physical Society and 1999 by the American Institute of Physics.

terminals. This measured voltage represents a direct measure of the resistance introduced by the grain boundary. A large bridge MR (27% at 77 K) is observed during magnetic field sweeps within $\pm$200 mT over a range of temperatures down to 77 K, with a strong low field hysteresis in bridge resistance at low temperatures (figure 34(b)). At higher temperatures, the magnitude of the peaks in MR decreases and the peaks disappear altogether at temperatures around 230 K. These results are qualitatively similar to those observed on polycrystalline films except for the magnitude of the low temperature MR, which is about a factor of two to three higher for the single grain boundary junctions. Interestingly, a small positive MR is observed above T_c, which is masked in experiments using polycrystalline samples by the contribution from the grains. Steenbeck *et al* [396], Westerburg *et al* [397], Evetts *et al* [398], Miller *et al* [399], Phillip *et al* [400], Mathieu *et al* [401] and several others [402–406] have also reported similar field dependence of LFMR in bicrystal grain boundaries.

4.2.2. Step-edge junctions. Ziese *et al* [407] investigated step-edge junctions made from LCMO films. $LaAlO_3$ substrates were patterned prior to film deposition by chemically assisted ion-beam etching such that an array of steps along [100] or [110] was formed. The steps were 100–200 nm high and 20 μm apart; the substrates contained 150 [100] or 200 [110] steps, respectively. 25 nm thick LCMO films were deposited on the patterned substrates using pulsed laser deposition. These films show large resistance anisotropy, the resistance showing intrinsic behavior for electric currents flowing along the steps and typical grain boundary behavior for currents across the steps. This resistance anisotropy can be related to disordered regions near the step edges. In comparison to epitaxial films, the magnetoresistance is strongly enhanced (figure 35). The magnetoresistance value at fixed field and temperature seems to be determined by the local defect structure and varies between different samples. After

annealing the film deposited on [100] step edges at 950 °C for 2 h in flowing oxygen, the resistance and magnetoresistance resumed the typical behavior of epitaxial films. Bosak *et al* [408] have also obtained low field magnetoresistance of step-edge junctions based on $La_{0.7}Sr_{0.3}MnO_3$ films on $SrTiO_3$ substrate. Similar results were obtained on 'scratch' junctions by Srinitiwarawong and Ziese [409].

4.2.3. Laser-patterned junctions. Another artificial junction, which is important for low field magnetotransport, is the laser-patterned planar junction. Bibes *et al* [410, 411] studied the temperature and magnetic field dependence of the magnetotransport properties of laser-patterned planar junctions. A 248 nm KrF excimer laser with a fluence of about 2.5 J cm^{-2} was used to define tracks of 10 and 40 μm width on $SrTiO_3$ substrates. These tracks consisted of overlapping discs of molten material, about 0.1–0.2 μm deep. Microcrack formation was observed within these disc regions. LSMO films were deposited by pulsed laser deposition on these patterned substrates. Strongly enhanced resistance was only found for the 40 μm wide tracks. However, both 10 and 40 μm tracks lead to a significantly enhanced low field magnetoresistance with the characteristic magnetic field and temperature dependence.

The above discussions make it evident that in the polycrystalline samples (both bulk and thin films) having natural grain boundaries as well as artificially engineered grain boundaries (bicrystal and step-edge junctions) the colossal magnetoresistance (CMR) effect can be observed at compatibly low magnetic fields (∼mT), which is important since it interfaces directly with the application aspect of CMR.

5. Recent observations of magnetoresistance in other materials and relevant mechanism

The discovery of the CMR effect in doped perovskite manganites revolutionized material science and a lot of effort has been carried out (and is still going on) to find materials with improved magnetoresistance around room temperature at low magnetic fields. The analogies with manganites and other magnetoresistive materials are based on the presence of a large magnetoresistance, a competition between FM and AFM states and universally accepted inhomogeneities. Based on the above analogies, the magnetoresistive family consists of a large number of materials having different crystalline structures. These materials are the following.

(i) *Mn-based pyrochlores.* $Tl_2Mn_2O_7$ show metal–insulator transition and large intrinsic magnetoresistance at a Curie temperature of 140 K with a saturation magnetic moment of 3 μ_B per formula unit, corresponding to a ferromagnetic ordering of the Mn^{4+} ions [412–421]. The pyrochlores are interesting in comparison with manganites as their large magnetoresistance does not arise from a conventional double-exchange mechanism [416]. Instead, the ferromagnetism is predominantly dominated by superexchange, and the conduction electrons likely arise from the Tl 6s band [417]. Thus in $Tl_2Mn_2O_7$ there are two separate electronic systems, a magnetic sublattice of Mn–O and a conducting sublattice of Tl–O indirectly coupled to it. Because of the lack of Mn^{3+}, there is no strong electron–lattice coupling driven by the Jahn–Teller energy gains. In the pyrochlore, a large degree of spin polarization appears to be due to the extremely small number of carriers [413]. The value of T_c, the magnitude of the resistivity peak near T_c for $Tl_2Mn_2O_7$ and the corresponding MR are generally altered by isovalent (Sc, Bi, Ru) or aliovalent substitutions [418–421]. Alonso *et al* observed room temperature MR and cluster glass behavior in $Tl_{2-x}Bi_xMn_2O_7$ [422].

(ii) *Cr-based chalcogenides.* Ramirez *et al* [423] have demonstrated moderately large high field magnetoresistance near the Curie temperature in the Cr-based chalcogenide spinels, i.e. $Fe_{1-x}Cu_xCr_2S_4$. The spinel ACr_2Ch_4 is a tetrahedrally coordinated compound, where cation A = Fe, Cu, Cd and Ch is a chalcogen, i.e. S, Se and Te [424]. However, unlike the perovskite manganites, they do not possess heterovalency, distortion-inducing ions, manganese, oxygen or a perovskite structure. The transport in these materials is due to electron hopping among d^5 states above a valence band comprised of chalcogenide p-levels [425]. Theoretical studies of the electronic structure indicate a half-metallic character with a gap in the minority density of states [426].

(iii) *Ordered double perovskite.* Another promising compound of the LFMR family is the double perovskite Sr_2FeMoO_6 [427] and Sr_2FeReO_6 [428] with comparatively high Curie temperature of 420 K and 400 K, respectively. The structure is obtained by doubling the perovskite unit cell, e.g. Sr_2FeMoO_6 has alternate stacking of $SrFeO_3$ and $SrMoO_3$ to form an ordered double perovskite structure. The highest Curie temperature was reported for Ca_2FeReO_6 with $T_c \sim 540$ K [429]. These materials are half-metallic in nature. Single crystals [430] do not show significant MR but a substantial low field magnetoresistance (∼5% at 300 K and ∼20% at 5 K for $H \sim 1$ T) [431, 432] often appears in polycrystalline samples that are likely to be of extrinsic origin from grain boundary or cation disorder scattering, similar to that of the grain boundary MR observed in manganites [433]. Westerburg *et al* [433] observed 5% MR under 8 T field at Curie temperature in Sr_2FeMoO_6. Serrate *et al* [434] have recently presented an excellent review on the structural, magnetic and transport properties of FeMo- and Re-based double perovskites with ferromagnetism above room temperature. In particular, they focus on the large intergrain magnetoresistance effect observed in polycrystalline samples and the possible implementation of these materials for device application.

(iv) *Hexaborides.* EuB_6 also shows a very large MR, but it is completely different from the manganites. EuB_6 is a ferromagnetic semimetal, and consequently the effective mass and the number of carriers is small [435, 436]. It shows two magnetic transitions at 12.5 and 15 K [437]. A spin-flip Raman scattering shows the existence of magnetic polarons [438]. Doped EuB_6 e.g. $Eu_{1-x}La_xB_6$ [439] and $EuB_{6-x}C_x$ [440] also show substantial MR. Other Eu-based materials, i.e. EuSe [441] and $Eu_{1-z}Gd_xSe$, also show MR similar to manganites.

(v) *Ruthenates.* Ruthenates are materials that are also receiving considerable attention currently [442]. In a single-layer material $Ca_{1-x}La_xRuO_4$ a dramatic decrease in the resistivity is observed upon La doping and the Mott insulator ($CaRuO_4$) eventually reaches a metallic state [443]. The resistivity versus temperature curves are similar in shape to those found in manganites. Both manganites and ruthenates present metallic and insulating states that can compete with each other. Ruthenates also show orbital ordering similar to manganites [444]. Recently, CaO *et al* [445] discovered tunneling magnetoresistance, due in part to the magnetic-valve effect, with a drop in the resistivity of the bilayer $Ca_3Ru_2O_7$ by three orders of magnitude. Very recently, Ohmichi *et al* [446] demonstrated the existence of two types of field-induced transitions at 6 and 15 T in $Ca_3Ru_2O_7$. They attributed these behaviors to strong coupling between spin, charge and lattice degrees of freedom in $Ca_3Ru_2O_7$, which can be controlled by in-plane field orientation. Another ruthenate, $SrRuO_3$, is a strongly correlated ferromagnetic d-band metal having orthorhombic structure. The Curie temperature in the bulk is 165 K; for thin films reduced Curie temperatures of 150 K were observed, possibly due to the strain effect [447, 448]. Near the Curie temperature a maximum in the MR was observed for $SrRuO_3$, that does not saturate in magnetic fields up to 8 T. The value of peak MR depends on the current and field direction, with values between -2 and -11%. Klein *et al* [449] interpreted this MR peak as arising from an increase of the magnetization and corresponding reduction of spin disorder scattering.

(vi) *Magnetite.* Fe_3O_4 is a ferrimagnetic oxide crystallizing in the inverse spinel structure and has the highest Curie temperature of 858 K among all magnetoresistive materials [450]. At room temperature, in this structure large O ions are located on a close-packed face-centered cubic lattice, whereas the Fe ions occupy interstitial sites. There are two kinds of cation sites, namely the tetrahedrally coordinated A site occupied only by Fe^{3+} ions and the octahedrally coordinated B site occupied by both Fe^{2+} and Fe^{3+} ions. The A- and B-site sublattices are ferrimagnetically aligned such that the net moment is equal to the magnetic moment $\mu = 4\ \mu_B$ of the Fe^{2+} ($3d^6$) ion [451]. Recently, Ziese *et al* [452] observed a few per cent MR in Fe_3O_4 single crystals at the Verwey transitions and explained it on the basis of the shift of the charge ordering/Verwey transition on application of magnetic field. The temperature dependence of resistivity is quite complex, changing from semiconducting to metallic behavior slightly above room temperature and back to semiconducting behavior near the Curie temperature [453]. Band structure calculations indicate a half-metallic nature with a gap in the major density of states [454]. Recently Liu *et al* [455] observed ∼7.4% MR at room temperature in polycrystalline Fe_3O_4 films (figure 36), which they ascribed to spin-dependent tunneling through the antiferromagnetically coupled grain boundaries.

(vii) *Chromium oxide.* CrO_2 is the only stoichiometric binary oxide that is a ferromagnetic metal having rutile structure. It is the simplest and best studied half-metal [456]. Band structure calculation of CrO_2 predicted 100% spin polarization at Fermi level [457] and spin-polarized photoemission and

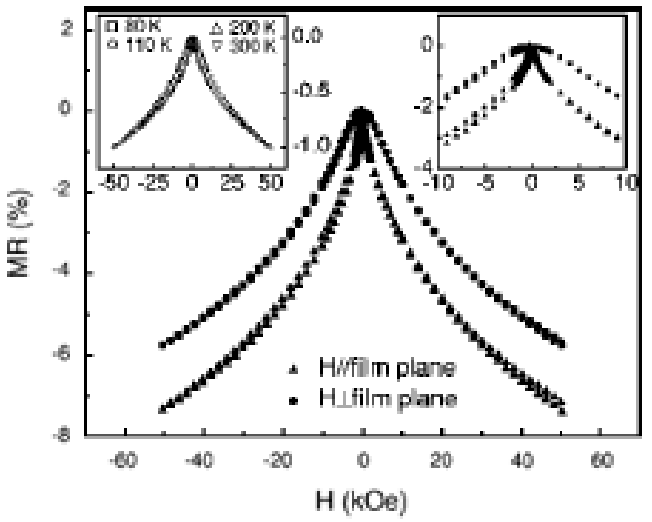

Figure 36. Parallel and perpendicular MR measured at 300 K. The inset shows normalized MR at different temperatures (left) and low field MR (right). Reproduced with permission from [455]. Copyright 2003 American Institute of Physics.

vacuum tunneling experiments showed nearly complete spin polarization 2 eV below E_F [458, 459]. The resistivity of CrO_2 varies widely, from semiconducting to metallic, and ranges over five orders of magnitude at low temperature [460]. Change in the slope of the resistivity is discernible near the Curie temperature of 390 K. The MR effect in CrO_2 is associated with transport of spin-polarized electrons from one FM region to another with a different direction of magnetization. These regions are not usually separated by a domain wall but by a grain boundary. The MR effect at low fields and low temperature can reach 50% in pressed CrO_2 powder [461, 462], and several hundred percent in planar manganite tunnel junctions [463], whereas small MR has been observed in CrO_2 tunnel junctions [464, 465].

(viii) *Diluted magnetic semiconductors.* At present diluted magnetic semiconductors (DMSs) are the hottest candidates for spintronic devices [466]. Most of the past work on DMSs has focused on (Ga, Mn)As and (In, Mn)As [467, 468]. But the problem with these DMSs is that they have low Curie temperature. Dietl *et al* [469] theoretically predicted that GaN and ZnO would exhibit ferromagnetism above room temperature on doping with Mn, provided that the hole density is sufficient high. Currently a number of excellent reviews are available which cover experimental as well as theoretical aspects of all types of DMSs including oxide-based DMSs, e.g. ZnO, TiO_2 and SnO_2 doped with Mn, Ni, Co, Fe, V etc [470–473]. Since then a great deal of effort has been focused on semiconductors, e.g. ZnO, TiO_2 and SnO_2 doped with ferromagnetic elements (Mn, Fe, Co, V, Ni etc) [474–490]. Among them a ZnO-based DMS would be very promising because of its widespread application in electronic devices, such as transparent conductors, gas sensors, varistors, ultraviolet laser sources and detectors [478–480]

Kim *et al* [481] measured the isothermal MR of $Zn_{1-x}Co_xO$:Al thin films for $x = 0.02$, 0.06, 0.10 and 0.15 at various temperatures. They observed three different types

of MR behavior below 20 K depending on the Co content, but above 50 K all samples exhibit a very small negative MR as observed in a ZnO:Al film without magnetic impurities. A large positive MR of ∼60% at 5 K under 2 T was observed in $Zr_{0.94}Fe_{0.05}Cu_{0.01}O$ below 100 K [482]. Despite non-magnetic elements, ZnO:S films also show a large MR of ∼26% at 3 K [483]. Similarly, Co-doped TiO_2 films also show MR under an 8 T magnetic field at 3 K which increases from ∼6% in an undoped TiO_2 film to ∼40% in 2% Co-doped TiO_2 film ($Ti_{0.98}Co_{0.02}O_{2-\delta}$) [484].

Prellier *et al* [485] have recently reviewed the oxide-based DMSs. They conclude that most of the Co-doped ZnO films exhibit FM above room temperature, and that in the case of Mn-doped ZnO thin films a definitive T_c is not found by some workers, but Sharma *et al* [486] recently reported room temperature ferromagnetism in Mn-doped ZnO bulk as well as thin films ($Zn_{1-x}Mn_xO$; $x = 0$, 0.01, 0.0 and 0.1). Thus the ferromagnetic behavior of Mn- and Co-doped ZnO have considerable doubt. Recently Rao *et al* [487] extensively studied the ferromagnetism of Mn- and Co-doped ZnO and pointed out that the presence of additional charge carriers is responsible for ferromagnetism rather than the mere doping of Mn and Co in ZnO, which is in agreement with the recent work of Spaldin [488].

(ix) *Doped silver chalcogenides.* Recently, an anomalously large MR was observed in two doped silver chalcogenides, $Ag_{2+\delta}Se$ and $Ag_{2+\delta}Te$, where the resistance displayed a positive linear dependence on the magnetic field over a temperature range 4.5–300 K without any sign of saturation at fields as high as 60 T. At room temperature and in a magnetic field of ∼55 kOe, Ag_2Se and Ag_2Te show ∼200% increase in resistance, which is close to CMR materials [491, 492]

(x) *Magnetic tunnel junctions.* Magnetic tunnel junctions (MTJs) show tunneling MR that is drawing considerable attention due to the advent of sophisticated thin film junction preparation techniques [493]. An MTJ consists of two ferromagnetic metallic layers separated by a thin insulating barrier layer. The insulating layer is so thin (a few nanometers or less) that electrons can tunnel through the barrier if a bias voltage is applied between the two metal electrodes through the insulator. The most important property of an MTJ is that the tunneling current depends on the relative orientation of the magnetization of the two FM layers, which can be changed by an applied magnetic field. This phenomenon is called TMR or JMR (junction magnetoresistance). TMR is a consequence of spin-dependent tunneling (SDT) due to an imbalance in the electric current carried by up-and down-spin electrons through a tunneling barrier. SDT was discovered in pioneering experiments by Tedrow and Meservey [494]. The relationship between SDT and TMR was explained by Julliere [495] within a simple model that quantifies the magnitude of TMR in terms of the spin polarization (SP) of the ferromagnetic electrodes as measured in the experiments on superconductors [496]. As per Julliere's model the TMR is given as

$$\mathrm{TMR} = \frac{2\rho_1\rho_2}{1-\rho_1\rho_2},$$

where $\rho_i = \frac{\rho_i^{\uparrow}-\rho_i^{\downarrow}}{\rho_i^{\uparrow}+\rho_i^{\downarrow}}$ $(i = 1, 2)$ is the effective spin polarization of two electrodes. For the case of two identical ferromagnets, the TMR is always −ve. It diverges for two half-metallic electrodes. It can be both +ve and −ve.

A few years ago, however, Miyazaki and Tezuka [496] demonstrated the possibility of large values of TMR in MTJs with Al_2O_3 insulating layers. Moodera *et al* [497] reported TMR values for a $Co/Al_2O_3/Ni_{80}Fe_{20}$ junction of 20.2%, 27.1% and 27.3% at 295, 77 and 4.2 K, respectively. Various workers have reported TMR values in excess of 100% at 4.2 K for ferromagnetic oxide tunneling junctions based on manganite electrodes [498–506]. Recently, extremely large TMR values up to 1800% were obtained by Bowen *et al* [507] in an LSMO/STO ($t_{STO} = 2.8$ nm)/LSMO/Co/Au structure. The extremely large TMR response (1800%) at 4 K leads to a spin polarization of the LSMO at the interface with STO of at least 95%. Moreover, the temperature dependence of the TMR in this optimally etched junction vanishes only at $T = 280$ K ($T/T_c = 0.7$). Strains as well as the mixed valency of Mn ions at the interface are the deciding factors to have large TMR response, as deduced from EELS measurements coupled with HREM observations by Pailloux *et al* [508]. Very recently, Yamada *et al* [509] atomically engineered the interface of LSMO with STO and LMO [LSMO(0.4)/LMO(2uc)]/STO(2 nm)/[LMO(2uc)/LSMO(0.4)] and observed an improved performance as compared to the direct-interface junction (LSMO/LMO/LSMO; LSMO/STO/LSMO).

(xi) *Nanocontacts.* Another type of material which is making news in the last couple of years is nanocontacts, which show ballistic magnetoresistance (BMR). When the size of the contact between two FM electrodes is of the order of nano- or atomic scale then the spin-polarized electron on its way through the contact will have less of a chance to accommodate itself to the spin regime of the secondary electrode (if it is different from that of the first electrode) and will consequently scatter more prominently, translating into a ballistic MR effect [510, 511]. Recently, Chopra and Hua (2002) of Sunny Buffalo reported remarkably large room temperature BMR of 3150% in fields of 500 Oe at room temperature in electrodeposited Ni nanocontacts [512]. In subsequent study they observed 10 000% BMR in fields of 3000 Oe at room temperature for stable Ni nanocontacts, which were made using only mechanically pulled Ni wires to eliminate the possibility of any extraneous chemical layer being present [513]. The BMR is formulated by Tatara *et al* [514] and is given by

$$\mathrm{BMR} = \left(\frac{2\rho^2}{1-\rho^2}\right)F,$$

where $\rho = (\frac{D_\uparrow - D_\downarrow}{D_\uparrow + D_\downarrow})$ describes the spin polarization, $D_\uparrow$ and $D_\downarrow$ are the densities of states for up and down spin at the Fermi level and F is a function that describe the non-conservation of conduction electron spin. If the domain wall width is comparable to or smaller than the electron wavelength, the spin should be conserved ($F = 1$) in the conduction process and the BMR is given only by degree of polarization [515, 516].

The BMR is a result of the spin-dependent scattering (SDS) of electrons across the nano- or point contact from a ferromagnetically aligned state (low resistance) to an antiferromagnetically aligned state (high resistance) in an applied field. In bulk ferromagnets, Cabrera and Falicov [515] and later Tatara and Fukuyana [516] have shown that the SDS by domain walls is negligible, owing to the adiabatic nature of electron transport across a wall, which is typically of the order of several tens of nanometers wide. The SDS, the nature of domain walls [517] and the geometry of nanocontacts [518] play a key role in the observed huge BMR effect but the cause of such a huge resistance change is not fully understood. Recently, a plausible mechanism for the observed large BMR was given by Tagirov *et al* [519] on the basis of spin splitting of quantized conduction states.

6. Envisaged applications of manganites

Perovskite manganites, initially, demonstrated a large potential for applications based on their various physical and chemical properties [232–235, 297, 298]. The magnetic field sensitivity of the transport properties, the strong metal insulator transition at the Curie temperature, the electric field polarizability of the material and its subsequent effect on the transport properties, the half metallicity of the electronic bands etc could possibly be exploited in a variety of devices. Based on the properties, a number of device approaches are being explored and few of them are described below.

(1) The magnetoresistance of manganites might be used in magnetic sensors; magnetoresistive read heads and magnetoresistive random access memory. Magnetic sensors can be made from either thin films or single crystals and can be used to sense the magnitude of a magnetic field in one or several directions by choosing the right crystal form and de-magnetizing factor. A good low field magnetoresistive response, however, can be obtained in manganite samples with a high density of grain boundaries and in tunnel spin valve structures. One of the first working devices of this kind was constructed by Sun *et al* [498]. It consists of two layers of ferromagnetic $La_{0.67}Ca_{0.33}MnO_3$, separated by an $SrTiO_3$ spacer layer, and shows a resistance decrease by a factor of two in a field of less than 200 Oe. The disadvantage of devices based on grain boundary magnetoresistance or on ferromagnetic tunneling junctions is that large magnetic field sensitivities are only achieved at temperatures below 200 K.

(2) The electric field effect has also been observed in manganites. Here the top layer can be paramagnetic, such as STO [520], or a ferroelectric layer, such as PZT ($PbZr_{0.2}Ti_{0.8}O_3$), and the bottom layer is a CMR material, but the changes are more profound in the case of PZT, where only 3% change in the channel resistance is measured over a period of 45 min at room temperature, which makes this material attractive for non-volatile ferroelectric field effect device applications [521, 522].

(3) The large temperature coefficient of resistance (TCR, calculated as $(1/R)(dR/dT)$) just below the resistivity peak makes these CMR materials interesting for use in bolometric detectors [523–525]. A bolometer is an instrument for detecting and measuring radiation. Indeed, the TCR can reach 15% per degree at 300 K [255], which is larger than that of VO_2, the material commonly used in bolometers.

(4) Since the properties of the CMR materials are quite spectacular at reduced temperatures, i.e. below 100 K, so at these low temperatures the combination of high-T_C superconducting cuprate thin films and CMR manganites could lead to hybrid HTSC–CMR structures [526, 527] These HTSC–CMR structures not only lead to potentially new spin-injection devices but also may serve as a useful medium for understanding some of the forefront theoretical ideas.

(5) Chemical applications include catalysis, such as catalysts for automobile exhausts, oxygen sensors and solid electrolytes in fuel cells. The catalytic activity is associated with the Mn^{3+}–Mn^{4+} mixed valence and the possibility of forming oxygen vacancies in the solid [528, 529].

7. Summary and future outlook

For over more than a decade, studies on manganites have been focused on both various details covering the underlying fundamental physics and on applied aspects; it is the former which has received most of the attention. This review embodies various aspects of CMR in doped manganites from its genesis through recent studies to the several efforts made for making the phenomenon intelligible. Many salient features such as double exchange, Jahn–Teller effect, charge/orbital/spin ordering, phase separation etc have recently emerged and these have been described in detail in this review. Emphasis has been placed on low-field-induced magnetoresistance, which is the most important aspect from the application point of view. Some important features are summarized below.

(A) The basic features, such as structure, T–x phase digram, occurrence of a variety of phenomena such as PM–FM transition, CO–OO ordering, phase separation etc, that result due to the interaction between the various degrees of freedom involving spin, lattice, orbit, and charge, have briefly discussed.

(B) Low field magnetoresistance (LFMR) is an extrinsic characteristic of polycrystalline manganites, and for a given material, magnetic field and temperature it is a function of the grain size. The LFMR component increases as the grain size is lowered. In general, LFMR shows monotonically decreasing trend as the temperature is increased, vanishing around the onset temperature of the PM–FM transition. However, there are exceptions, and nearly constant LFMR has been reported in lower temperature range of the FM regime.

(C) The concept of spin-polarized tunneling (SPT) across the grain boundary (it acts as a barrier) of two misaligned grains has often been employed to explain the LFMR in polycrystals. A decrease in the grain size results in increased surface to volume ratio and a more disordered

grain boundary. This leads to an increased barrier across the grain boundary. However, the concept of spin-dependent scattering (SDS) at the grain boundary is also invoked, especially in composites.

(D) LFMR has also been observed around T_C/T_{IM} in epitaxial films, and this of course cannot be explained by either SPT or SDS. Here the strain and lattice relaxation play the key role. Chemical as well as lattice defects can lead to formation of polaron clusters just below T_C. These defects act as pinning centers for magnetic domain walls and increase their density, leading to enhancement of a very low field component of the magnetoresistance that is not observed at low temperature. The origin of the larger MR around T_C than the one predicted from a double-exchange mechanism in LCMO is the delocalization of the polaron clusters below T_{MI} by moderate external magnetic fields (mostly below 5 kOe).

(E) That LFMR has strong correlation with grain boundaries has also been supported by investigations of transport across artificially patterned boundaries, e.g. in thin epitaxial films on bicrystal substrates.

(F) Phase separation is believed to be one of the key mechanisms that govern the overall landscape in manganites. The important role of PS has been recognized in LFMR also, both in polycrystalline and single-crystalline materials. The decrease in grain size leads to a kind of electronic PS due to the breaking of Mn–O–Mn bonds and enhances the barrier across the grain boundaries.

The magnitude of the extrinsic LFMR of the polycrystalline manganites seems to have limiting value $\sim$ 30% at 4.2 K and $H \sim 3$ kOe. So the future course of investigation should focus on the LFMR in epitaxial thin films, which has been found to be larger than 30% at $H = 3$ kOe around T_C/T_{IM}. Irrespective of the temperature scale, the magnetic field sensitivity of the manganites is still much smaller than that of the conventional GMR materials being used. Thus before any real device application the field sensitivity of the manganites has to be drastically improved. In this regard, the rich T–x phase diagram of the manganites holds the key and any materials tailoring for achieving the large LFMR should exploit this. In manganites, the T–x phase diagram shows strong phase coexistence with occurrence of a variety of phases such as PM, FM, CO–OO, AFM metal and AFM insulator. Consequently, in any materials tailoring the multicritical regions of the phase diagram hold the key to have significant low field magnetoresistance at room temperature.

Acknowledgments

Authors wish to thank Professors A R Verma, C N R Rao, C M Srivastava, Vikram Kumar, S B Ogale, J Kumar and R S Tiwari for valuable discussions and suggestions. We would like to offer our sincere thanks to Professors T V Ramakrishnan and A K Raychaudhari for valuable discussions and a critical reading of the manuscript. This work was supported financially by UGC, DST and CSIR, New Delhi.

References

[1] Rao C N R and Raveau B 1998 *Transition Metal Oxides: Structure, Properties and Synthesis of Ceramic Oxides* 2nd edn (New York: Wiley)
[2] Cross L E 1987 *Ferroelectrics* **76** 241
[3] Schmid H 1994 *Ferroelectrics* **162** 317
[4] Bednorz J G and Muller K F 1986 *Z. Phys.* B **64** 189
[5] Chu C W, Hor P H, Gao L, Huang Z J and Wang Y Q 1987 *Phys. Rev. Lett.* **58** 405
[6] Putlin S N, Antipov E V, Chmaissem O and Marezio M 1993 *Nature* **362** 226
[7] For comprehensive reviews, see for example: Tokura Y (ed) 2000 *Colossal Magnetoresistive Oxides* (London: Gordon and Breach)
Salamon M B and Jaime M 2001 *Rev. Mod. Phys.* **73** 583
Ramirez A P 1997 *J. Phys.: Condens. Matter* **9** 8171
Coey J, Viret M and von Molnar S 1999 *Adv. Phys.* **48** 167
Ziese M 2002 *Rep. Prog. Phys.* **65** 143
Tokura Y 2006 *Rep. Prog. Phys.* **69** 797
Gorkov L P and Kresin V Z 2004 *Phys. Rep.* **400** 149
Serrtae D, de Teresa J M and Ibarra M R 2007 *J. Phys.: Condens. Matter* 1 **9** 023201
[8] Maeno Y, Hashimoto H, Yoshida K, Nishizaki S, Fujita T, Bednorz J G and Lichtenberg F 1994 *Nature* **372** 532
[9] Fiebig M 2005 *J. Phys. D: Appl. Phys.* **38** R123
Prellier W, Singh M P and Murugavel P 2006 *J. Phys.: Condens. Matter* **17** R157
[10] Cheong S W and Mostovoy M 2007 *Nat. Mater.* **6** 13
Ramesh R and Spaldin N A 2007 *Nat. Mater.* **6** 21
Eerenstein W, Mathur N D and Scott J F 2006 *Nature* **442** 759
[11] Prinz G A and Hathaway K 1995 *Phys. Today* **48** (4) 24
Simonds J L 1995 *Phys. Today* **48** (4) 26
[12] Comstock R L 1999 *Introduction to Magnetism and Magnetic Recording* (New York: Wiley)
[13] Moser A, Takano K, Margulies D T, Albrecht M, Sonobe Y, Ikeda Y, Sun S and Fullerton E E 2002 *J. Phys. D: Appl. Phys.* **35** R157
[14] Prize G A 1998 *Science* **282** 1660
[15] Wolf S A, Awschalom D D, Buhrman R A, Daughton J M, von Molnar S, Roukes M L, Chtchelkanova A Y and Treger D M 2001 *Science* **294** 1488
[16] Ziese M and Thornton M J (ed) 2001 *Spin Electronics* (Heidelberg: Springer)
[17] Awschalom D D, Flatte M E and Samarth N 2002 *Sci. Am.* **284** 67
[18] Hong J, Kane J, Hashimoto J, Yamagishi M, Noma K and Kanai H 2001 *TMRC 2001: 12th Magnetic Recording Conf. (Minneapolis, MN)* **38** 15
[19] Zhang Z *et al* 2002 *Intermag Europe (Amsterdam, The Netherlands, April–May 2002)*
[20] Wood R 2000 *IEEE Trans. Mag.* **36** 36
[21] Pippard A B 1984 *Magnetoresistance* (Cambridge: Cambridge University Press)
Pippard A B 1989 *Magnetoresistance in Metals* (Cambridge: Cambridge University Press)
[22] Watts S M, Wirth S, von Molnar S, Barry A and Coey J M D 2000 *Phys. Rev.* B **61** 9621
[23] Ashcroft N and Mermin B 1976 *Solid State Physics* (New York: Holt Rinehart and Winston)
[24] Coey J M D 1999 *J. Appl. Phys.* **85** 5576
[25] Binasch G, Grunberg P, Saurenbach F and Zinn W 1989 *Phys. Rev.* B **39** 4828
[26] Baibich M N, Broto J M, Fert A, Dau F N V, Petroff F, Eitenne P, Creuzel G, Friedrich A and Chazelas J 1988 *Phys. Rev. Lett.* **61** 2472
[27] Parkin S S P, More N and Roche K P 1990 *Phys. Rev. Lett.* **64** 2304
[28] Parkin S S P, Li Z G and Smith D J 1991 *Appl. Phys. Lett.* **58** 2710

[29] Parkin S S P, Bhadra R and Roche K P 1991 *Phys. Rev. Lett.* **66** 2152
[30] Levy P M 1992 *Science* **156** 1972
[31] Berkowitz A E, Mitchell J R, Carey M J, Young A P, Zhang S, Spada F E, Parker F T, Hutten A and Thomas G 1992 *Phys. Rev. Lett.* **68** 3745
[32] Xiao J Q, Jiang J S and Chien C L 1992 *Phys. Rev. Lett.* **68** 3749
[33] Hylton T L, Coffey K R, Parker M A and Howard J K 1993 *Science* **261** 1021
[34] Chein C L 1995 *Annu. Rev. Mater. Sci.* **25** 129
[35] Abeles B, Sheng P, Coutts M D and Arie Y 1975 *Adv. Phys.* **24** 407
[36] Helman J S and Abeles B 1976 *Phys. Rev. Lett.* **37** 1429
[37] Parkin S S P and York B R 1993 *Appl. Phys. Lett.* **62** 1842
[38] Parkin S S P 1995 *Annu. Rev. Mater. Sci.* **25** 357
[39] Fert A and Campbell I A 1976 *J. Phys. F: Met. Phys.* **6** 849
[40] Mathon J 1991 *Contemp. Phys.* **32** 143
[41] Edwards D M, Muniz R B and Mathon J 1991 *IEEE Trans. Mag.* **27** 3548
[42] Mott N F 1964 *Adv. Phys.* **13** 325
[43] Dorleijn J W 1976 *Phil. Res. Rep.* **31** 287
Campbell I A and Fert A 1982 *Ferromagnetic Materials* vol 3, ed E P Wohlfarth (Amsterdam: North-Holland) p 747
[44] Possiter P L 1987 *The Electrical Resistance of Metals and Alloys* (Cambridge: Cambridge University Press)
[45] Christides C 2001 *Handbook of Surfaces and Interfaces of Materials* vol 4 *Solid Thin Films and Layers* ed H S Nalwa (New York: Academic) pp 65–130
[46] Tsymbal E Y and Pettifor D G 2001 *Solid State Physics* vol 56, ed H Ehrenreich and F Spaepen (New York: Academic) p 113
[47] Chahara K, Ohno T, Kasai M and Kozono Y 1993 *Appl. Phys. Lett.* **63** 1990
[48] von Helmolt R, Wecker J, Holzapfel B, Schultz M and Samwer K 1993 *Phys. Rev. Lett.* **71** 2331
[49] Jin S, Tiefel T H, McCormack M, Fastnacht R A, Ramesh R and Chen L H 1994 *Science* **264** 413
[50] Jonker G H and van Santen J H 1950 *Physica* **16** 337
[51] van Santen J H and Jonker G H 1950 *Physica* **16** 559
[52] Jonker G H and van Santen J H 1953 *Physica* **19** 120
[53] Volger J 1954 *Physica* **20** 49
[54] Jonker G H 1954 *Physica* **20** 1118
[55] Wollan E O and Koehler W C 1955 *Phys. Rev.* **100** 545
[56] Searle C W and Wang S T 1969 *Can. J. Phys.* **47** 2703
Searle C W and Wang S T 1970 *Can. J. Phys.* **48** 2023.
[57] Jirak Z, Vratislav S and Zajicek J 1979 *Phys. Status Solidi* a **52** K39
[58] Pollert E, Krupicka S and Kuzmicova E 1982 *J. Phys. Chem. Solids* **43** 1137
[59] Kusters R M, Singleton D A, Keen D A, McGreevy R and Hayes W 1989 *Physica* **115B** 362
[60] Ju H L, Kwon C, Li Q, Green R L and Venkatesan T 1994 *Appl. Phys. Lett.* **65** 2108
[61] Xiong G C, Li Q, Ju H L, Bhagat S M, Lofland S E, Green R L and Venkatesan T 1995 *Appl. Phys. Lett.* **67** 3031
[62] Zener C 1951 *Phys. Rev.* **81** 440
Zener C 1951 *Phys. Rev.* **82** 403
[63] Goodenough J B and Loeb A L 1955 *Phys. Rev.* **98** 391
[64] Goodenough J B 2004 *Rep. Prog. Phys.* **67** 1915
Li C, Soh K C K and Wu P 2004 *J. Alloys Compounds* **372** 40
[65] Prellier W, Haghiri-Gosnet A M, Mercey B, Lecoeur Ph, Hervieu M, Simon Ch and Raveau B 2000 *Appl. Phys. Lett.* **77** 1023
[66] Zhao Y G, Rajeswari M, Srivastva R C, Biswas A, Ogale S B, Kang D J, Prellier W, Chen Z, Green R L and Venkatesan T 1999 *J. Appl. Phys.* **86** 6327
[67] Jahn H A and Teller E 1937 *Proc. R. Soc.* A **161** 220
[68] Goodenough J B 1999 *Aust. J. Phys.* **52** 155
[69] van Tendeloo G, Lebedev O I, Hervieu M and Raveau B 2004 *Rep. Prog. Phys.* **67** 1315
[70] Goldschmidt V M 1958 *Goechemistry* (Oxford: Oxford University Press)
[71] Goodenough J B, Kafalas J A and Longo J M 1972 *Preparation Methods in Solid State Chemistry* ed P Hagenmuller (New York: Academic)
Manthiram A and Goodenough J B 1991 *J. Solid State Chem.* **92** 231.
[72] Shannon R D and Prewitt C T 1969 *Acta Crystallogr.* B **25** 725
Shannon R D and Prewitt C T 1970 *Acta Crystallogr.* B **26** 1046.
[73] Goodenough J B 1966 *Magnetism and the Chemical Bond* (New York: Wiley–Interscience)
[74] Dai P, Zhang J, Mook H A, Liou S H, Dowben P A and Plummer E W 1995 *Phys. Rev.* B **54** 3694
[75] Radaelli P G, Iannone G, Marezio M, Hwang H Y, Cheong S W, Jorgensen J D and Argyriou D N 1997 *Phys. Rev.* B **56** 8265
[76] Radaelli P G, Marezio M, Hwang H Y, Cheong S W and Batlogg B 1996 *Phys. Rev.* B **54** 8992
[77] Garcia-Munoz J L, Fontcuberta J, Suaaidi M and Obradors X 1996 *J. Phys.: Condens. Matter* **8** L787
[78] Hwang H Y, Cheong S W, Radaelli P G, Marezio M and Batlogg B 1995 *Phys. Rev. Lett.* **75** 914
[79] Zhou J P, McDevitt J T, Zhou J S, Yin H Q, Goodenough J B, Gim Y and Jia Q X 1999 *Appl. Phys. Lett.* **75** 1146
[80] Sun J R, Rao G H and Liang J K 1997 *Appl. Phys. Lett.* **70** 1900
[81] Dho J, Kim W S and Hur N H 2001 *Phys. Rev. Lett.* **87** 187201
[82] Kawano H, Kajimoto R, Kubota M and Yoshizawa H 1996 *Phys. Rev.* B **53** R14709
[83] Kawano H, Kajimoto R, Kubota M and Yoshizawa H 1996 *Phys. Rev.* B **53** 2202
[84] Schiffer P, Ramirez A P, Bao W and Cheong S W 1995 *Phys. Rev. Lett.* **75** 3336
[85] Cheong S W and Hwang H Y 2000 Ferromagnetism versus charge/orbital ordering in mixed-valent manganites *Colossal Magnetoresitance Oxides* ed Y Tokura (London: Gordon and Breach)
[86] Kajimoto R, Yoshizawa H, Tomioka Y and Tokura Y 2002 *Phys. Rev.* B **66** 180402(R)
[87] Tomioka Y and Tokura Y 2000 Metal–insulator phenomena relevant to charge/orbital ordering in perovskite type manganese oxides *Colossal Magnetoresitance Oxides* ed Y Tokura (London: Gordon and Breach)
[88] Yao Y K, Duewer F, Yang H, Yi D, Li J W and Xiang X D 2000 *Nature* **406** 704
[89] Cahn R W 2001 *Nature* **410** 643
[90] Chen S H, Cheong S W and Hwang H Y 1997 *J. Appl. Phys.* **81** 4326
[91] Coey J M D, Viret M, Ranno L and Ounadjela K 1995 *Phys. Rev. Lett.* **75** 3910
[92] Urshibara A, Moritomo Y, Arima T, Asamitsu A, Kido G and Tokura Y 1995 *Phys. Rev.* B **51** 14103
[93] Khomskii D I 2004 *Colossal Magnetoresistance* ed T Chatterji (Dordrecht: Kulwer–Academic) (*Preprint* cond-mat/0104517)
[94] van den Brink J, Khaliullin G and Khomskii D I 2004 *Colossal Magnetoresistance* ed T Chatterji (Dordrecht: Kulwer–Academic) (*Preprint* cond-matt/0206053)
[95] Dagotto E, Hotta T and Moreo A 2001 *Phys. Rep.* **344** 1
[96] Tomioka Y, Asamitus A, Kuwahara H, Moritoma Y and Tokura Y 1996 *Phys. Rev.* B **53** R1689
[97] Kajimoto R, Yoshizawa H, Kawano H, Kuwahara H, Tokura Y, Ohoyama K and Ohashi M 1999 *Phys. Rev.* B **60** 9506

[98] Cox P A 1995 *Transition Metal Oxides: An Introduction to Their Electronic Structure and Properties* (Oxford: Clarendon)
[99] Pickett W E and Singh D J 1995 *Phys. Rev.* B **53** 1146
[100] Orbach R and Stapleton H J E 1972 *Spin-Lattice Relaxation Electron Paramagnetic Resonance* ed S Geschwind (New York: Plenum) chapter 2
[101] Kanamori J 1960 *J. Appl. Phys.* Suppl **31** 14S
[102] Millis A J, Littlewood P B and Shraiman B I 1995 *Phys. Rev. Lett.* **74** 5144
[103] Roder H, Zang J and Bishop A R 1996 *Phys. Rev. Lett.* **76** 1536
[104] Millis A J 1998 *Nature* **392** 147
[105] Rao C N R, Arulraj A, Cheetham A K and Raveau B 2000 *J. Phys.: Condens. Matter* **12** R83
[106] Anderson P W and Hasegawa H 1955 *Phys. Rev.* **100** 675
[107] de Gennes P 1960 *Phys. Rev.* **118** 141
[108] Alexandro A S and Bratkovsky A M 1998 *Phys. Rev. Lett.* **82** 141
[109] Goodenough J B 1955 *Phys. Rev.* **100** 564
[110] Kubo K and Ohata N 1972 *J. Phys. Soc. Japan* **33** 21
[111] Furukawa N 1994 *J. Phys. Soc. Japan* **63** 3214
Furukawa N 1995 *J. Phys. Soc. Japan* **64** 2734
Furukawa N 1995 *J. Phys. Soc. Japan* **64** 3164
[112] Furukawa N 2000 *J. Phys. Soc. Japan* **6** 1954
[113] Millis A J 1996 *Phys. Rev.* B **53** 8434
[114] Millis A J, Shraiman B I and Mueller R 1996 *Phys. Rev. Lett.* **77** 175
[115] Millis A J, Mueller R and Shraiman B I 1996 *Phys. Rev.* B **54** 5389
Millis A J, Mueller R and Shraiman B I 1996 *Phys. Rev.* B **54** 5405.
[116] Neumeier J J, Hundley M, Thompson J D and Heffner R H 1995 *Phys. Rev.* B **52** R 7006
[117] Tyson T Y, Mustre de Leon J, Conradson S D, Bishop A R, Neumeier J J, Roder H and Zhang J 1996 *Phys. Rev.* B **53** 13985
[118] Mahesh R and Itoh M 1999 *Aust. J. Phys.* **52** 235
[119] Snyder G J, Hiskes R, Di Carolis S, Beasley M R and Geballe T H 1996 *Phys. Rev.* B **53** 14434
Ziese M and Srinitiwarawong C 1998 *Phys. Rev.* B **58** 11519.
[120] Palstra T T M, Ramirez A P, Cheong S W, Zegarski B R, Schiffer P and Zaanen J 1997 *Phys. Rev.* B **56** 5104
[121] Zhou J S, Goodenough J B, Asamitsu A and Tokura Y 1997 *Phys. Rev. Lett.* **79** 3234
[122] Jaime M, Hardner H T, Salamon M B, Rubinstein M, Darsey P and Emin D 1997 *Phys. Rev. Lett.* **78** 951
[123] Kim K H, Jung J H and Noh T W 1998 *Phys. Rev. Lett.* **81** 1517
Ishikawa T, Kimura T, Katsufuji T and Tokura Y 1998 *Phys. Rev.* B **57** R8079
[124] Nucara A, Perucchi A, Calvani P, Aselage T and Emin D 2003 *Phys. Rev.* B **68** R174432
[125] Wang L, Yin J, Huang S, Hunag X, Xu J, Liu Z and Chen K 1999 *Phys. Rev.* B **60** 6976
[126] Adams C P, Lynn J W, Mukovskii Y M, Arsenov A A and Shulyatev D A 2000 *Phys. Rev. Lett.* **85** 3954
Zhang J, Dai P, Fernandez-Baca J A, Plummer E W, Tomioka Y and Tokura Y 2001 *Phys. Rev. Lett.* **86** 3823.
[127] de Teresa J M, Ibarra M R, Algarabel A P, Ritter C, Marquina C, Blasco J, Garcia J deL Moral A and Arnold Z 1997 *Nature* **387** 256
[128] Kapusta Cz, Riedi P C, Koceraba W, Tomka G J, Ibarra M R, de Teresa J M, Viret M and Coey J M D 1999 *J. Phys.: Condens. Matter* **11** 4079
[129] Babushkina N A, Belova L M, Yu Gorbenko O, Kaul A R, Bosak A A, Ozhogin V I and Kugel K I 1998 *Nature* **391** 159
Zhou J S and Goodenough J B 1998 *Phys. Rev. Lett.* **80** 2665
[130] Ju H L, Sohn H C and Krishnan K M 1997 *Phys. Rev. Lett.* **79** 3230
[131] Chuang Y D, Gromko A D, Dessau D S, Kimura T and Tokura Y 2002 *Science* **292** 1509
[132] Lanzara A, Siani N L, Brunelli M, Natali F, Bianconi A, Radaelli P G and Cheong S W 1998 *Phys. Rev. Lett.* **81** 878
[133] Yoon S, Liu H L, Schollerer G, Cooper S L, Han P D, Payne D A, Cheong S W and Fisk Z 1998 *Phys. Rev.* B **58** 2795
Bjornsson P, Rubhausen M, Backstrom J, Kall M, Eriksson S, Eriksen J and Borjesson L 2000 *Phys. Rev.* B **61** 1193
[134] Zang J, Bishop A R and Roder H 1996 *Phys. Rev.* B **53** R8840
[135] Achutharaman V S, Kraus P A, Vasko V A, Nordman C A and Goldman A M 1995 *Appl. Phys. Lett.* **67** 1019
[136] Mitchell J F, Argyriou D N and Jorgensen J D 2000 *Colossal Magnetoresistance Oxide* ed Y Tokura (London: Gordon and Breach) (and reference therein)
[137] Goodenough J B 1997 *J. Appl. Phys.* **81** 5330
Goodenough J B 1999 *Aust. J. Phys.* **52** 155
Goodenough J B 1992 *Ferroelectrics* **130** 77
[138] Alexandrov A S and Bratkowsky A M 1999 *J. Phys.: Condens. Matter* **11** 1989
Alexandrov A S and Bratkowsky A M 1999 *Phys. Rev.* B **60** 6215
Alexandrov A S, Zhao G M, Keller H, Lorenz B, Wang Y S and Chu C W 2001 *Phys. Rev.* B **58** R140404
[139] Nagaev E L 1996 *Usp. Fiz. Nauk.* **166** 833
[140] Ramakrishnan T V, Krishnamurthy H R, Hassan S R and Venketeswara Pai G 2004 *Phys. Rev. Lett.* **92** 157203
Ramakrishnan T V 2007 *J. Phys.: Condens. Matter* **19** 125211
[141] Mannella N, Yang W L, Zhou X J, Zheng H, Mitchell J F, Zaanen J, Devereaux T P, Nagaosa N, Hussain Z and Shen Z X 2005 *Nature* **238** 474
[142] Verwey E J 1939 *Nature* **144** 327
[143] Garcia J and Subias G 2004 *J. Phys.: Condens. Matter* **16** R145
[144] Chen C H, Cheong S W and Cooper A S 1993 *Phys. Rev. Lett.* **71** 2461
[145] Battle P D, Gibb T C and Lightfoot P 1990 *J. Solid State Chem.* **84** 271
[146] Jirak Z, Krupicka S, Simsa Z, Dlouha M and Vratislav S 1985 *J. Magn. Magn. Mater.* **53** 153
[147] Tomioka Y, Asamitsu A, Moritomo Y, Kuwahara H and Tokura Y 1995 *Phys. Rev. Lett.* **74** 5108
[148] Ramirez A P, Schiffer P, Cheong S W, Chen C H, Bao W, Palstra T T M, Gammel P L, Bishop D J and Zegarski B 1996 *Phys. Rev. Lett.* **76** 3188
[149] Chen C H and Cheong S W 1996 *Phys. Rev. Lett.* **76** 4042
Chen C H, Cheong S W and Hwang H Y 1997 *J. Appl. Phys.* **81** 4326
[150] Cheong S W, Hwang H Y, Chen C H, Batlogg B, Rupp L W Jr and Carter S A 1994 *Phys. Rev.* B **49** 7088
[151] Radaelli P G, Cox D E, Marezio M and Cheong S W 1997 *Phys. Rev.* B **55** 3015
[152] Mori S, Chen C H and Cheong S W 1998 *Nature* **392** 473
[153] Kuwahara H, Tomioka Y, Asamitsu A M and Tokura Y 1995 *Science* **270** 961
[154] Moritomo Y, Kiwahara H, Tomioka Y and Tokura Y 1997 *Phys. Rev.* B **55** 7549
[155] Kiryukhin V, Casa D, Hill J P, Keimer B, Vigliante A, Tomioka Y and Tokura Y 1997 *Nature* **386** 813
[156] Asamitsu A, Tomioka Y, Kuwahara H and Tokura Y 1997 *Nature* **388** 50
[157] Parashar S, Ebenso E E, Raju A R and Rao C N R 2000 *Solid State Commun.* **114** 295
[158] Miyano K, Tanaka T, Tomioka Y and Tokura Y 1997 *Phys. Rev. Lett.* **78** 4257
[159] Kawano H, Kajimoto R, Yoshizawa H, Tomioka Y, Kuwahara H and Tokura Y 1997 *Phys. Rev. Lett.* **78** 4253

[160] Knizek K, Jirak Z, Pollert E and Zounova F 1992 *J. Solid State Chem.* **100** 292
[161] Raveau B, Hervieu M, Maignan A and Martin C 2001 *J. Mater. Chem.* **11** 29
[162] Tomioka Y, Okuda T, Okunoto Y, Asamitsu A, Kuwahara H and Tokura Y 2001 *J. Alloys Compounds* **326** 27
[163] Rao C N R and Raveau B (ed) 1998 *Colossal Magnetoresistance Charge Ordering and Related Properties of Manganese Oxides* (Singapore: World Scientific)
[164] Loudon J C, Mathur N D and Midgley P A 2002 *Nature* **420** 797
[165] Mori S, Asaka T and Matsui Y 2002 *J. Electron Microsc.* **51** 225
[166] Sagdeo P R, Shahid A and Lalla N P 2006 *Solid State Commun.* **137** 158
[167] Cepas O, Krishnamurthy H R and Ramakrishnan T V 2006 *Phys. Rev.* B **73** 035218
[168] Tokura Y and Nagaosa N 2000 *Science* **288** 462
Orenstein J and Millis A J 2000 *Science* **288** 468
[169] Rao C N R and Vanitha P V 2002 *Curr. Opin. Solid State Mater. Sci.* **6** 97
Rao C N R, Kundu Asish K, Seikh Md M and Sudheendra L 2004 *Dalton Trans.* **19** 3003
[170] Dagotto E, Burgy J and Moreo A 2003 *Solid State Commun.* **126** 9
Mathur N D and Littlewood P 2003 *Phys. Today* **56** 25
[171] Tanquada J M, Sternlied B J, Axe J D, Nakamura Y and Uchida S 1995 *Nature* **375** 561
[172] Chernyshev A L, Castro Neto A H and Bishop A R 2000 *Phys. Rev. Lett.* **84** 4922
[173] Belevtsev B I 2004 *Low Temp. Phys.* **30** 421
[174] Sigmund E and Muller K A (ed) 1994 *Phase Separation in Cuprate Superconductors* (Heidelberg: Springer)
[175] Burley J C, Mitchell J F and Short S 2004 *Phys. Rev.* B **69** 054401
Kundu A K, Nordblad P and Rao C N R 2006 *J. Solid State Chem.* **179** 923
[176] Nagaev E L 1967 *JETP Lett.* **6** 18
Nagaev E L 1968 *Sov. Phys. Lett.* **27** 122
Nagaev E L 1972 *JETP Lett.* **16** 3948
[177] Nagaev E L 1986 *Physics of Magnetic Semiconductors* (Moscow: Mir Publisher)
Nagaev E L 2001 *Phys. Rep.* **346** 387
[178] Wakai H 2001 *J. Phys.: Condens. Matter* **13** 1627
[179] Guha A, Khare N, Raychaudhuri A K and Rao C N R 2000 *Phys. Rev.* B **62** R11941
[180] Kim R H, Uehara M, Hess C, Sharma P A and Cheong S W 2000 *Phys. Rev. Lett.* **84** 2961
[181] Hardy V, Wahl A and Martin C 2001 *Phys. Rev.* B **64** 064402
[182] Moreo A, Yunoki S and Dagotto E 1999 *Science* **283** 2034
[183] Dagotto E (ed) 2002 *Nanoscale Phase separation and Colossal Magnetoresistance* (Berlin: Springer)
[184] Dagotto E, Hotta T and Moreo A 2001 *Phys. Rep.* **344** 1
[185] Moreo A, Mayr M, Feiguin A, Yunoki S and Dagotto E 2000 *Phys. Rev. Lett.* **84** 5568
[186] Uehara M, Mori S, Chen C H and Cheong S W 1999 *Nature* **399** 560
[187] Fath F, Freisem S, Menovsky A A, Tomioka Y, Aarts J and Mydosh J A 1999 *Science* **285** 1540
[188] Biswas A, Elizabeth S, Raychaudhuri A K and Bhat H L 1999 *Phys. Rev.* B **59** 5368
[189] Smolyaninova V N, Xie X C, Zhang F C, Rajeswari M, Greene R L and Das Sarma S 2000 *Phys. Rev.* B **62** R6093
[190] Bibes M, Balcells L, Valencia S, Fontcuberta J, Wojcik M, Jedryka E and Nadolski S 2001 *Phys. Rev. Lett.* **87** 067210
[191] Renner C, Aeppli G, Kim B G, Soh Y A and Cheong S W 2002 *Nature* **416** 518
[192] Zhang L, Israel C, Biswas A, Greene R L and de Lozanne A 2002 *Science* **298** 805
[193] Booth C H, Bridges F, Kwei G H, Lawrence J M, Connelius A L and Neumeier J J 1998 *Phys. Rev. Lett.* **80** 853
Booth C H, Bridges F, Kwei G H, Lawrence J M, Connelius A L and Neumeier J J 1998 *Phys. Rev.* B **57** 10440
[194] Billinge S J L, Profen Th, Petkov V, Sarrao J L and Kycia S 2000 *Phys. Rev.* B **62** 1203
[195] Dai P, Fernandez-Baca J A, Wakabayashi N, Plummer E W, Tomioka Y and Tokura Y 2000 *Phys. Rev. Lett.* **85** 2553
[196] Yoon S, Liu H, Schollerer G, Cooper S, Han P D, Payne D A, Cheong S W and Fisk Z 1998 *Phys. Rev.* B **58** 2795
[197] Chechersky V, Nath A, Michel C, Hervieu M, Gosh K and Green R L 2000 *Phys. Rev.* B **62** 5316
[198] Heffner R H, Sonier J E, Maclaughlin D E, Nieuwenhuys G J, Luke G M, Uemura Y J, Ratcliff W II, Cheong S W and Balakrishnan G 2001 *Phys. Rev.* B **63** 094408
[199] Massa N E, Tolentino H, Salva H, Alonso J A, Martinze-lopez M J and Casais M T 2001 *J. Magn. Magn. Mater.* **233** 91
[200] Hirai Y *et al* 2000 Univ of Wisconsin Madison, Preprint
[201] Babushkina N A, Belova L M, Gorbenko O Yu, Kaul A R, Bosak A A, Ozhogin V I and Kugel K I 1998 *Nature* **391** 159
[202] Woodfiled B F, Wilson M L and Byers J M 1997 *Phys. Rev. Lett.* **78** 3201
[203] Moskvin A S, Zenkov E V, Sukhoroukov Yu P, Mostovsh-Chikova E V, Loshkareva N N, Kaul A R and Gorbenko O Yu 2003 *J. Phys.: Condens. Matter* **15** 2635
[204] Savosta M M, Novak P, Marysko M, Jirak Z, Hejtmanek J, Englich J, Kohout J, Martin C and Raveau B 2000 *Phys. Rev.* B **62** 9532
[205] Ma Y Q *et al* 2004 *J. Phys.: Condens. Matter* **16** 7447
Ma Y Q *et al* 2004 *Phys. Rev.* B **69** 134404
[206] Podzorov V, Uehara M, Gershenson M E, Koo T Y and Cheong S W 2000 *Phys. Rev.* B **61** R3784
[207] Hardner H T, Weissman M B, Jamie M, Treece R E, Dorsey P C, Horwitz J S and Chrisey D B 1997 *J. Appl. Phys.* **81** 272
[208] Alers G P, Ramirez A P and Jin S 1996 *Appl. Phys. Lett.* **68** 3649
[209] Raquet B, Anane A, Wirth S, Xiong P and Von Molnar S 2000 *Phys. Rev. Lett.* **84** 4485
[210] Merithew R D, Weissman M B, Hess F H, Spradling P, Nowak E R, O'Donnell J, Eckstein J, Tokura Y and Tomioka Y 2000 *Phys. Rev. Lett.* **84** 3442
[211] Anane A, Raquet B, von Molnar S, Pinsard-Gaudart L and Revcolevschi A 2000 *J. Appl. Phys.* **87** 5025
[212] Podzorov V, Gershenson M E, Uehara M and Cheong S W 2001 *Phys. Rev.* B **64** 115113
[213] Sarma D D *et al* 2004 *Phys. Rev. Lett.* **93** 097202
[214] Viret M, Ott F, Renard J P, Glattli H, Pinsard-Gaudart L and Revcolevschi A 2004 *Phys. Rev. Lett.* **93** 217402
[215] Saurel D, Brulet A, Heinemann A, Martin C, Mercone S and Simon C 2006 *Phys. Rev.* B **73** 094438
[216] Ma J X, Gillaspie D T, Plummer E W and Shen J 2005 *Phys. Rev. Lett.* **95** 237210
[217] Dagotto E 1994 *Rev. Mod. Phys.* **66** 763
[218] Bastiannsen P J M and Knops H J F 1998 *J. Phys. Chem. Solids* **59** 297
[219] Mayr M, Moreo A, Verges J A, Arispe J, Feiguin A and Dagotto E 2001 *Phys. Rev. Lett.* **86** 135
[220] Weibe A, Loos J and Fehske H 2001 *Phys. Rev.* B **64** 104413
[221] Lynn J W, Erwin R W, Borchers J A, Huang Q, Santoro A, Peng J L and Li Z Y 1996 *Phys. Rev. Lett.* **76** 4046
[222] Mira J, Rivas J, Rivadulla F, Vazquez-Vazquez C and Lopez Quintela M A 1999 *Phys. Rev.* B **60** 2998
[223] Zeise M 2001 *J. Phys.: Condens. Matter* **13** 2919

[224] Lyuksyutov I F and Pokrovsky V L 1999 *Mod. Phys. Lett.* B **13** 379
[225] Varma C 1996 *Phys. Rev.* B **54** 7328
[226] Yunoki S J, Hu J, Malvezzi A l, Moreo A, Furukawa N and Dagatto E 1998 *Phys. Rev. Lett.* **80** 845
[227] Gorkov L P 1998 *Sov. Phys.—Usp.* **41** 589
Gorkov L P and Kresin V Z 1998 *JETP Lett.* **67** 985
[228] Dzero M O, Gorkov L P and Kresin V Z 2000 *Eur. Phys. J.* B **14** 459
[229] Jaime M, Lin P, Chun S H, Salamon M, Dorsey P and Rubinstein M 1999 *Phys. Rev.* B **60** 1028
[230] Ahn K H, Lookman T and Bishop A R 2004 *Nature* **428** 401
[231] Sagdeo P R, Shahid A and Lalla N P 2006 *Phys. Rev.* B **74** 214118
[232] Shenoy V B, Gupta T, Krishnamurthy H R and Ramakrishnan T V 2007 *Phys. Rev. Lett.* **98** 097201
[233] Dorr K 2006 *J. Phys. D: Appl. Phys.* **39** R125
[234] Haghiri-Gosnet A M and Renard J P 2003 *J. Phys. D: Appl. Phys.* **36** R127 (and reference therein)
[235] Prellier W, Mercey B and Haghiri-Gosnet A M 2003 *Encyclopedia of Nanoscience and Nanotechnology* vol X, ed H S Nalwa (Stevenson Ranch, CA: American Scientific Publishers) pp 1–18 (and reference therein)
Prellier W, Lecoeur Ph and Mercey B 2001 *J. Phys.: Condens. Matter* **13** R915 (and reference therein)
[236] Hwang H Y, Cheong S W, Ong N P and Batlogg B 1996 *Phys. Rev. Lett.* **77** 2041
[237] Mahesh R, Mahendiran R, Raychaudhuri A K and Rao C N R 1996 *Appl. Phys. Lett.* **68** 2291
[238] Wang X L, Dou S X, Liu H K, Ionescu M and Zeimetz B 1998 *Appl. Phys. Lett.* **73** 396
[239] Bibes M, Balcells L, Fontcuberta J, Wojcik M, Nadolski S and Jedryka E 2003 *Appl. Phys. Lett.* **82** 98
[240] Hueso L E, Rivasa J, Rivadulla F and Lo'pez-Quintela M A 1999 *J. Appl. Phys.* **86** 3881
[241] Zhang S and Yang Z 1996 *J. Appl. Phys.* **79** 7398
[242] Kim Y N, Kim J C, Lee E K, Hwang Y S, Hur N H, Yun Y J, Park G S and Kim J T 2004 *J. Appl. Phys.* **95** 7088
[243] Dey P and Nath T K 2005 *Appl. Phys. Lett.* **87** 162501
Dey P and Nath T K 2006 *Phys. Rev.* B **73** 214425
[244] Raychaudhuri P, Sheshadri K, Taneja P, Bandyopadhyay S, Ayyub P, Nigam A K, Pinto R, Chaudhary S and Roy S B 1999 *Phys. Rev.* B **59** 13919
[245] Lee S, Hwang H Y, Shraiman B I, Ratcliff W D and Cheong S W 1999 *Phys. Rev. Lett.* **82** 4508
[246] Yuan S L *et al* 2003 *Phys. Rev.* B **68** 172408
[247] Rivas J, Hueso L E, Fondado A, Rivadullo F and Lopez-Quintela M A 2000 *J. Magn. Magn. Mater.* **21** 57
[248] Nam Y S, Ju H L and Park C W 2001 *Solid State Commun.* **119** 613
[249] Sánchez R D, Rivas J, Vázquez-V ázquez C, López-Quintela M A, Causa M T, Tovar M and Oseroff S B 1996 *Appl. Phys. Lett.* **68** 134
[250] Shankar K S, Kar S, Subbanna G N and Raychaudhuri A K 2004 *Solid State Commun.* **129** 479
[251] Vazquez-vazquez C, Blanco M C, Lopez-quintela M A, Sanchez R D, Rivas J and Oseroff S B 1998 *J. Mater. Chem.* **8** 991
[252] Siwach P K, Goutam U K, Srivastava P, Singh H K, Tiwari R S and Srivastava O N 2006 *J. Phys. D: Appl. Phys.* **39** 14
[253] Peng H B, Zhao B R, Xie Z, Lin Y, Zhu B Y, Hao Z, Ni Y M, Tao H J, Dong X L and Xu B 1999 *Appl. Phys Lett.* **74** 1606
[254] Gleiter H 1992 *Adv. Mater.* **4** 474
[255] Berkowitz A E, Kodama R H, Makhloul S A, Parker F T, Spada F E, McNiff E J Jr and Foner S 1999 *J. Magn. Magn. Mater.* **196/197** 591
[256] Zhang N, Ding W, Zhong W, Xing D and Du Y 1997 *Phys. Rev.* B **56** 8138
[257] Calderón M J, Brey L and Guinea F 1999 *Phys. Rev.* B **60** 6698
[258] Balcells L, Foncuberta J, Martínez B and Obradors X 1998 *Phys. Rev.* B **58** R14697
[259] Norton D P 2004 *Mater. Sci. Eng.* B **R43** 139
[260] Mathews S, Ramesh R, Venkatesan T and Bendetto J 1998 *Science* **276** 238
[261] Goyal A, Rajeswari M, Shreekala R, Lofland S E, Bhagat S M, Boettcher T, Kwon C, Ramesh R and Venkatesan T 1997 *Appl. Phys. Lett.* **71** 2535
[262] Kida N and Tonouchi M 2001 *Appl. Phys. Lett.* **78** 4115
[263] Venktaesan T *et al* 1999 *Mater. Sci. Eng.* B **63** 36
[264] Dorr K, De Teresa J M, Muller K H, Eckert D, Walter T, Vlakhov E, Nenkov K and Schultz L 2000 *J. Phys.: Condens. Matter* **12** 7099
[265] Rentler P, Bensaid A, Herbstritt F, Hofener C, Marx A and Gross R 2000 *Phys. Rev.* B **62** 11619
[266] Chen C C and de Lozanne A 1997 *Appl. Phys. Lett.* **71** 1424
[267] Wang L M, Sung H H, Su B T, Yang H C and Horng H E 2000 *J. Appl. Phys.* **88** 4236
[268] Ponnambalam V, Parashar S, Raju A R and Rao C N R 1999 *Appl. Phys. Lett.* **74** 206
[269] Singh H K, Khare N, Siwach P K and Srivastava O N 2000 *J. Phys. D: Appl. Phys.* **33** 921
[270] Khare N, Singh H K, Siwach P K, Moharil U P, Gupta A K and Srivastava O N 2001 *J. Phys. D: Appl. Phys.* **34** 673
[271] Bae S Y and Wang S X 1996 *Appl. Phys. Lett.* **69** 121
[272] Gupta A, Gong G Q, Xiao G, Dumcombe P R, Lecoeur P, Trouilloud P, Wang Y Y, Dravid V P and Sun J Z 1996 *Phys. Rev.* B **54** R15629
[273] Walter T, Dorr K, Muller K H, Holzapfel B, Eckert D, Wolf M, Schlafer D, Schultz L and Grotzschel R 1999 *Appl. Phys. Lett.* **74** 2218
[274] Cheng S L and Lin J G 2005 *J. Appl. Phys.* **98** 114318
[275] Liu X, Jiao Z, Nakamura K, Hatano T and Zeng Y 2000 *J. Appl. Phys.* **87** 2431
[276] Pignard S, Vincent H, Senateur J P, Frohlich K and Souc J 1998 *Appl. Phys. Lett.* **73** 999
[277] Steenbeck K and Hiergeist R 1999 *Appl. Phys. Lett.* **75** 1778
[278] Ibarra M R, Algarabel P A, Marquina C, Blasco J and Garcia J 1995 *Phys. Rev. Lett.* **75** 3541
[279] Biswas A, Rajeswari M, Srivastava R C, Venkatesan T, Greene R L, Li Q, de Lozanne A L and Millis A J 2001 *Phys. Rev.* B **63** 184424
[280] De Teresa J M, Ibarra M R, Blasco J, Garcia J, Marquina C, Algarabel P A, Arnold Z, Kamenev K, Ritter C and von Helmolt R 1996 *Phys. Rev.* B **54** 1187
[281] Koo T Y, Park S H, Lee K B and Jeong Y H 1997 *Appl. Phys. Lett.* **71** 977
[282] Zandbergen H W, Freizem S, Nojima T and Aarts J 1999 *Phys. Rev.* B **60** 10259
[283] Venimadhar A, Hegde M S, Rawat R and Das I 2001 *J. Appl. Phys.* **89** 8057
[284] Prellier W, Biswas A, Rajeswari M, Venkatesan T and Greene R L 1999 *Appl. Phys. Lett.* **75** 397
[285] Klein J, Philipp J P, Carbone G, Vigliante A, Alff L and Gross R 2002 *Phys. Rev.* B **66** 052414
[286] Wu X W, Rzchowski M S, Wang H S and Li Q 2000 *Phys. Rev.* B **61** 501
[287] Millis A J, Darling T and Migliori A 1998 *Appl. Phys. Lett.* **83** 1588
[288] Izumi M, Ogimoto Y, Konisihi Y, Manako T, Kawasaki M and Tokura Y 2001 *Mater. Sci. Eng.* B **84** 53
[289] Zhang J, Tanaka H, Kanki T, Choi J H and Kawai T 2001 *Phys. Rev.* B **64** 184404
[290] Kanki T, Tanaka H and Kawai T 2001 *Phys. Rev.* B **64** 224418

Kanki T, Tanaka H and Kawai T 2004 *Phys. Rev.* B **70** 125109
[291] Gommert E, Cerva H, Wecker J and Samwer K 1999 *J. Appl. Phys.* **85** 5417
[292] Kwon C *et al* 1997 *J. Magn. Magn. Mater.* **172** 229
[293] Razavi F S, Gross G, Habermeier H U, Lebedev O, Amelinckx S, Van Tendeloo G and Vigliante A 2000 *Appl. Phys. Lett.* **76** 155
[294] Dho J, Hur N H, Kim I S and Park Y K 2003 *J. Appl. Phys.* **94** 7670
[295] Jin S, Tiefel T H, McCormack M, Obryan H M, Chen L H, Ramesh R and Schurig D 1995 *Appl. Phys. Lett.* **67** 557
[296] Konishi Y, Fang Z, Izumi M, Manako T, Kasai M, Kuwahara H, Kawasaki M, Terakura K and Tokura Y 1999 *J. Phys. Soc. Japan* **68** 3790
[297] Wu Y, Suzuki Y, Rudiger U, Yu J, Kent A D, Nath T K and Eom C B 1999 *Appl. Phys. Lett.* **75** 2295
[298] Suzuki Y and Hwang H Y 1999 *J. Appl. Phys.* **85** 4797
[299] Nelson C S *et al* 2004 *J. Phys.: Condens. Matter* **16** 13
[300] Wu I, Ogale S B, Shinde S R, Biswas A, Polletto T, Greene R L and Millis A J 2003 *J. Appl. Phys.* **93** 5507
[301] Dale D, Fleet A, Brock J D and Suzuki Y 2003 *Appl. Phys. Lett.* **82** 3725
[302] Valencia S, Balcells L, Fontcuberta J and Martinez B 2003 *Appl. Phys. Lett.* **82** 4531
[303] Kanki T, Li R W, Naitoh Y, Tanaka H, Matsumoto T and Kawai T 2003 *Appl. Phys. Lett.* **83** 1184
[304] de Andres A, Rubio J, Castro G, Taboada S, Martinez J L and Colino J M 2003 *Appl. Phys. Lett.* **83** 713
[305] Wang H S, Li Q, Liu K and Chien C L 1999 *Appl. Phys. Lett.* **74** 2212
[306] Li Q, Wang H S, Hu Y F and Wertz E 2000 *J. Appl. Phys.* **87** 5573
[307] Miniotasa A, Vailionis A, Svedberg E B and Karlsson U O 2001 *J. Appl. Phys.* **89** 2134
[308] Campillo G, Berger A, Osorio J, Pearson J E, Bader S D, Baca E and Prieto P 2001 *J. Magn. Magn. Mater.* **237** 61
[309] Lu J, Wang Z L, Kwon C and Jia Q X 2000 *J. Appl. Phys.* **88** 4032
[310] Biswas A, Rajeswari M, Srivastava R C, Li Y H, Venkatesan T, Greene R L and Millis A J 2000 *Phys. Rev.* B **61** 9665
[311] Pradhan A K, Sahu D R, Roul B K and Feng Y 2002 *Appl. Phys. Lett.* **81** 3597
[312] Murugavel P, Lee J H, Yoon J G, Noh T W, Chung J S, Heu M and Yoon S 2003 *Appl. Phys. Lett.* **82** 1908
[313] Klein J, Philipp J B, Reisinger D, Opel M, Marx A, Erb A, Alff L and Gross R 2003 *J. Appl. Phys.* **93** 7373
[314] Siwach P K, Singh H K and Srivastava O N 2006 *J. Phys.: Condens. Matter* **18** 9783
[315] Prasad R, Gaur A, Siwach P K, Varma G D, Kaur A and Singh H K 2007 *J. Phys. D: Appl. Phys.* **40** 2954
[316] Yeh N C, Vasquez R P, Beam D A, Fu C C, Huynh J and Beach G 1997 *J. Phys.: Condens. Matter* **9** 3713
[317] de Andres A, Taboda S, Colino J M, Rameriz R, Garcia-Hernandez M and Marteniz J L 2002 *Appl. Phys. Lett.* **81** 319
[318] Li J, Wang P, Xiang J Y, Zhu X Z, Peng W, Chen Y F, Zheng D N and Li Z W 2005 *Appl. Phys. Lett.* **86** 112514
[319] Siwach P K, Singh H K, Singh D P, Khare N and Srivastava O N 2003 *J. Phys. D: Appl. Phys.* **36** 1361
[320] Rajeswari M *et al* 1998 *Appl. Phys. Lett.* **73** 2672
[321] Nam B C, Kim W S, Choi H S, Kim J C, Hur N H, Kim I S and Park Y K 2001 *J. Phys. D: Appl. Phys.* **34** 54
[322] Wu W, Wong K H, Li X G, Choy C L and Zhang Y H 2000 *J. Appl. Phys.* **87** 3006
[323] Shreekala R *et al* 1999 *Appl. Phys. Lett.* **74** 2857
[324] Prokhorov V G, Kaminsky G G, Komashko V A, Lee Y P, Park J S and Ri H C 2002 *Appl. Phys. Lett.* **80** 2707
[325] Khare N, Singh D P, Singh H K, Gupta A K, Siwach P K and Srivastava O N 2004 *J. Phys. Chem. Solids* **65** 867
[326] Huang Y-H, Yan C-H, Luo F, Song W, Wang Z-M and Liao C-S 2002 *Appl. Phys. Lett.* **81** 76
[327] Yan X-B, Liu Y-H, Wang C-J and Mei L-M 2005 *J. Phys. D: Appl. Phys.* **38** 3360
[328] Pal S, Banerjee A, Chatterjee S, Nigam A K, Chaudhuri B K and Yang H D 2003 *J. Appl. Phys.* **94** 3485
[329] Huang Y H, Yan C H, Luo F, Song W, Wang Z M and Liao C S 2002 *Appl. Phys. Lett.* **81** 76
[330] Yan X-B, Liu Y-H, Huang B-X, Wang C-J and Mei L-M 2005 *Solid State Commun.* **135** 170
[331] Huang Y H, Huang K F, Luo F, He L L, Wang Z M, Liao C S and Yan C H 2003 *J. Solid State Chem.* **174** 257
[332] Li J, Huang Q, Li Z W, You L P, Xe Y and Ong C K 2001 *J. Phys.: Condens. Matter* **13** 3419
[333] Rajeswari M, Goyal A, Raychaudhuri A K, Robson M C, Xiong G C, Kwon C, Ramesh R, Greene R L, Venkatesan T and Lakeou S 1996 *Appl. Phys. Lett.* **69** 851
[334] Shlyakhtin O A, Shin K H and Oh Y-J 2002 *J. Appl. Phys.* **91** 7403
[335] Balcells L I, Carrillo A E, Martinez B and Fontcuberta J 1999 *Appl. Phys. Lett.* **74** 4014
[336] Petrov D K, Krusin-Elbaum L, Sun J Z, Feild C and Duncombe P R 1999 *Appl. Phys. Lett.* **75** 995
[337] Das D, Chowdhury P, Das R N, Srivastava C M, Nigam A K and Bahadur D 2002 *J. Magn. Magn. Mater.* **238** 178
[338] Xia Z C *et al* 2003 *J. Phys. D: Appl. Phys.* **36** 217
[339] Xia Z C *et al* 2002 *J. Phys. D: Appl. Phys.* **35** 177
[340] Das D, Srivastava C M, Bahadur D, Nigam A K and Malik S K 2004 *J. Phys.: Condens. Matter* **16** 4089
[341] Shilpi K, Taran S, Chaudhuri B K, Sakata H, Sun C P, Huang C L and Yang H D 2005 *J. Phys. D: Appl. Phys.* **38** 3757
[342] Huang Q, Li J, Huang X J, Ong C K and Gao X S 2001 *J. Appl. Phys.* **90** 2924
[343] Yan C-H, Xu Z-G, Zhu T, Wang Z-M, Cheng F-X, Huang Y-H and Liao C-S 2000 *J. Appl. Phys.* **87** 5588
[344] Yuan X-B, Liu Y-H, Wang C-J and Mei L-M 2005 *J. Phys. D: Appl. Phys.* **38** 3360
[345] Yan C-H, Huang Y-H, Chen X, Liao C-S and Wang Z-M 2002 *J. Phys.: Condens. Matter* **14** 9607
[346] Huang Y-H, Chen X, Wang Z-H, Liao C-S, Yan C-H, Zhao H-W and Shen B-G 2002 *J. Appl. Phys.* **91** 7733
[347] Kumar J, Singh R K, Siwach P K, Singh H K, Singh R and Srivastava O N 2006 *J. Magn. Magn. Mater.* **299** 155
Kumar J, Singh R K, Siwach P K, Singh H K, Singh R, Katria N D and Srivastava O N 2008 *J. Alloys Compounds* **455** 289
[348] Gupta S, Ranjit R, Mitra C, Raychaudhuri P and Pinto R 2001 *Appl. Phys. Lett.* **78** 362
[349] Yan C-H, Luo F, Huang Y-H, Li X-H, Wang Z-M, Liao C-S, Zhao H-W and Shen B-G 2002 *J. Appl. Phys.* **91** 7406
[350] Liu J-M, Yuan G L, Sang H, Wu Z C, Chen X Y, Liu Z G, Du Y W, Huang Q and Ong C K 2001 *Appl. Phys.Lett.* **78** 1110
[351] Sun J R, Shen B G, Yeung H W and Wong H K 2002 *J. Phys. D: Appl. Phys.* **35** 173
Sun J R, Shen B G, Yeung H W and Wong H K 2002 *Appl. Phys.Lett.* **88** 192514
[352] Bahadur D and Das D 2003 *Proc. Indian Acad. Sci. (Chem. Sci.)* **115** 587
[353] Chaudhuri B K, Banerjee A and Pal S 2004 *Encyclopedia of Nanoscience and Nanotechnology* vol V, ed H S Nalwa (Stevenson Ranch, CA: American Scientific Publishers) pp 41–52 (and reference therein)
[354] Yao L D, Zhang W, Zhang J S, Yang H, Li F Y, Liu Z X, Jin C Q and Yu R C 2007 *J. Appl. Phys.* **101** 063905
[355] Moshnyaga V *et al* 2003 *Nat. Mater.* **2** 247

[356] Kang B S, Wang H, MacManus-Driscoll J L, Li Y, Jia Q X, Mihut I and Betts J B 2006 *Appl. Phys. Lett.* **88** 192514
[357] Moritomo Y, Asamitsu A, Kuwahara H and Tokura Y 1996 *Nature* **380** 141
[358] Kimura T, Tomioka Y, Kuwahara H, Asamitsu A, Tamura M and Tokura Y 1996 *Science* **274** 1698
[359] Fukumura T, Sugawara H, Hasegawa T, Tanaka K, Sakaki H, Kimura T and Tokura Y 1999 *Science* **284** 1969
[360] Asano H, Hayakawa J and Matsui M 1996 *Appl. Phys. Lett.* **68** 3638
[361] Asano H, Hayakawa J and Matsui M 1997 *Phys. Rev.* **B56** 5395
[362] Asano H, Hayakawa J and Matsui M 1997 *Appl. Phys. Lett.* **70** 2303
[363] Hirota K, Moritomo Y, Fujioka H, Kubota M, Yoshizawa H and Endoh Y 1998 *J. Phys. Soc. Japan* **67** 3380
[364] Hur N H, Kim J T, Yoo K H, Park Y K, Park J C, Chi E O and Kwon Y W 1998 *Phys. Rev.* B **57** 10740
[365] Li Q, Gray K E, Mitchell J F, Berger A and Osgood R 2000 *Phys. Rev.* B **61** 9542
[366] Welp U, Berger A, Vlasko-Vlasov V K, Li Q, Gray K E and Mitchell J F 2000 *Phys. Rev.* B **62** 8615
[367] Li Q, Gray K E and Mitchell J F 1999 *Phys. Rev.* B **59** 9357
[368] Welp U, Berger A, Miller D J, Vlasko-Vlasov V K, Li Q, Gray K E and Mitchell J F 2000 *J. Appl. Phys.* **87** 5043
[369] Kimura T and Tokura Y 2000 *Annu. Rev. Mater. Sci.* **30** 451
[370] Nair S and Banerjee A 2004 *Phys. Rev.* B **70** 104428
[371] Shen C H, Liu R S, Hu S F, Lin J G, Huang C Y and Sheu S H 1999 *J. Appl. Phys.* **86** 2178
[372] Zhang J, Wang F, Zhang P and Yan Q 1999 *Solid State Commun.* **109** 401
[373] Zhou T J, Yu Z, Ding S Y, Qiu L and Du Y W 2002 *Appl. Phys.* A **74** 163
[374] Zhu H, Tan S, Tong W and Zhang Y 2002 *Appl. Phys. Lett.* **80** 3778
[375] Rodrguez-Martinez Lide M and Attfield J P 1996 *Phys. Rev.* B **54** R15622
[376] Damay F, Martin C, Maignan A and Raveau B 1997 *J. Appl. Phys.* **82** 6181
[377] Chi E O, Kwan Y U, Kim J T and Hur N H 1999 *Solid State Commun.* **110** 569
[378] Zhang J, Yan Q, Wang F, Ywan P and Zhang P 2001 *J. Phys.: Condens. Matter* **13** 917
[379] Zhu H, Zhu D and Zhang Y 2002 *J. Appl. Phys.* **92** 7355
[380] Singh H K, Gupta A K, Siwach P K and Srivastava O N 2004 *J. Magn. Magn. Mater.* **292** 483
[381] Konishi Y, Kimura T, Izumi M, Kawasaki M and Tokura Y 1998 *Appl. Phys. Lett.* **73** 3004
[382] Philipp J B, Klein J, Recher C, Walther T, Mader W, Schmid M, Suryanarayanan R, Alff L and Gross R 2002 *Phys. Rev.* B **65** 184411
[383] Siwach P K, Singh H K and Srivastava O N 2006 *J. Phys. D: Appl. Phys.* **39** 3731
[384] Zhang C L, Chen X J, Almasan C C, Gardner J S and Sarro J L 2002 *Phys. Rev.* B **65** 134439
[385] Mitchell J F, Argyriou D N, Berger A, Gray K E, Osborn R and Welp U 2001 *J. Am. Phys. Chem.* **105** 10731
[386] Ju H L, Gopalakrishnan J, Peng J L, Li Q, Xiong G C, Venkatesan T and Greene R L 1995 *Phys. Rev.* B **51** 6143
[387] Fu Y 2000 *Appl. Phys. Lett.* **77** 118
[388] de Andres A, Garcia-Hernandez M, Martinez J L and Prieto C 1999 *Appl. Phys. Lett.* **74** 3884
[389] Huesco L E, Rivas J, Rivadulla F and Lopez-Quintela M A 1999 *J. Appl. Phys.* **86** 3881
[390] Lopez-Quintela M A, Huesco L E, Rivas J and Rivadulla F 2004 *Nanotechnology* **14** 212
[391] Li X W, Gupta A, Xiao G and Gong G Q 1997 *Appl. Phys. Lett.* **71** 1124
[392] Todd N K, Mathur N D, Issac S P, Evetts J E and Blamire M G 1999 *J. Appl. Phys.* **85** 7263
[393] Sun J Z, Abraham D W, Rao R A and Eom C B 1999 *Appl. Phys. Lett.* **74** 3017
[394] Raju A R, Aiyer H N, Venkatanagarajuna B, Mahendiren R, Raychaudhari A K and Rao C N R 1997 *J. Phys. D: Appl. Phys.* **30** L71
[395] Mathur N D, Burnell G, Issac S P, Jackson T J, Teo B S, MacManus Driscoll J L, Cohen L F, Evetts J E and Blamire M G 1997 *Nautre* **387** 266
Mathur N D, Littlewood P B, Todd N K, Isaac S P, Teo B-S, Kang D-J, Tarte E J, Barber Z H, Evetts J E and Blamire M G 1999 *J. Appl. Phys.* **86** 6287
[396] Steenbeck K, Eick T, Kirsch K, O'Donnel K and Steinbeiss E 1997 *Appl. Phys. Lett.* **71** 968
Steenbeck K, Eick T, Kirsch K, Schmidt H G and Steinbeiss E 1998 *Appl. Phys. Lett.* **73** 2506.
[397] Westerburg W, Martin F, Friedrich S, Maier M and Jakob G 1999 *J. Appl. Phys.* **86** 2173
[398] Evetts J E, Blamire M G, Mathur N D, Issac S P, Teo B S, Cohen L F and Macmanus-Driscoll J L 1998 *Phil. Trans. R. Soc.* A **356** 1593
[399] Miller D J, Lin Y K, Vlasko-Vlasov V and Welp U 2000 *J. Appl. Phys.* **87** 6758
[400] Philipp J B, Höfener C, Thienhaus S, Klein J, Alff L and Gross R 2000 *Phys. Rev.* B **62** R9248
[401] Mathieu R, Svedlindh P, Gunnarsson R and Ivanov Z G 2001 *Phys. Rev.* B **63** 132407
[402] Gutpa A and Sun J Z 1999 *J. Magn. Magn. Mater.* **200** 24
[403] Sun J Z and Gupta A 1998 *Annu. Rev. Mater. Sci.* **28** 45
[404] Blamire M G, Schneider C W, Hammeri G and Mannhart J 2003 *Appl. Phys. Lett.* **82** 2670
[405] Vertruyen B, Cloots R, Rulmont A, Dhalenne G, Ausloos M and Vanderbemden Ph 2001 *J. Appl. Phys.* **90** 5692
[406] Gunnarsson R, Ivanov Z G, Dubourdieu C and Roussel H 2002 *Phys. Rev.* B **66** 024404
[407] Ziese M, Heydon G, Hohne R, Esquinazi P and Dienelt J 1999 *Appl. Phys. Lett.* **74** 1481
Glaser A and Ziese M 2002 *Phys. Rev.* B **66** 0944
[408] Bosak A A, Dubourdieu C, Chaudouet P, Senateur J-P and Fournier T 2003 *J. Appl. Phys.* **94** 5021
[409] Srinitiwarawong C and Ziese M 1998 *Appl. Phys. Lett.* **73** 1140
[410] Bibes M, Martynez B, Fontcuberta J, Trtik V, Benytez F, Sanchez F and Varela M 1999 *Appl. Phys. Lett.* **75** 2120
[411] Bibes M, Martynez B, Fontcuberta J, Trtik V, Benitez F, Ferrater C, Sanchez F and Varela M 1999 *Phys. Rev.* 9579
[412] Ramirez A P and Subramanian M A 1997 *Science* **277** 546
[413] Shimakawa Y, Kubo Y and Manako T 1996 *Nature* **379** 53
[414] Cheon S W, Hwang H Y, Batlogg B and Rupp L W 1996 *Solid State Commun.* **98** 163
[415] Hwang H Y and Cheong S W 1997 *Nature* **389** 942
[416] Subramanian M A, Toby B H, Ramirez A P, Marshall W A, Sleight A W and Kwei G H 1996 *Science* **273** 81
[417] Singh D J 1997 *Phys. Rev.* B **55** 313
[418] Alonso A, Velasco P, Martinze-Lope M J, Casais M T, Martinez J L, Fernandez-Diaz M T and de Paoli J M 2004 *Appl. Phys. Lett.* **76** 3274
[419] Alonso J A, Martinze-Lope M J, Casais M T, Velasco P, Martinez J L, Fernandez-Diaz M T and de Paoli J M 1999 *Phys. Rev.* B **60** R15024
[420] Velasco P, Alonso J A, Martinez-lope M J, Casais M T, Martinez J L, Fernandez-Diaz M T and de Paoli J M 2001 *Phys. Rev.* B **64** 184436
[421] Venkatesan M, Velasco P, Alonso J A, Martinez J L and Coey J D 2004 *J. Phys.: Condens. Matter* **16** 3465
[422] Alonso J A, Martinez J L, Martinez-lope M J, Casais M T and Fernandez-Diaz M T 1999 *Phys. Rev. Lett.* **82** 189
[423] Ramirez A P, Cava R J and Krajewski J 1997 *Nature* **387** 268

[424] Yang Z, Tan S, Chen Z and Zhang Y 2000 *Phys. Rev.* B **62** 13872
[425] Lotgering P K, Van Stapele P R P, Steen Van Der G H A M and Wieringer J S 1969 *J. Phys. Chem. Solids* **30** 799
[426] Park M S, Kwon S K, Youn S J and Min B I 1999 *Phys. Rev.* B **59** 10018
[427] Kobayashi K S, Kimura T, Sawada H, Terakura T and Tokura Y 1998 *Nature* **395** 677
[428] Manako T, Izumi M, Konishi Y, Kobayashi K I, Kawasaki M and Tokura Y 1999 *Appl. Phys. Lett.* **74** 2215
[429] Longo J M and Ward R 1961 *J. Am. Chem. Soc.* **83** 1088
[430] Tomioka Y, Okuda T, Okimoto Y, Kumai R, Kobayashi K I and Tokura Y 2000 *Phys. Rev.* B **61** 422
[431] Kim T H, Uehara M, Cheong S W and Lee S 1999 *Appl. Phys. Lett.* **74** 1737
[432] Shinde S R, Ogale S B, Greene R L, Venkatesan T, Tsoi K, Cheong S W and Millis A J 2003 *J. Appl. Phys.* **93** 1605
[433] Garcia-Hernandez M, Martinez J L, Martinez-lope M J, Casais M T and Alonso J A 2001 *Phys. Rev. Lett.* **86** 2443
Westerburg R, Reisinger D and Jakob G 2000 *Phys. Rev.* B **62** R767
[434] Serrate D, De Teresa J M and Ibarra M R 2007 *J. Phys.: Condens. Matter* **19** 023201
[435] Massida S, Continenza A, de Pascele T M and Monnier R 1997 *Z. Phys.* B **102** 82
[436] Aronson M C, Sarrao J L, Fisk Z, Whitton W and Brandt B L 1999 *Phys. Rev.* B **59** 4720
[437] Sillow S, Prasad I, Aronson M C, Sarrao J L, Fisk Z, Hristova H, Lacerda A H, Hundley M F, Vigliante A and Gibbs D 1998 *Phys. Rev.* B **57** 5860
[438] Nyhus P, Yoon S, Kauffman M, Cooper S L, Fisk Z and Sarrao J 1997 *Phys. Rev.* B **56** 2717
[439] Snow C S, Cooper S L, Young D P, Fisk Z, Comment A and Ansermet J P 2001 *Phys. Rev.* B **64** 174412
[440] Taraseon J M, Soubeyroux J L, Etourneau J, Georges R and Coey J M D 1981 *Solid State Commun.* **37** 133
[441] Von Molnar S and Methfessel S 1967 *J. Appl. Phys.* **38** 959
[442] Maeono Y, Hashimoto H, Yoshida K, Nishizaki S, Fujita T, Bednorz J G and Lichtenberg F 1994 *Nature* **372** 532
[443] Cao G, McCall S, Dobrosavljevic V, Alexander C S, Crow J E and Guertin R P 2000 *Phys. Rev.* B **61** R5053
[444] Hotta T and Dagotta E 2002 *Phys. Rev. Lett.* **88** 017201
[445] Cao G, Balicas L, Kin Y, Dagotto E, Crow J E, Nelson C S and Hill J P 2002 *Preprint* cond-mat/0205151
[446] Ohmichi E, Yoshida Y, Ikeda S I, Shirakawa N and Osada T 2004 *Phys. Rev.* B **70** 104414
[447] Klein L, Dodge J S, Ahn C H, Synder G, Geballe T H, Beasley M R and Kapitulnik A 1996 *Phys. Rev. Lett.* **77** 2774
[448] Cao G, McCall S, Shepard M, Crow J E and Guertin R P 1997 *Phys. Rev.* B **56** 321
[449] Kelin L, Marshall A F, Reiner J W, Ahn C H, Geballe J H, Beasley M R and Kapitulnik A 1998 *J. Magn. Magn. Mater.* **188** 319
[450] Brabers V A M 1995 *Handbook of Magneitc Materials* vol 8 ed K H J Buschow (Amsterdam: North-Holland)
[451] Garcia J and Subias G 2004 *J. Phys.: Condens. Matter* **16** R145
[452] Ziese M and Blythe H J 2000 *J. Phys.: Condens. Matter* **12** 13
[453] Todo S, Siratori K and Kimura S 1995 *J. Phys. Soc. Japan* **64** 2118
Verwey E J 1939 *Nature* **144** 327
[454] Yanase A and Hamada N 1999 *J. Phys. Soc. Japan* **68** 1607
[455] Liu H, Jiang E Y, Bai H L, Zheng R K, Wei H L and Zhang X X 2003 *Appl. Phys. Lett.* **83** 3531
[456] Coey J M D and Venkatesan M 2002 *J. Appl. Phys.* **91** 8345
[457] Schwarz K 1986 *J. Phys. F: Met. Phys.* **16** L211
[458] Kamper K P, Schmitt W, Guntherodt G, Gambino R J and Ruf R 1987 *Phys. Rev. Lett.* **59** 2788
[459] Wiesendanger R, Guntherodt H J, Guntherodt G, Gambino R J and Ruf R 1990 *Phys. Rev. Lett.* **65** 247
[460] Hwang H Y and Cheong S W 1997 *Science* **278** 1607
[461] Coey J M D, Berkowitz A E, Balcells L I, Purtis F F and Barry A 1998 *Phys. Rev. Lett.* **80** 3815
[462] Dai J and Tang J 2001 *Phys. Rev.* B **63** 054434
[463] Coey J M D, Viret M and von Molnar S 1999 *Adv. Phys.* **48** 167
[464] Barry A, Coey J M D and Viret M 2000 *J. Phys.: Condens. Matter* **12** L173
[465] Gupta A, Li X W and Xiao G 2000 *J. Appl. Phys.* **87** 6073
[466] Ohno H 1998 *Science* **281** 951
Sharma S D 2001 *Am. Sci.* **89** 516
Zutic I, Fabian J and Sarma S D 2004 *Rev. Mod. Phys.* **76** 323
[467] Koshihara S, Oiwa A, Hirasawa M, Katsumoto S, Iye Y, Urano C, Takagi H and Munekata H 1997 *Phys. Rev. Lett.* **78** 4617
[468] Nazmul M, Ahsan S and Tanatka Y 2002 *Preprint* cond-matt/0208299
[469] Dietl T, Ohno H, Matsukura F, Cibert J and Ferrand D 2000 *Science* **287** 1019
[470] Pearton S J *et al* 2003 *J. Appl. Phys.* **93** 1
[471] Dietl T 2002 *Semicond. Sci. Technol.* **17** 377
[472] Pearton S J *et al* 2004 *J. Phys.: Condens. Matter* **16** R209
[473] Timm C 2003 *J. Phys.: Condens. Matter* **15** R1865
[474] Matosumoto Y, Murakomi M, Shono T, Hasegawa T, Fukumura T, Kawasaki M, Ahmet P, Chikyow T, Koshihara S and Koinuma H 2001 *Science* **291** 854
[475] Pearton S J, Heo W H, Ivill M, Norton D P and Steiner T 2004 *Semicond. Sci. Technol.* **19** R59
[476] Kimura H, Fukumura T, Kawasaki M, Inaba K, Hasegawa T and Koinuma H 2002 *Appl. Phys. Lett.* **80** 94
[477] Ogale S B *et al* 2003 *Phys. Rev. Lett.* **91** 077205
[478] Sharma P, Sreenivas K and Rao K V 2003 *J. Appl. Phys.* **93** 3963
[479] Pearton S J, Norton D P, Ip K, Hea Y W and Steiner T 2005 *Prog. Mater. Sci.* **50** 293
[480] Reshchikov M A, Dogan S, Avrutin V, Cho S J and Morkoc H 2005 *J. Appl. Phys.* **98** 041301
[481] Kim J H, Kim H, Kim D, Ihm Y E and Choo W K 2003 *Physica* B **327** 304
[482] Han S J, Song J W, Yang C H, Park S H, Park J H, Jeong Y H and Rhie K W 2002 *Appl. Phys. Lett.* **81** 4212
[483] Yoo Y Z, Jin Z W, Chikyow T, Fukumara T, Kawasaki M and Koinuma H 2002 *Appl. Phys. Lett.* **81** 3798
[484] Shinde S R *et al* 2003 *Phys. Rev.* B **67** 115211
[485] Prellier W, Fouchet A and Mercey B 2003 *J. Phys.: Condens. Matter* **15** R1583 (and reference therein)
[486] Sharma P, Gupta A, Rao K V, Owens F J, Sharma R, Ahuja R, Osorio Guillen J M, Johansson B and Gehring G A 2003 *Nat. Mater.* **2** 673
[487] Rao C N R and Deepak F L 2005 *J. Mater. Chem.* **15** 573
[488] Spaldin N A 2004 *Phys. Rev.* B **69** 125201
[489] Wang Z L 2004 *J. Phys.: Condens. Matter* **16** R829
[490] Janisch R, Gopal P and Spaldin N 2005 *J. Phys.: Condens. Matter* **17** R657
[491] Xu R, Husmann A, Rosenbaum T F, Saboungi M L, Enderby J E and Littlewood P B 1997 *Nature* **390** 57
[492] Parish M M and Littlwood P B 2003 *Nature* **426** 162
[493] Tsymbal Y E, Mryasov O N and LeClair P R 2003 *J. Phys.: Condens. Matter* **15** R109
[494] Meservey R and Tedrow P M 1994 *Phys. Rep.* **238** 173
[495] Julliere M 1975 *Phys. Lett.* A **54** 225
[496] Miyazaki T and Tezuka N J 1995 *J. Magn. Magn. Mater.* **139** L231
[497] Moodera J S, Nowak J and van de Veerdonk R J M 1998 *Phys. Rev. Lett.* **80** 2941

[498] Sun J Z, Gallagher W J, Duncombe P R, Krusin-Elbaum L, Altoman R A, Gupta A, Lu Y, Gong G Q and Xiao G 1996 *Appl. Phys. Lett.* **69** 3266
[499] Li X W, Lu Y, Lu Y, Gong G Q, Xiao G, Gupta A, Leocoeur P, Sun J Z, Wang Y Y and Dravid V P 1997 *J. Appl. Phys.* **81** 5509
[500] Sun J Z, Krusin-Elbaum I, Duncombe P R, Gupta A and Laibowitz R B 1997 *Appl. Phys. Lett.* **70** 1769
[501] Viret M, Drouet M, Nassar J, Contour J P, Fermon C and Fert A 1997 *Europhys. Lett.* **39** 545
[502] Moon-Ho J, Mathur N D, Todd N K and Blamire M G 2000 *Phys. Rev.* B **61** R14905
[503] Moon-Ho J, Mathur N D, Evetts J E and Blamire M G 2000 *Appl. Phys. Lett.* **77** 3803
[504] Obata T, Manako T, Shimakawa Y and Kubo Y 1999 *Appl. Phys. Lett.* **74** 290
[505] Yin H Q, Zhou J S and Goodenough J B 2000 *Appl. Phys. Lett.* **77** 714
[506] Noh J S, Nath T K, Eom C B, Sun J Z, Tian W and Pan X Q 2001 *Appl. Phys. Lett.* **79** 233
[507] Bowen M, Bibes M, Barthelemy A, Contour J P, Anane A, Lemaitre Y and Fert A 2003 *Appl. Phys. Lett.* **82** 233
[508] Paillous F, Imhoff D, Sikora T, Barthelemy A, Maurice J L, Contour J P, Colliex C and Fert A 2002 *Phys. Rev.* B **66** 014417
[509] Yamada H, Ogawa Y, Ishii Y, Sato H, Kawasaki M, Akoh H and Tokura Y 2004 *Science* **305** 646
[510] Garcia N, Munoz M and Zhao Y W 1999 *Phys. Rev. Lett.* **82** 2923
[511] Garcia N, Munoz M, Qian G G, Rohrer H, Sareliev I G and Zhao Y W 2001 *Appl. Phys. Lett.* **79** 4550
[512] Chopra H D and Hua S Z 2002 *Phys. Rev.* B **66** 020403(R)
[513] Hua S Z and Chopra H D 2003 *Phys. Rev.* B **67** 060401(R)
[514] Tatara G, Zhao Y W, Munoz M and Garcia N 1999 *Phys. Rev. Lett.* **83** 2030
[515] Cabrera G C and Falicov L M 1974 *Phys. Status Solidi* b **61** 539
[516] Tatara G and Fukuyama H 1997 *Phys. Rev. Lett.* **78** 3773
[517] Bruno P 1999 *Phys. Rev. Lett.* **83** 2425
[518] Coey J M D, Berger L and Labaye Y 2001 *Phys. Rev.* B **64** 020407(R)
[519] Tagirov L R, Vodopyanov B P and Efetov K B 2002 *Phys. Rev.* B **65** 214419
[520] Ogale S B, Talyansky V, Chen C, Ramesh R, Greene R L and Venkatesan T 1996 *Phys. Rev. Lett.* **77** 1159
[521] Mathews S, Ramesh R, Venkatesan T and Benedetto J 1997 *Science* **276** 238
[522] Es-Souni M, Girdauskaite E, Iakovlev S, Solterbeck C H and Zaporojtchenko V 2004 *J. Appl. Phys.* **96** 5691
[523] Choudhary R J, Ogale S A, Shinde S R, Hullavarad S, Ogale S B, Bathe R N, Patil S I and Kumar R 2004 *Appl. Phys. Lett.* **84** 3846
[524] Rajeswari M, Chen C, Goyal A, Kwon C, Robson M C, Ramesh R, Venkatesan T and Lakeou S 1996 *Appl. Phys. Lett.* **68** 3555
[525] Lisauskas A, Khartsec S I and Grishin A 2000 *Appl. Phys. Lett.* **77** 756
[526] Fu C C, Huang Z and Yeh N C 2002 *Phys. Rev.* B **65** 224516
[527] Chen Z Y, Biswas A, Zutic I, Wu T, Ogale S B, Greene R L and Venkatesan T 2001 *Phys. Rev.* B **63** 212508
[528] Mcevoy S J 2001 *J. Mater. Sci.* **36** 1087
[529] Mori M, Sammes N M, Suda E and Takeda Y 2003 *Solid State Ion.* **164** 1